Observing and Modeling Ice-Sheet Surface Mass Balance

Lenaerts, J.T.M.; Medley, Brooke; van den Broeke, Michiel R.; Wouters, Bert

DOI
10.1029/2018RG000622

Publication date
2019

Document Version
Final published version

Published in
Reviews of Geophysics

Citation (APA)
Lenaerts, J. T. M., Medley, B., van den Broeke, M. R., & Wouters, B. (2019). Observing and Modeling Ice-Sheet Surface Mass Balance. *Reviews of Geophysics*, *57*(2), 376-420. https://doi.org/10.1029/2018RG000622

Reviews of Geophysics

REGULAR ARTICLE
10.1029/2018RG000622

Observing and Modeling Ice Sheet Surface Mass Balance

Jan T. M. Lenaerts[1], Brooke Medley[2], Michiel R. van den Broeke[3], and Bert Wouters[3,4]

[1]Department of Atmospheric and Oceanic Sciences, University of Colorado Boulder, Boulder, CO, USA, [2]Cryospheric Sciences Laboratory, NASA GSFC, Goddard, MD, USA, [3]Institute for Marine and Atmospheric Research, Utrecht University, Utrecht, The Netherlands, [4]Faculty of Civil Engineering and Geosciences, Delft University of Technology, Delft, The Netherlands

Abstract Surface mass balance (SMB) provides mass input to the surface of the Antarctic and Greenland Ice Sheets and therefore comprises an important control on ice sheet mass balance and resulting contribution to global sea level change. As ice sheet SMB varies highly across multiple scales of space (meters to hundreds of kilometers) and time (hourly to decadal), it is notoriously challenging to observe and represent in models. In addition, SMB consists of multiple components, all of which depend on complex interactions between the atmosphere and the snow/ice surface, large-scale atmospheric circulation and ocean conditions, and ice sheet topography. In this review, we present the state-of-the-art knowledge and recent advances in ice sheet SMB observations and models, highlight current shortcomings, and propose future directions. Novel observational methods allow mapping SMB across larger areas, longer time periods, and/or at very high (subdaily) temporal frequency. As a recent observational breakthrough, cosmic ray counters provide direct estimates of SMB, circumventing the need for accurate snow density observations upon which many other techniques rely. Regional atmospheric climate models have drastically improved their simulation of ice sheet SMB in the last decade, thanks to the inclusion or improved representation of essential processes (e.g., clouds, blowing snow, and snow albedo), and by enhancing horizontal resolution (5–30 km). Future modeling efforts are required in improving Earth system models to match regional atmospheric climate model performance in simulating ice sheet SMB, and in reinforcing the efforts in developing statistical and dynamic downscaling to represent smaller-scale SMB processes.

Plain Language Summary Ice sheets, the largest class of glaciers, contain the majority of ice on Earth. The amount of ice contained in ice sheets changes constantly with the addition of new snow and ice, and melting taking place at the surface, base, and terminus of ice sheets. The balance between these inputs and outputs is known as the "mass balance." Processes affecting the addition and removal of snow on top of the ice sheet are termed the "surface mass balance" and include rainfall, moisture evaporation, snow-transporting winds, and melting due to temperature changes. Scientists can now monitor these processes with tools on-site, such as automated weather stations, Global Positioning Systems, and sensors that record high-energy radiation (cosmic rays) originating outside the Earth's atmosphere. Several methods are also available where Earth-orbiting satellites measure how ice is changing. Data collected in these ways have revealed how the surface mass balance varies over time and space. A better understanding of these processes is critical to predicting future behavior of ice sheets and their effect on sea level. Improvements to regional-scale models in the past decade have allowed good simulations of surface mass balance, and the next step is to build models that work at a global scale.

GRAND CHALLENGES CENTENNIAL COLLECTION

Key Points:
- Emerging (remote) observational techniques provide enhanced insights in spatial and temporal variability of ice sheet surface mass balance (SMB)
- Regional climate models can be used to assess ice sheet SMB, although deficiencies remain in representing subgrid processes
- In the near future, Earth System Models can be used to assess internal variability, forced change, and positive feedbacks on ice sheet SMB

Supporting Information:
- Supporting Information S1
- Date Set S1
- Date Set S2
- Date Set S3

Correspondence to:
J. T. M. Lenaerts,
jan.lenaerts@colorado.edu

Citation:
Lenaerts, J. T. M., Medley, B., van den Broeke, M. R., & Wouters, B. (2019). Observing and modeling ice sheet surface mass balance. *Reviews of Geophysics*, *57*. https://doi.org/10.1029/2018RG000622

Received 13 NOV 2018
Accepted 19 MAR 2019
Accepted article online 21 MAY 2019

1. Introduction

Earth's ice sheets—the Greenland Ice Sheet (GrIS) in the Arctic and the Antarctic Ice Sheet (AIS) roughly centered around the South Pole—collectively contain more than two thirds of the planet's freshwater (Church et al., 2013). If melted completely, global mean sea level would be about 65 m higher than today (Alley et al., 2005). Observations show that both ice sheets are currently losing mass at accelerating rates (E. Rignot et al., 2011; Shepherd et al., 2012, 2018), in spite of large natural interannual variability. Even in a scenario of strong climate change mitigation, in which global mean temperature rise is limited to less than 2 °C relative to preindustrial values, ice sheets will continue to lose mass but are not likely to pass tipping points, in which case mass loss would become irreversible (Pattyn et al., 2018). In high-emission scenarios, however, projected mass loss from the ice sheets becomes highly uncertain, especially for the AIS; some

models predict AIS mass losses in excess of one meter of global sea level equivalent at the end of the 21st century, with multiple meters of potential additional sea level rise in the centuries thereafter (DeConto & Pollard, 2016).

1.1. Ice Sheet Mass Balance and Surface Mass Balance

Ice sheet mass loss/gain is commonly expressed as a negative/positive ice sheet mass balance (MB; Cogley et al., 2011). Ice sheet MB is determined by two main classes of processes: (1) surface mass fluxes (referred to as the surface mass balance, SMB) and (2) the flux of ice across the grounding line (referred to as ice discharge, D). The MB of the grounded ice sheet is defined as MB = SMB − D, which implies that both SMB and D have units of mass change with time (usually expressed in Gt per year, where 1 Gt = 10^{12} kg is equivalent to the mass of 1 km^3 of water). SMB generally is a positive term (as D is positive) but may also be negative, in which case MB becomes negative, a situation that is sometimes referred to as a tipping point for ice sheet mass loss (Robinson et al., 2012). Once it has crossed the grounding line, ice becomes afloat and forms ice shelves, which are prevalent on the AIS but rare on the GrIS. The MB of these ice shelves comprises of the difference of D + SMB (the incoming mass fluxes), and the two outgoing mass fluxes, (1) melting of the ice shelf base that is in contact with the ocean (basal melting), and (2) iceberg calving at the ice shelf front (Depoorter et al., 2013).

SMB components and relevant processes are visualized in Figure 1. During precipitation and condensation (dew formation) and deposition (riming), mass accumulates at the surface. Mass is lost when meltwater is not retained in the firn by refreezing and/or capillary forces and leaves the ice sheet as runoff; snow can also be redistributed by the wind (erosion/deposition) and/or sublimate, either from the surface or from drifting snow particles. Once accumulated, snow slowly changes into ice via the intermediate product firn, representing a layer of old (i.e., multiyear), compressed snow. The firn layer can be anything between 0 and 130 m thick, depending on the local climate (Ligtenberg et al., 2011). Because the firn layer plays such an important role in the ice sheet MB, in this paper we consider firn processes (meltwater percolation, retention, and refreezing) to be part of the SMB, although formally this use is referred to as "climatic mass balance" (Cogley et al., 2011). Mass is also lost by the movement of glacier ice from the interior ice sheet to the margins, driven by basal sliding and internal deformation, followed by solid ice discharge (D) when the ice crosses the grounding line and starts to float on the ocean.

The GrIS and AIS are remarkably different in many of their global characteristics (Figure 1). The AIS (12.9 million km^2) is about 7.5 times larger in area than the GrIS (1.7 million km^2), contains about eight times more ice (58.2 vs. 7.3 m sea level equivalent; Church et al., 2013), and is characterized by a generally colder, windier, and drier surface climate. An exception to that is the Antarctic Peninsula, which operates in similar ways to the GrIS, with narrow outlet glaciers draining into fjords (Figure 1) and which experiences a much warmer and overall wetter climate than the remainder of the AIS. Moreover, although both ice sheets are currently losing mass (i.e., their MB is negative), they do so at different rates via different mechanisms. While currently increasing AIS mass loss is solely attributed to an increase in D owing to glacier acceleration in spatially limited regions (Mouginot et al., 2014; Rignot et al., 2011; Rignot et al., 2019; Shepherd et al., 2018), GrIS mass loss is dominated by a decrease in SMB that has occurred essentially along its entire margin since the early 1990s (van den Broeke et al., 2016). Temporal SMB trends and their impact on ice sheet MB are discussed in sections 4 and 5.

To understand fully the physical processes that determine ice sheet MB, four different balances must be explicitly solved, one of which is SMB (Figure 2). Ice sheet SMB comprises the sum of multiple components; it is intimately linked to the liquid water balance, which describes sources and sinks of liquid water at the surface (melt, rain, and condensation) and in the firn layer (i.e., percolation/refreezing/retention of liquid water) as well as the surface energy balance (SEB), which determines the energy available for melt, evaporation/condensation, or sublimation/deposition. These processes will be discussed in section 1.2.

Thus far, we have defined SMB as an ice sheet-integrated quantity. To evaluate changes at the process scale, we also study values of "local" SMB, expressed in millimeter water equivalent (w.e.) $year^{-1}$ or kg m^{-2} $year^{-1}$ (referred to as "specific SMB," or "SSMB"). Following this definition, the ice sheet accumulation/ablation zones (Figure 1; see Glossary) comprise all locations where SSMB > 0/SSMB < 0, respectively.

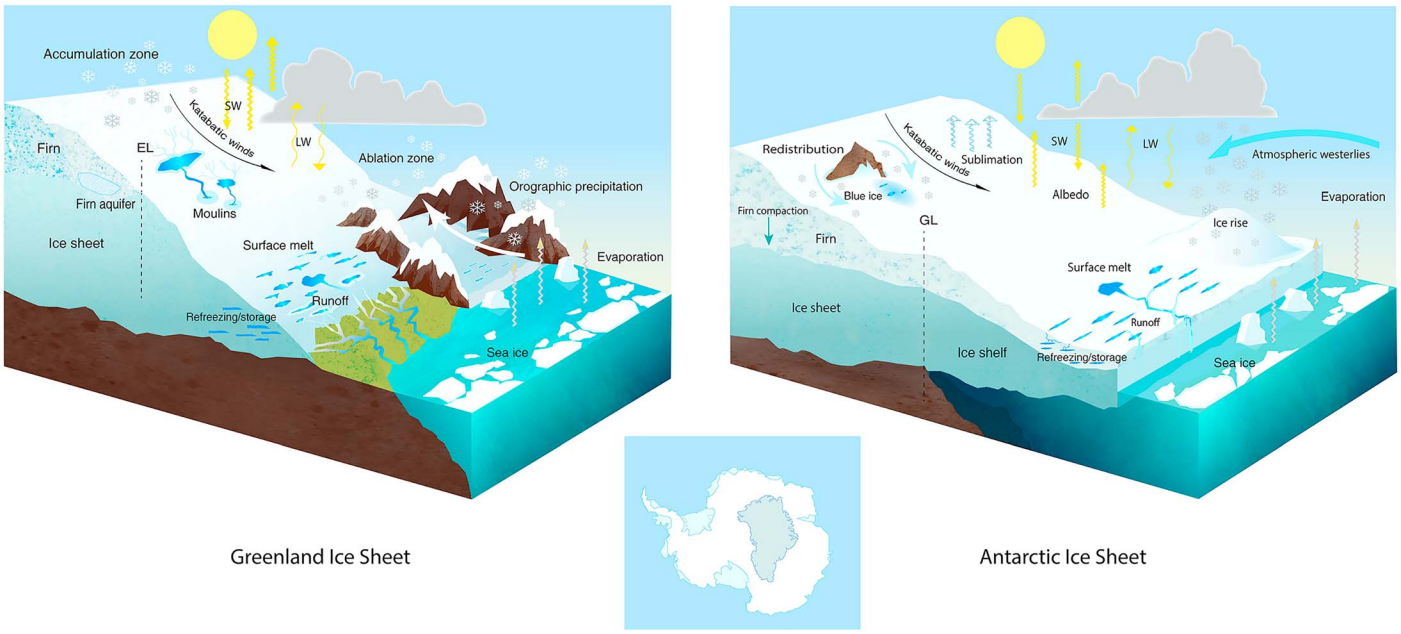

Figure 1. Illustration of all relevant surface mass balance processes on the Greenland (left) and Antarctic (right) ice sheets. Some processes are only indicated on the left or right, depending on where they are most important. The inset below shows a size comparison of the ice sheets, with the Antarctic ice sheet in white and the Greenland ice sheet in grey (Credit: Marlo Garnsworthy, Wordy Bird Studio).

1.2. Components of Surface Mass Balance

1.2.1. Precipitation

The dominant source of mass for ice sheets is precipitation, the transfer of ice particles (snow) or water droplets (rain) from the atmosphere to the ice sheet surface. Atmospheric ice and water can coexist in atmospheric clouds, depending on the thermodynamic characteristics of the atmosphere. Cloud droplets form by condensation onto atmospheric aerosols that act as cloud condensation nuclei. Over ice sheets, cloud condensation nuclei predominantly originate from in-cloud ice particles, sea salt, and—to a lesser degree—biogenic nuclei, sulphates, dust, and black carbon from long-range pollution sources or wildfires (Bromwich et al., 2012; Lathem et al., 2013). Clouds over ice sheets typically contain only ice particles (when temperatures less than -40 °C) or are mixed-phase clouds (Bromwich et al., 2012; Shupe et al., 2013), which contain both (supercooled) liquid water droplets and ice. In mixed-phase clouds, ice precipitation particles (snowflakes) predominantly grow through deposition of water molecules onto them, at the expense of supercooled liquid water droplets that evaporate (the Wegener-Bergeron-Findeisen, or simply Bergeron process).

Ice sheet mass balance (MB, Gt yr $^{-1}$)

$$MB = \text{Surface mass balance} - \text{Discharge}$$

Surface mass balance (SMB, Gt yr $^{-1}$)

$$SMB = \text{Precipitation} - \text{Runoff} - \text{Sublimation/Evaporation} - \text{Blowing snow erosion}$$

Liquid water balance (LWB, Gt yr $^{-1}$)

$$\text{Runoff} = \text{Melt} + \text{Rainfall} + \text{Condensation} - \text{Refreezing} - \text{Retention}$$

Surface energy balance (SEB, W m $^{-2}$)

$$\text{Melt} = SW_{net} + LW_{net} + SHF + LHF + G_s$$

Figure 2. The four equations governing ice sheet MB and components. The colored vertical arrows show how the equations are linked. The SEB components are (all defined at the surface, and positive means that the flux is directed toward the surface): net shortwave radiation (SW_{net}), net longwave radiation (LW_{net}), sensible heat flux (SHF), latent heat flux (LHF), and ground/soil heat flux (G_s).

Besides this process, ice crystals can change by fragmentation (large ice particles break into smaller ones), accretion (supercooled liquid freezing onto an existing ice crystal), and aggregation (snowflakes merging). As the temperature in the atmosphere over ice sheets is usually below the freezing point, precipitation generally falls as snow. If temperatures in a sufficiently deep atmospheric layer exceed the melting point, however, snowflakes melt as they fall, and precipitation falls on the surface as rain. While other, convective-weather precipitation types (hail, graupel, etc.) are considered rare over ice sheets (Serreze & Hurst, 2000), the cold and dry GrIS and AIS interior areas frequently experience "clear-sky precipitation" (Bromwich, 1988). This type of precipitation falls from surface-based clouds of ice crystals, often referred to as "diamond dust," and typically occurs during cold and quiet conditions (Ricaud et al., 2017; Sato et al., 1981). Being frequently observed in the interiors of the AIS and GrIS, especially in winter (von Walden et al., 2003), locally diamond dust can contribute significantly (30–80%) to the total annual accumulation (Radok & Lile, 1977; Ricaud et al., 2017).

1.2.2. Surface Melt, Refreezing, Retention and Runoff

Melting (i.e., the phase change from solid to liquid state) of the surface snow and ice occurs when the surface temperature reaches the melting point (0 °C), while excess energy is available. Snow and ice can also melt at some small (<10 cm) depth below the surface (subsurface melt), caused by penetration of solar radiation (Brandt & Warren, 1993). The amount of energy available for melt is determined by the SEB, the sum of radiative, turbulent, and conductive subsurface heat fluxes, ignoring heat from rain (Figure 2; see Glossary). Meltwater generated at the surface can have five different pathways: (1) It collects at the surface in the form of supraglacial meltwater lakes (Koenig et al., 2015; Moussavi et al., 2016); (2) it runs off supraglacially (Bell et al., 2017; Smith et al., 2015); (3) it percolates into the snowpack or runs off englacially through vertical pathways in the ice (moulins) or is diverted laterally when it encounters an impermeable layer, such as ice or bedrock (Chandler et al., 2013); (4) it percolates into the snowpack and is stored in liquid form in weathered ice crusts (Cooper et al., 2018), firn aquifers (Forster et al., 2014), or subsurface lakes (Lenaerts et al., 2016); and (5) it percolates into the snowpack, refreezes, and is stored in the firn as ice (Harper et al., 2012). The pathway of surface meltwater thus strongly depends on surface and firn characteristics (section 1.3); in turn, meltwater pathways affect surface snow and firn characteristics (de la Peña et al., 2015; Machguth et al., 2016; Nienow et al., 2017).

1.2.3. Evaporation and Sublimation

Evaporation (i.e., the phase change from liquid to vapor state) can occur when liquid water is exposed at the ice sheet surface, that is, after melt, condensation, or rainfall. Over snow surfaces, liquid water will quickly penetrate the snowpack, preventing significant evaporation from occurring. However, standing water can be found on impermeable ice, mostly in the form of water collecting in topographic depressions of the ice sheet surface in the GrIS ablation zone (McMillan et al., 2007; Sundal et al., 2009), and on or near some Antarctic ice shelves (Kingslake et al., 2017; Langley et al., 2016; Lenaerts, Lhermitte, et al., 2017). Sublimation, the direct phase change between solid and vapor state, occurs more commonly on ice sheets (Bintanja, 1998; Box & Steffen, 2001; Lenaerts & van den Broeke, 2012; van den Broeke, 1997; van Lipzig et al., 2004). Sublimation represents a turbulent moisture flux and exists in two dominant forms. First, surface sublimation (SU_s) depends on the magnitude of the surface-to-air humidity gradient and the wind speed, which represents the wind shear required to generate turbulence (vertical mixing) in the stably stratified surface layer. Sublimation peaks when the sun heats the surface (i.e., typically in the summer season), the near-surface air is dry, and wind speed is significant but not so high as to induce drifting snow (King et al., 2001). Second, sublimation is favored when snow particles become entrained in the near-surface atmosphere (Liston & Sturm, 2002; Schmidt, 1982), referred to as drifting snow/blowing snow sublimation (SU_{ds}). Because the drifting particles are better ventilated than those at the surface, this type of sublimation is more efficient than surface sublimation (Bintanja, 2000, 2001; Déry et al., 1998). Drifting and blowing snow occurs in high-wind conditions, which prevail in katabatic wind zones over much of the AIS (Lenaerts & van den Broeke, 2012; Palm et al., 2011) and large parts of the GrIS, particularly in winter (Lenaerts, van den Broeke, van Angelen, et al., 2012; Lenaerts, van den Broeke, van de Berg, et al., 2012; Lenaerts, van den Broeke, Déry, et al., 2012; Lenaerts, van den Broeke, Scarchilli, et al., 2012).

1.2.4. Snow Erosion

During drifting and blowing snow conditions, suspended snow particles are (partly) sublimated and/or deposited elsewhere (Essery et al., 1999; Palm et al., 2011). Depending on the surface characteristics and near-surface wind field, this leads to snow redistribution (Lenaerts, van den Broeke, Déry, et al., 2012). In

locations where the near-surface air flow diverges and/or accelerates, snow will be eroded and—if not sublimated while entrained in the atmosphere—redeposited in areas where the flow convergences and/or decelerates. This implies net snow erosion (ER_{ds} positive, surface mass loss) in the former and net snow deposition (ER_{ds} negative, surface mass gain) in the latter regions (Das et al., 2013; Frezzotti et al., 2007; Scambos et al., 2012).

1.3. Factors Driving SMB and SMB Components

1.3.1. Large-Scale Atmospheric Circulation—Greenland

GrIS SMB is strongly controlled by synoptic (100- to 1,000-km scale) and large-scale (>1,000 km) atmospheric dynamics. The transport of air masses with varying temperature and moisture content toward the GrIS affects all SMB components. Precipitation on the GrIS is mostly generated by advection of relatively mild, moist air by low-pressure systems branching off the North Atlantic storm track, an elongated band of high cyclonic activity running southwest-northeast across the North Atlantic Ocean basin, from the east coast of North America to Iceland and Scandinavia. When mild and moist air encounters the ice sheet, it is forced to rise, expand, and cool, leading to orographically induced precipitation. As a result, the depth and position of low-pressure systems determine the spatial and temporal distribution of precipitation on the GrIS (Berdahl et al., 2018). In winter, when atmospheric baroclinicity resulting from horizontal temperature gradients peaks, cyclonic activity is focused around Iceland (generating the climatological "Iceland Low"), and weather systems regularly reach the south and southeastern coasts of Greenland. In this area and season, cyclonic activity can be enhanced by the presence of the ice sheet, generating so-called "lee cyclogenesis" (Schuenemann et al., 2009). In summer, the storm track is less well developed, less symmetrical, and narrower (Chen et al., 1997; Ohmura & Reeh, 1991). In this season, the atmospheric flow is more frequently blocked by the GrIS and can become more north-south oriented. Synoptic weather systems more frequently approach from the west or south and travel into Baffin Bay, where they become stagnant, bringing precipitation to the GrIS west coast for prolonged periods (Schuenemann et al., 2009). This seasonality in storm track behavior and resulting precipitation patterns explains the remarkable variation in seasonality between west Greenland, where precipitation peaks in summer, and south(-east) Greenland, where precipitation peaks in winter (Berdahl et al., 2018).

The North Atlantic Oscillation (NAO; Hurrell et al., 2013) index is usually defined as the normalized sea level pressure difference between the Azores and Iceland. With generally low pressure around Iceland and high pressure around the Azores, the NAO index is usually positive, indicative of a well-developed and zonally directed North Atlantic large-scale atmospheric circulation. However, the NAO can become zero or negative when the pressure gradient is small or reversed, implying a weak and/or wavy jet stream and blocking conditions. Generally, such a small or negative NAO index is associated with dry conditions over the northern and western GrIS and wet conditions over the southern portion of the GrIS (Appenzeller et al., 1998; Bromwich et al., 1999; Lewis et al., 2017). As these two signals tend to compensate each other, the total GrIS precipitation does not correlate significantly with NAO (Hanna et al., 2011). More importantly, a weak NAO is associated with anomalously warm conditions and upper-air ridging over Greenland in summer (Figure 3), which can be quantified by the Greenland Blocking Index (Hanna et al., 2016). A weak NAO and high Greenland Blocking Index in summer, such as predominantly observed between 2003 and 2012 (Fettweis et al., 2013; Hanna et al., 2018) in turn leads to anomalously high surface melt on the western GrIS, with 2012 as a peak anomaly. The summer NAO index has returned to positive values, and Greenland SMB has increased to average 1961–1990 values in recent years (2017 and 2018; see www.polarportal.org). Other climate indices that are commonly used to characterize atmospheric circulation variability in the middle to high northern latitudes include the Arctic Oscillation, which is similar to NAO in that it expresses the zonality of the midlatitude jet stream over the North Atlantic, and the Atlantic Multidecadal Oscillation, both of which can explain some degree of variability of GrIS SMB (Hanna et al., 2011; Lewis et al., 2017). Regarding links to tropical climate variability, it has been suggested that the recent weak NAO (and consequent high GrIS summer melt) is caused by anomalous Rossby wave activity originating in the tropical Pacific (Ding et al., 2014). However, on longer time scales, there is little evidence of significant correlations between GrIS SMB and various tropical climate variability indices (Hanna et al., 2006), such as the El Niño Southern Oscillation (ENSO) or the Pacific Decadal Oscillation.

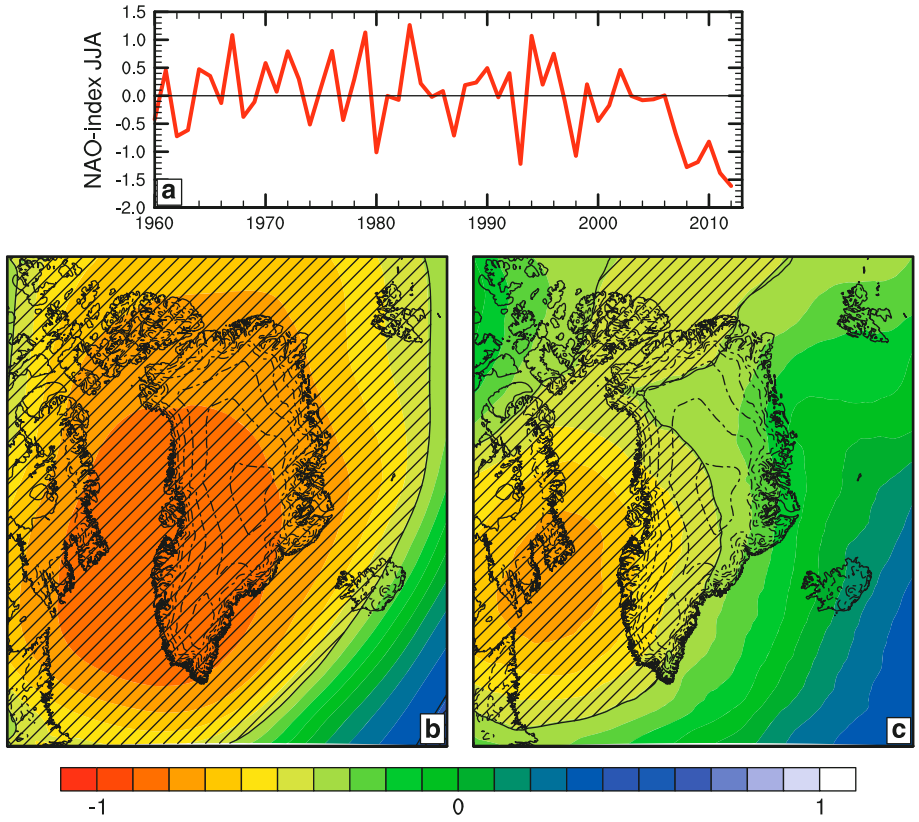

Figure 3. Averaged June–August (JJA) index for the North Atlantic Oscillation (NAO; data from the National Oceanic and Atmospheric Administration). Correlation fields between the JJA NAO index and the 500-hPa geopotential height (b) and temperature (c) from RACMO2 for 1960–2012; hatched area indicates the 99% confidence level. Source: van Angelen et al. (2014).

1.3.2. Large-Scale Atmospheric Circulation—Antarctica

Owing to its greater geographical symmetry relative to the large-scale circulation and sheer size, the precipitation climate of the AIS is remarkably different to that of the GrIS. The circumpolar pressure trough (CPT), a band of low-pressure systems in high southern latitudes, is deeper and more symmetrical than the storm track in the Northern Hemisphere, since fewer topographical barriers exist to disturb the large-scale atmospheric flow, and fewer continents are nearby to generate high pressure during winter. Therefore, the CPT features prominently in zonally average pressure distribution, and the meridional transport of heat and moisture is less determined by topography, with the notable exception of the Antarctic Peninsula, a mountain range that extends northward between roughly 60°S to 75°S.

Three climatological low-pressure systems are embedded in the CPT (Marshall, 2009), generating a zonal wave three atmospheric pattern in maps of average surface pressure (Raphael, 2004). The deepest climatological low-pressure system is the Amundsen Sea Low (Turner et al., 2013, 2017), centered around 130°W, followed by the low-pressure system off Wilkes Land in the South-Central Pacific Ocean (around 100°E), and another system off Dronning Maud Land in the South Atlantic Ocean (around 20°E). The CPT around Antarctica and hence the position of these three climatological low-pressure systems contract and expand twice a year—in austral spring and autumn—in response to peaks in the meridional temperature gradient and hence baroclinicity, known as the semiannual oscillation (Meehl, 1991; van Loon, 1967). This oscillation induces meridional circulation changes that profoundly affect seasonality in precipitation (Marshall, 2009) and temperature (van den Broeke, 1998), particularly in coastal regions. The largest intra-annual and interannual variability in SMB is found on the east side of those low-pressure systems, where southward moisture transport is most pronounced (Marshall, 2009). This is especially true around the Amundsen-Bellingshausen region, which is sometimes termed the “pole of variability” (Lachlan-Cope et al., 2001).

Antarctic precipitation is strongly controlled by the meridional (southward) transport of moisture from lower latitudes. The strength and zonality of the midlatitude westerlies are expressed by circulation indices such as the Antarctic Oscillation or Southern Annular Mode (SAM). The correlation between SAM and integrated Antarctic SMB is weak (Medley & Thomas, 2019), as the SAM-forced precipitation signal predominantly reflects a spatial redistribution (van den Broeke & van Lipzig, 2004), where regional accumulation decreases are compensated for by increases elsewhere (Fyke et al., 2017). In particular, in response to a positive SAM, precipitation is lower in the western part of West Antarctica (around the Ross Ice Shelf), while it is higher on the eastern side on the Antarctic Peninsula (Medley & Thomas, 2019). There is a wide body of literature discussing the role of tropical variability in shaping Antarctic climate, in particular ENSO, but also the Atlantic Multidecadal Oscillation, the Madden-Julian Oscillation, and Pacific Decadal Oscillation, as summarized by Yuan et al. (2018). Overall, the tropical-high latitude connection is complex and manifests itself on subseasonal to multidecadal time scales. For example, the recent atmospheric warming on the Antarctic Peninsula in the 1990s (Vaughan et al., 2003) and subsequent cooling after 1998 (Oliva et al., 2017) are most likely linked to natural variations in the strength of the midlatitude westerlies (Turner et al., 2016). ENSO modulates heat and moisture transport onto the West AIS, affecting temperature and precipitation patterns. In response to ENSO, eastern West Antarctica experiences anomalously low sea surface temperatures (SSTs) and an atmospheric moisture flux directed away from the ice sheet, while western West Antarctica (the region around the Ross ice shelf) experiences higher than normal SSTs and anomalously high southward moisture fluxes (Marshall et al., 2017; Marshall & Thompson, 2016). Additionally, recent work suggests that stratospheric ozone depletion, apart from impacting Southern Ocean sea ice and atmospheric dynamics, has led to a spatial redistribution of Antarctic snowfall, and an increase in total snowfall (Lenaerts et al., 2018).

Source regions of precipitation vary strongly for both ice sheets, depending on the distance to the coast, seasonality, and large-scale atmospheric circulation (Delaygue et al., 2000; Reijmer & van den Broeke, 2001; Sodemann et al., 2008). In general, coastal regions receive most of their precipitation from nearby ocean areas, while high-elevation snowfall is sourced from remote, lower-latitude regions, especially on the AIS (Delaygue et al., 2000; Sodemann & Stohl, 2009). The largest precipitation events are caused by "atmospheric rivers," long-fetched channels of high atmospheric moisture that protrude from the tropics or midlatitudes all the way to high latitudes (Gorodetskaya, Tsukernik, et al., 2014; Mattingly et al., 2018; Nash et al., 2018). In middle- and high-elevation areas of the AIS, atmospheric rivers generate 30–100% of the annual precipitation (Gorodetskaya et al., 2013; Schlosser et al., 2010), depending on their strength, location, and frequency.

1.3.3. Topography and Winds

Ice sheets represent extensive and highly elevated (>3 km asl) surfaces with a relatively flat and homogeneous interior and steeper and more complex coastal topography, which have a profound impact on their climate and SMB. First, ice sheets interact with the prevalent atmospheric flow on multiple spatial scales. They generate planetary Rossby waves (James, 2006; Löfverström et al., 2014), which describe the large-scale atmospheric circulation at midlatitudes. The topography of the ice sheet periphery is often relatively steep, rising vertically by ~1 km over a horizontal distance of 100 km or less, leading to orographic precipitation. This is the main driver of coastal precipitation on both ice sheets (Bromwich, 1988; Chen et al., 1997) and can result in high (multiple meters) annual snowfall amounts in areas where topography is steepest, that is, close to the ice sheet edge or in mountainous areas, and aligned perpendicular to the prevalent atmospheric flow, such as in southeast Greenland and the Antarctic Peninsula (van den Broeke et al., 2006; Ettema et al., 2009, section 3). Note that a positive feedback is active, as high precipitation amounts lead to a steeper ice sheet profile. Second, the ice sheet topography shapes the near-surface wind field (Bromwich et al., 1996; Parish & Bromwich, 1987). Because net radiation is generally negative at the ice sheet surface, the near-surface air is cooled, and the dominant ice sheet wind regime is katabatic (van den Broeke et al., 2002). If allowed enough time, this gravity-driven flow of cold air from the ice sheet interior to the coast is turned along the ice sheet contours by the Coriolis force and maintains a downslope component near the surface owing to friction (van den Broeke et al., 2003). The katabatic wind field, and resulting snow redistribution, is subsequently altered by smaller-scale topography: It is channeled and accelerated in narrow glacial valleys (Bromwich et al., 1990; Gallée et al., 1994; Lenaerts, van den Broeke, van Angelen, et al., 2012; Lenaerts, van den Broeke, van de Berg, et al., 2012; Lenaerts, van den

Broeke, Déry, et al., 2012; Lenaerts, van den Broeke, Scarchilli, et al., 2012) and is slowed down and deflected by large obstacles, such as nunataks or topographic promontories. On ice shelves, in the absence of a significant surface slope, katabatic forcing is weak, and synoptic pressure gradients determine the wind field. In the escarpment zone, katabatic winds can be significantly enhanced by synoptic pressure gradients resulting from cyclonic activity over the Southern Ocean for the AIS (van den Broeke et al., 2002, 2003) or in Baffin Bay for the GrIS (van Angelen et al., 2011). Isolated mountain ranges, such as that in the AP, force upslope flow on their windward side, resulting in orographic precipitation, but also generate downslope flow on their leeward side. As it descends dry adiabatically (warming ~10 K/km), the downslope flowing air to the east of the AP mountain range is generally warm and dry and referred to as foehn winds (Elvidge et al., 2015), locally resulting in surface melt (Luckman et al., 2014), even in midwinter (Kuipers Munneke, Luckman, et al., 2018). Other local and regional wind phenomena include barrier winds, which result from the damming of cold air against a topographic barrier (Petersen et al., 2009; van den Broeke & Gallée, 1996), and tip jets, which are driven by orographic descent or flow distortion by an isolated topographic ridge and consequent flow acceleration (Doyle & Shapiro, 1999; Våge et al., 2009). Barrier winds are common on the east and west coasts of Greenland (Harden et al., 2011; van den Broeke & Gallée, 1996), east of the AP (Parish, 1983; Turner et al., 2002), and on the Ross Ice Shelf along the Transantarctic Mountains (Steinhoff et al., 2008). The existence of a tip jet is well documented for south Greenland (Doyle & Shapiro, 1999; Moore et al., 2005) but also occurs commonly in, for example, coastal West Antarctica (Lenaerts, Lhermitte, et al., 2017; Lenaerts, Ligtenberg, et al., 2017; Lenaerts, van Tricht, et al., 2017).

1.3.4. Clouds, Turbulence, Albedo, and Radiation

Ice sheet SMB, and each of its components, is tightly coupled to the exchange of momentum, heat, and moisture between the ice sheet surface and the turbulent near-surface atmosphere, referred to as the atmospheric surface layer. Turbulent heat and moisture fluxes are part of the SEB, the sum of all the incoming and outgoing energy fluxes at the surface skin layer (Figure 2; see Glossary). Clouds play a pivotal role in determining the SEB through the competing effects of decreasing downwelling solar (shortwave) radiation while enhancing downward thermal (longwave) radiation. The net cloud radiative effect, defined as the difference in surface net all-wave radiation between average conditions (including clouds) and clear skies, depends on cloud structure, height, and frequency of occurrence (Chen et al., 2000; Shupe et al., 2004; Wang et al., 2005). In polar regions, and over highly reflective snow and ice surfaces, the longwave cloud effect generally dominates the shortwave cloud effect, so that clouds generally result in a net warming of the surface (Curry et al., 1993; Zhang et al., 1996); that is, the net cloud radiative effect is positive. This warming effect by clouds is sometimes referred to as the radiation paradox (Bintanja & van den Broeke, 1995), as its sign is opposite to that of the typical midlatitude cloud effect. This also suggests that clouds over ice sheets can promote surface melting, as has been observed on Larsen C Ice Shelf (King et al., 2015), the GrIS (van Tricht et al., 2016), the grounded parts of the AIS (Hoffman et al., 2008), as well as Arctic sea ice (Kay & Gettelman, 2009).

Surface broadband albedo is the wavelength-integrated shortwave reflectivity of the surface and determines which fraction of the incoming shortwave radiation is reflected and which part is absorbed by the surface. The spectral (wavelength-dependent) albedo of clean, dry snow is high (0.8–0.9) in the near-UV and visible wavelengths but decreases rapidly at larger wavelengths (Wiscombe & Warren, 1980). Snow albedo depends on a variety of atmospheric and surface factors, most prominently snow grain size, cloud cover, solar zenith angle, impurity content, and the presence of liquid water in the snow (Flanner & Zender, 2006; Kuipers Munneke et al., 2008; Wiscombe et al., 1980). Usually, freshly accumulated dry snow grains are relatively small (order 100 μm) and grow in time, driven by temperature and vapor gradients in the snowpack. This decreases snow albedo as larger grains predominantly scatter in the forward direction, that is, into the snowpack, enhancing the chances of absorption (Flanner & Zender, 2006). When surface snow melts, the liquid water will promote (wet) snow grain growth and quickly lower surface albedo (clean wet snow has an albedo of ~0.7, depending on liquid water content and other factors mentioned above). This highlights the powerful positive snowmelt-albedo feedback, by which, in the absence of fresh snow accumulation, even a small amount of liquid water can decrease snow albedo, further promoting melt. Snow albedo increases with higher solar zenith angle, as the chances of forward scattering and absorption decrease at low sun angles (Wang & Zender, 2010).

Lastly, snow albedo depends on the presence and concentration of impurities; at small wavelengths, even in very small quantities dust and black carbon are efficient absorbers of shortwave radiation (Dumont et al., 2014; Flanner & Zender, 2006; Warren & Wiscombe, 1980).

Locally, the firn layer can be fully removed by melt, runoff, and/or sublimation; glacier ice is then exposed at the surface, which has a much lower albedo than that of snow (0.55 for clean ice without impurities, down to 0.3 or lower for impurity-rich ice). Exposed glacier ice is rare in Antarctica, as it requires ablation (i.e., a negative SSMB) at low temperatures: only approximately 0.8–1.6% of the surface of the AIS consists of bare or so-called "blue" ice area (Winther et al., 2001), where clean (blue-colored) glacier ice is (semi) continuously exposed at the surface. These blue-ice areas appear to be self-sustaining (Ligtenberg et al., 2014), as they promote surface sublimation, surface and subsurface melt (Liston et al., 2005), and/or blowing snow sublimation and erosion (Lenaerts, Lhermitte, et al., 2017), mechanisms by which any accumulated snow is efficiently removed. In Greenland, about 10% of the ice sheet consists of seasonally snow-free ablation area (SSMB < 0). A portion of the ablation area in west Greenland is characterized by a relatively lower albedo (the so-called dark zone), where algae (Stibal et al., 2017), dust (Wientjes et al., 2011), and/or black carbon (van Angelen et al., 2012) lower ice albedo to values of 0.3 or less. Even lower broadband albedo values are found in ice-free regions, that is, rocks that are exposed above the ice sheet surface (nunataks), and seasonally snow-free tundra adjacent to the ice sheet, both of which through convection can generate warm air in summer that enhances surface melting of the neighboring snow and ice (Kingslake et al., 2017).

Turbulent heat exchange between the ice sheet surface and the atmosphere can be either direct (sensible heat flux) or in the form of latent heat (through evaporation/sublimation or condensation/riming). The turbulent heat fluxes of sensible (SHF) and latent (LHF) heat are driven by wind shear and vertical gradients in potential temperature and specific humidity, respectively. When the radiation balance is negative (longwave cooling exceeds shortwave warming, i.e., during the polar winter or at night in summer), the surface temperature will sink below the air temperature, creating a surface-based temperature inversion, a common phenomenon over ice sheets. The inversion can be as large as 30 K over interior East Antarctica (Phillpot & Zillman, 1970) and results in a downward directed SHF (cooling the air and heating the surface). When the surface melts, the surface temperature cannot exceed 0 °C, which means that when the air is warmer than 0 °C, a temperature inversion is again present and SHF is once more directed downward, further promoting melt. In both cases, under these statically stable conditions, wind (shear) is required to generate turbulence in the stably stratified surface layer. In the presence of a surface slope, this wind shear is "automatically" generated by katabatic winds (van den Broeke, van As, et al., 2005; van den Broeke, Smeets, et al., 2009). As a result, SHF can become an important energy source for surface melting in the marginal GrIS, especially when winds are strong over a rough ice surface, further enhancing turbulence intensity (Fausto et al., 2016). Under those conditions, and when the ambient atmosphere is sufficiently warm and moist, LHF can also become a heat source for the surface, in spite of the saturated surface. Under nonmelting conditions, sublimation (negative LHF) can become an important heat sink for the ice sheet snow surface, especially in summer when the sun heats the surface (Kuipers Munneke, Luckman, et al., 2018; Kuipers Munneke, Smeets, et al., 2018).

1.3.5. Firn Characteristics

Liquid water produced at the surface of the ice sheets seldomly runs off directly to the ocean. A thick (up to 130 m; Ligtenberg et al., 2011) layer of firn (compressed, multiyear snow with a density lower than 830 kg/m^3) covers the accumulation zone of the ice sheet (~90% of the total area of the GrIS, ~99% of the AIS). The firn layer acts as a runoff buffer by retaining liquid water from melt and rain, as liquid water percolates into the cold firn column, it can be refrozen and stored. Current estimates indicate that almost half and virtually all of the meltwater produced on the GrIS and AIS, respectively, is refrozen and stored in the firn (van Angelen et al., 2013; Harper et al., 2012; Kuipers Munneke, Picard, et al., 2012; Pfeffer et al., 1990; Steger et al., 2017). Without this refreezing, all meltwater produced at the surface—even if temporarily stored in the firn as liquid water—would run off into the ocean unimpeded, enhancing the AIS and GrIS contribution to sea level rise (van Angelen et al., 2013). During the spring of 2014, before the onset of the melt season, liquid water was discovered at 5- to 20-m depth in the firn layer of southeast GrIS (Forster et al., 2014). This body of perennial liquid water, aptly named the perennial firn aquifer, was later found to extend all the way along the southeastern coast to the southern tip of the ice sheet (Miège et al., 2016), with

smaller aquifers being present along the southwestern and northwestern ice sheet margin. Formation of a firn aquifer requires high summer melt rates and high snowfall rates, to isolate the meltwater from the cold atmosphere so as to prevent refreezing during winter (Kuipers Munneke et al., 2014).

1.3.6. Sea Ice—Ocean Conditions

Oceanic conditions nearby the ice sheets, such as nearby sea-surface temperatures (SST) and sea-ice concentration, are able to modulate ice sheet SMB through various mechanisms. Sea-ice-free and/or warmer surface waters promote evaporation, increasing the moisture content of the atmosphere and enhancing precipitation in nearby areas, including the ice sheet coastal areas (van Lipzig et al., 2002). At the same time, open water also acts to warm the atmosphere through the exchange of sensible heat (Deser et al., 2010). Existing literature, focusing on the Arctic region and the GrIS, suggests a weak effect of Arctic sea ice decline on the recent increase in GrIS surface melting (Liu et al., 2016; Noël et al., 2014; Rennermalm et al., 2009; Stroeve et al., 2017). Alternatively, increasing SST and decreasing sea-ice concentration might also enhance winter snowfall on the GrIS, potentially reducing summer melting through the resulting higher surface albedo (Day et al., 2013). Recent work indicates that similar interactions exist over Antarctica (Kittel et al., 2018; Krinner et al., 2014; Picard et al., 2012). On smaller scales, the generation of open water areas (polynyas) close to the ice sheet margins by strong offshore (katabatic) winds will increase heat and moisture fluxes to the atmosphere. For example, it has been suggested that the springtime opening of the North Water Polynya (in northern Baffin Bay) has triggered early GrIS melt (Stroeve et al., 2017). Large, ocean-forced polynyas regularly develop in the Weddell Sea (Carsey, 1980), impacting regional atmospheric conditions (Weijer et al., 2017). As of yet, little is known about the possible effects of such large polynyas on AIS ice-shelf and ice sheet climate and SMB. Lastly, changing oceanic conditions also indirectly affect ice sheet SMB by regulating large-scale atmospheric circulation (Overland et al., 2012).

2. Methods to Estimate Ice Sheet SMB

Here, we very briefly summarize both traditional and newly emerging techniques for measuring ice sheet SMB. The review by Eisen et al. (2008) presents detailed descriptions of SMB observation methods used in Antarctica, which we briefly summarize.

2.1. Observations

Neglecting effects of horizontal ice flow that advects firn layers with it, at locations where accumulation exceeds ablation (SSMB > 0), a porous firn column is present (Ligtenberg et al., 2011) that is capable of storing meltwater as it percolates into the subsurface, either by refreezing or by capillary forces. If all meltwater is retained, runoff equals zero and SMB equals accumulation, providing the conceptual basis for traditional observations of SMB (e.g., snow stakes and GPR surveys, firn/ice cores); however, sampling must be deep enough to include the retained meltwater and the density of the accumulated material must be determined. In ice sheet ablation zones (SSMB < 0), measurements of surface ablation (using stakes or sonic height rangers) can be directly used to infer the SSMB, because the density of the ablated material (glacier ice) is reasonably well known (830–917 kg/m^3); alternatively, if properly allowing for dynamic effects, repeat satellite and airborne altimetry can be used to assess ablation (Sutterley et al., 2018). The techniques described below use these principles to directly or indirectly measure SMB and/or its components. Because several of the techniques rely on the measurement of height (or volume) change for conversion to mass, we first discuss an important correction for firn density. Another correction, for longitudinal strain, is described in the Glossary.

The compaction of fresh snow into solid ice is a slow process that depends on the firn temperature and overburden pressure (Herron & Langway, 1980). In the accumulation zone, assessment of SSMB in water or ice equivalents requires knowledge of the depth-varying density of the firn column. Density can be measured in situ by weighing a known volume of firn, either in bulk samples from a snow pit or segments of firn cores. These measurements are limited in vertical resolution by the sampling frequency and volume and are prone to measurement error; more recent techniques allow for finer-scale sampling and improved accuracy (Hawley et al., 2008). Such methods include (1) dielectric profiling that links conductivity and permittivity to firn density (Wilhelms, 2005), (2) borehole optical stratigraphy (Hawley & Morris, 2006), (3) measurements of neutron-scattering properties of the firn (Morris & Cooper, 2003), (4) gamma-ray

attenuation (Gerland et al., 1999), and (5) the Snow MicroPen snow penetration instrument (Proksch et al., 2015).

Numerous models of firn densification have been proposed, both steady state (Herron & Langway, 1980; Spencer et al., 2001) and time dependent (Arthern et al., 2010; Arthern & Wingham, 1998; Goujon et al., 2003; Li & Zwally, 2011; Ligtenberg et al., 2011; Simonsen et al., 2013). These models provide estimates of firn density with depth that are particularly useful when detailed in situ density measurements are lacking, for example, in the case of airborne and ground-based radar profiling of isochrones. Next, when converting the surface height change to a fixed anchor point in the firn (e.g., stakes and Global Positioning System [GPS] Interferometric Reflectometry) into SMB, a correction for the firn compaction between the surface and the anchor point must be applied. Finally, the SMB observation needs to be corrected for longitudinal strain (see Glossary), which is based on simple (Dansgaard & Johnsen, 1969; Nye, 1963) to more sophisticated (Huybrechts et al., 2009) ice-flow models.

2.1.1. Stakes

Perhaps the most traditional way to measure SMB is to a place a stake vertically in the firn or ice that protrudes above the surface (Black & Budd, 1964; Dibb & Fahnestock, 2004; Gow, 1965; McConnell et al., 1997). Immediately upon installation, an initial measurement of the distance between the top of the stake and the surface is made. Upon return, this measurement is repeated, and the difference between final and initial reading reflects the relative change in surface height relative to the level where the stake is anchored (units of meters). In the accumulation zone, the height change represents a seasonal snow depth change and requires multiplying with a bulk density (in units kg/m^3) to yield SSMB (in units kg/m^2 or mm w.e. over time, i.e., the measurement interval). In the ablation zone, stakes are used to estimate ice ablation (Braithwaite, 1995; van de Wal et al., 2005), and the observed height decrease is converted to SMB using the density of glacier ice.

Given the high small-scale spatial variability (SSV) of SSMB, especially in the interior dry snow zone, a single stake record does not necessarily represent the SMB of a larger area. For instance, interactions between the stake and the local wind field challenge interpretation of the record. To reduce associated uncertainties and quantify SSV, stakes can be combined into an array or farm (Frezzotti et al., 2005; Kameda et al., 2008) or along a transect (Frezzotti et al., 2007; Minghu et al., 2011). Because stakes require revisiting, these observations are typically limited in space and time, and to easily accessible regions. Stake measurements are not appropriate for SSMB measurements in the percolation zone, where surface meltwater can percolate down into the firn and be retained below the stake base.

2.1.2. Snow Pits

Seasonal differences in snow metamorphism allow for visual distinction of summer and winter snow as observed in snow pits (Benson, 1962). Specifically, the layering sequence of fine-grained winter accumulation and coarse-grained summer accumulation (depth hoar) is preserved within the firn (Alley et al., 1997). Although visual stratigraphic detection of annual layers is sometimes subjective, it is still a frequently used method for determining snow accumulation rates within snow pits and even with ice cores, mainly because it yields rapid results.

2.1.3. Firn/Ice Cores

Firn and ice cores provide SSMB estimates that vary in time span and resolution, depending on the length of the core, the accumulation rate, and the type of dating. The dating techniques rely on the fact that distinctive time markers are preserved within the firn and ice column. Several time markers or even annually resolved layers enable the construction of an SSMB time series.

2.1.3.1. Multidecadal Ice-Core Records

The deposition of volcanic and/or radioactive material over polar ice sheets results in reference horizons that can be used as time markers. Long-term, bulk accumulation rates can be determined by estimating the mass of snow, firn,and/or ice between well-dated horizons, including the surface. The sequence of bomb tests during the mid-1950s and early-1960s left a unique signature of enhanced β-activity that, when detected, provides a well-known tie point for absolute dating of the ice (Picciotto & Wilgain, 1963). Similarly, deposition of volcanic sulfate aerosols provides well-dated reference horizons, and their unique sequences are also well preserved in ice cores (Cole-Dai et al., 2000; Zielinski et al., 1994). The use of reference horizons is most suitable in regions where snow accumulation rates are relatively low, challenging the detection of annual snow layers.

2.1.3.2. Annual Ice-Core Records

Annually resolved SSMB records are useful, as they allow for assessment of the local and global drivers of change when analyzed in combination with atmospheric data (Thomas et al., 2015, 2017). Chemical detection of seasonally varying parameters, such as oxygen/hydrogen-isotopic composition and concentrations of hydrogen peroxide, dust, and/or nonsummer sea salt sulfate, allows for objective determination of annual layers (Herron, 1982; McConnell et al., 2002). When combined with volcanic or radioactive time markers, uncertainty is largely reduced, yielding time series of annual snow accumulation. Several drilling programs have used a multiparameter approach for assessment of accumulation changes over Greenland (Mosley-Thompson et al., 2001) and Antarctica (Kaspari et al., 2004; Oerter et al., 2000).

As with stake measurements, ice cores provide SSMB estimates for a single location, where local SSV due to wind redistribution (e.g., sastrugi) imparts additional noise on the record. If the accumulation rate is sufficiently low, this glaciological noise can overwhelm the large-scale variability. Thus, the common interannual variability between measured and modeled accumulation rates in these low accumulation areas (e.g., East Antarctic Plateau) is often quite small, especially when compared to high accumulation regions (e.g., Antarctic Peninsula, Thomas et al., 2017). Regionally colocated cores are often stacked to minimize the impact of SSV (Banta et al., 2008; Fisher et al., 1985; Frezzotti et al., 2013; McConnell, Mosley-Thompson, et al., 2000).

2.1.4. Ground-Penetrating Radar

Ground- (or ice-) penetrating radar (GPR) is a nondestructive method of mapping the internal stratigraphy of the firn and ice column along a transect. Because radar-derived accumulation measurements capture the spatial variability better than widely spaced point measurements, they provide a more accurate representation of the spatial mean and thus are more appropriate for MB studies (Richardson et al., 1997). Moreover, they sometimes go back in time hundreds of years, enabling quantification of long-term accumulation variability. Three-dimensional mapping of the firn (i.e., in various horizontal directions) also allows us to quantify the impact of SSV on SMB estimation. As for ice cores, GPR analysis relies on the assumption that stratigraphic reference horizons can be dated in either an absolute or relative sense. It relies on the assumption that each radar horizon represents an isochrone, that is, is representative of a single deposition event. In the upper layers of the firn, where ice crystal fabric is relatively constant, and in absence of volcanic ash layers of melt layers that can impact conductivity, stratigraphic horizons in radargrams represent contrasts in dielectric permittivity, which are likely caused by seasonal variations in the physical and chemical properties of the firn (Arcone et al., 2005; Eisen et al., 2008).

Ground-based radar imaging of both near-surface (Anschutz et al., 2007, 2008; Eisen et al., 2005; Frezzotti et al., 2007; Rotschky et al., 2004; Sinisalo et al., 2004; Spikes et al., 2004; Urbini et al., 2008) and deep (Huybrechts et al., 2009; MacGregor et al., 2009; Nereson et al., 2000; Siegert & Payne, 2004; Waddington et al., 2007) internal horizons has provided the basis for calculating recent and historical spatiotemporal snow accumulation rates over Antarctica. In the last decade however, airborne-based GPR has revolutionized observational ice sheet accumulation observations. The Center for Remote Sensing of Ice Sheets began development of several airborne radar systems, capable of surveying to different depths and at varying vertical resolutions, around the year 2000 (Kanagaratnam et al., 2004, 2007). Their continued improvement over the years accelerated in 2009 with the start of NASA Operation IceBridge (OIB) campaigns that are currently scheduled to run through 2019. The Center for Remote Sensing of Ice Sheets (CRESIS) "snow" and "accumulation" radars measure shallow (10 m) to intermediate (100 m) depths at respective vertical resolutions of ~3 and ~40 cm in firn, making them ideal candidates for measuring annual and multiannual accumulation rates (Rodriguez-Morales et al., 2014). Using spatial extrapolation techniques, the relative (i.e., relative to a "background" large-scale SMB value) or absolute SSMB derived from these OIB flight lines can be used to map drainage basin-scale SMB, for instance over the Pine Island and Thwaites glacier catchments (see Glossary, Medley et al., 2013, 2014), and for the GrIS interior (Lewis et al., 2017; Overly et al., 2016) and Southeast (Koenig et al., 2016). Until late 2019, OIB flies annual campaigns over both ice sheets, including extensive portions of the GrIS, West Antarctica, and the Antarctic Peninsula; however, much of this vast archive of data has yet to be analyzed, leaving significant room for future analysis.

Estimation of SSMB from GPR begins with tracking the internal horizons, which is accomplished manually or in a semiautomated approach. Measured or modeled firn depth-density profiles are used to convert the radar measurements of two-way travel time τ (in seconds) to depth d (in meters) via a density-dependent

mixture model (Looyenga, 1965) of dielectric permittivity ε_d ($\boldsymbol{d = c\tau/2\varepsilon_d^{1/2}}$). The spatially varying depths are next converted to water or ice equivalents using the cumulative mass (depth-integrated density) profiles (Medley et al., 2015). To estimate accumulation rates, the relative or absolute ages of the horizons of interest must be determined. Most studies rely on complementary firn or ice-core depth-age relationships along the radar profile to date the tracked horizons (Spikes et al., 2004). Where the vertical resolution of the radar system is sufficiently fine (5–10 cm) relative to the mean annual accumulation (>1 m), recent studies have avoided the need for ancillary ice core data by assuming that adjacent horizons are annually spaced (Medley et al., 2013; Scott et al., 2010). Once adjacent markers have been dated and their relative age difference assessed, accumulation rates are determined by dividing the water or ice-equivalent thicknesses between markers by the age difference.

2.1.5. Automatic Weather Stations

Most automatic weather stations (AWSs) are equipped with an acoustic depth gauge (or sonic altimeter), which measures the vertical distance between the sensor (anchored in or placed on the snow surface at time of deployment) and the surface, which is displaced in time in response to accumulation and ablation. Knowing snow density, this measurement can be converted to an SSMB time series by taking the difference between the actual distance and the initial distance at each time of measurement. Although representing only a single location, and with data quality that can be poor at times during blowing snow or fog conditions, this technique can provide a semicontinuous SSMB record at high (typically hourly) temporal resolution (van den Broeke et al., 2004; Gorodetskaya et al., 2013; Qin et al., 2004).

In addition, in combination with an SEB model (van den Broeke, van As, et al., 2005; van den Broeke, Reijmer, et al., 2005), AWSs can provide in situ estimates of the SEB, which are urgently needed to improve models of the ice sheets and their projections (Trusel et al., 2015). This requires the operation of high-quality instrumentation (Figure 2) (van den Broeke, van As, et al., 2005; van den Broeke, Reijmer, et al., 2005). An SEB model yields the turbulent latent heat flux to quantify sublimation, melt energy for the production rate of liquid water, and the subsurface heat flux, that is, the molecular conduction of heat into/away from the subsurface. The latter heat flux determines refreezing and hence runoff rates in the percolation zone. AWS data are indispensable for validating and calibrating, for example, satellite-derived surface temperature (Reeves Eyre & Zeng, 2017) and melt (Trusel et al., 2012; Trusel et al., 2013). In contrast to Greenland, where melt is significant and even almost continuous during summer at lower elevations (Kuipers Munneke, Luckman, et al., 2018; Kuipers Munneke, Smeets, et al., 2018), melt in Antarctica is often a subtle and intermittent process, requiring accurate observations as melt energy represents the (small) difference of various large energy fluxes (van den Broeke, Bamber, et al., 2009; van den Broeke, König-Langlo, et al., 2009; van den Broeke, Smeets, et al., 2009).

Recent investments have been made in developing a new generation of AWSs, for a multitude of reasons. First, the rapid expansion and high level of international collaboration in polar research implies that several teams of researchers and technicians from all countries and institutes must be capable of easily deploying, maintaining and checking AWSs on glaciers and ice sheets. Second, these activities must be performed as time efficiently as possible, while not compromising the personnel security and long-term reliability of the AWS. And third, the number of batteries of any type involved in transport and AWS operation must be reduced as much as possible to enhance transportation safety, to protect the environment, and to reduce operational costs. An example of a new design AWS that considers these restrictions is the iWS (intelligent Weather Station for polar use; van den Broeke et al., 2013). The iWS unit is much smaller than the previous generation of AWSs but includes all meteorological sensors (except wind speed and radiation, which are installed externally), as well as an ultrasonic height ranger, an electronic compass and inclinometer and a GPS, data storage module, and satellite and Bluetooth connectivity. This new design uses ~95% less energy than AWS of the previous generation, using the latest sensor technology, a small solar panel, and efficient energy usage. The station has been successfully deployed on the GrIS and AIS (Figure 4).

2.1.6. GPS Interferometric Reflectometry

A recent innovative technique uses the reflected signal recorded by GPS antennas to obtain surface height changes within an area surrounding the GPS antenna (Larson et al., 2015; Shean et al., 2017; Siegfried et al., 2017). This technique requires the continuous operation of dual-frequency geodetic GPS receivers. The interference pattern of the combined direct and reflected signals can be directly related to the distance between the antenna phase center and the snow surface; thus, a continuous time series

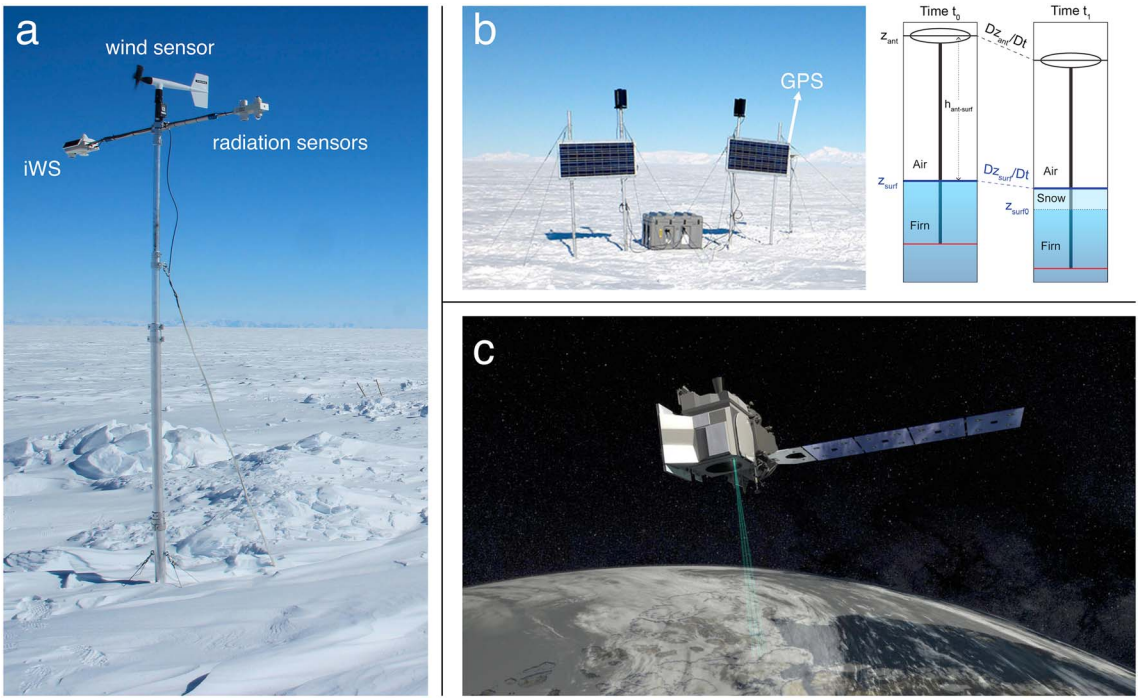

Figure 4. Examples of emerging measurement techniques. (a) iWS installed in high-accumulation area in South-East Greenland (installed in April 2014. Courtesy: Clément Miège, Rutgers University); (b) Using Global Positioning System (GPS; example on the left, courtesy: Matthew Siegfied) reflections to detect surface height changes (Dz_{surf}/Dt in sketch on the right). Right sketch taken from Shean et al. (2017); (c) ICESat-2 laser altimeter, launched in September 2018 (source: icesat2-gsfc.nasa.gov).

of surface height change (relative to the GPS antenna) can be derived in a fashion similar to sonic ranging (see section 2.1.3.2). Height changes can then be converted to SSMB if the density of the accumulated snow is known.

By adjusting the height of the antenna, the total area over which the reflected signal is returned to the GPS antenna is adjusted, allowing for precise tuning of the area-integrated height change. The areal-integration of the height change is unique to the GPS interferometry approach and minimizes the impact of local-scale SSV, which makes for an ideal comparison of SSMB with atmospheric models (Siegfried et al., 2017). With an average accuracy of about 1 cm (Larson et al., 2015), the technique provides accumulated height change at daily resolution, a significant resolution improvement over the more traditional SSMB methods, potentially identifying snow accumulation at the event level.

2.1.7. Cosmic Ray Neutron-Sensing Device

Cosmic ray neutron detection for snowpack monitoring has a long history within the field of snow science, yet until recently has been underutilized in ice sheet studies. Cosmic ray neutrons are formed through collision of the high-energy radiation (cosmic rays) with the mass of our Earth's atmosphere, creating the secondary neutrons that then rain down toward the surface. Water attenuates the cosmic ray neutrons, prohibiting transmission to the sensing device. Therefore, the mass of snow that accumulates on top of the device directly determines the attenuation of cosmic-ray neutrons reaching the device. This concept was already proven successful decades ago in alpine conditions (Kodama, 1980; Kodama et al., 1975; Kodama et al., 1979). Recently, Howat et al. (2018) investigated the applicability of a commercially available cosmic ray neutron-sensing device for measuring SSMB on the GrIS. The device records hourly neutron counts; however, the surface flux of cosmic ray neutrons is not constant, and corrections are applied based on the variations in the incoming cosmic ray flux and barometric pressure (Howat et al., 2018). The former is assessed through placement of a secondary neutron-sensing device above the surface.

Howat et al. (2018) summarize several advantages to using a neutron-sensing device including the following: (1) It provides direct mass change measurements that integrate all the components of

SSMB without the need for ancillary density measurements to convert from volume to mass; (2) measurements are integrated over a larger area (tens of square meters), reducing the impact of SSV in a similar fashion to the GPS-Interferometric Reflectometry technique, although the spatial scale of integration is less quantifiable; (3) reduction of power constraints relative to comparable instruments, such as active radars, as the passive sensor has very low power consumption, which is critical in polar winter; (4) measurements are frequent (approximately hourly) and continuous, providing measurements at the event scale; and finally (5) the device is sensitive enough to survey the lowest accumulation areas, such as the interior of the ice sheets, where frequent redistribution and drifting making stratigraphic interpretation difficult.

Some limitations of the technique include (1) the precision of accumulated snow-mass measurements decreases with burial as the neutron count decreases, suggesting that its use over long periods of time or in high-accumulation areas might be limited; (2) its applicability in the percolation zone is unknown, as meltwater percolation and refreezing might impact the sensor; and (3) a better understanding between the relationship with drifting snow at the surface and observed mass change is required for proper validation with independent observations.

2.1.8. Airborne and Satellite Altimetry

Airborne and spaceborne observations of ice sheet height changes are comprised of several signals: short- and long-term variability in (1) SSMB, (2) firn compaction rates, (3) ice dynamical imbalance, (4) solid earth deformation, and (5) basal melt rate and other oceanic signals such as tides and sea level change (over floating ice shelves only; Pritchard et al., 2012). They differ from traditional ground-based height measurements in that they are relative to a reference ellipsoid (e.g., WGS-84 for ICESat-2) rather than an anchor point at or just below the surface. Thus, without ancillary information, it is impossible to isolate the contribution to integrated height change of these individual components, some of which are not even associated with a change in ice mass.

Altimetry-based MB studies often utilize models of SMB and firn compaction to effectively remove the height change signal due to surface process in order to assess the ice dynamical change (Csatho et al., 2014; Shepherd et al., 2012, 2018; Zwally et al., 2005; Zwally et al., 2015). Progress toward measuring ablation from airborne altimetry, however, indicates that under specific circumstances SSMB can be estimated, providing excellent validation data for SMB models. For instance, Sutterley et al. (2018) suggested that the isolation of the height signal due to SSMB is possible by restricting focus to regions where (1) no firn column exists (i.e., the ablation zone) as defined by regional atmospheric climate model (RCM) output and (2) the underlying ice flow velocities fall under a reasonable threshold (<100 m/year), minimizing the impact of ice dynamics. After the rates of uplift due to Glacial Isostatic Adjustment (GIA) are removed, the remaining height change signal can be attributed to ice ablation (Sutterley et al., 2018).

Existence of long-term records of both radar and laser altimetry combined with newly emerging models of SMB indicates that future altimetry studies can provide insight into modeled SMB. Although altimetry studies are limited in their ability to directly measure SMB, they have great potential to provide additional insight in distinguishing between the abilities of various SMB models to represent Greenland and Antarctic SMB, as evidenced by prior studies that related observed height change to precipitation (Davis et al., 2005; McConnell, Arthern, et al., 2000; McConnell, Mosley-Thompson, et al., 2000), and ultimately to modeled height change due to surface processes (Kuipers Munneke et al., 2015; Ligtenberg et al., 2011). The latter studies indicate that height changes due to SMB can dominate the entire height-change signal. Recent intercomparisons of ice sheet MB methodologies (Shepherd et al., 2012, 2018) indicate that there is common overlap in the results between altimetry and other independent techniques (i.e., gravimetry; see section 2.1.9).

The initial framework laid out by Sutterley et al. (2014) utilized IceBridge and ICESat data that provide only intermittent snapshots in time and space, yet due to the paucity of field observations, still provided several orders of magnitude more observations of height change. Further refinement of the spatial and temporal resolution is expected with NASA's ongoing ICESat-2 laser altimetry mission (Figure 4), launched in September 2018, that provides complete ice sheet-wide height change at the seasonal scale (91-day repeat cycle; Markus et al., 2017).

Due to their large (several tens of kilometers) footprint, conventional radar altimeters struggled to generate precise height change measurements on the more steeply sloping regions of the ice sheet, including the ablation zone in Greenland (Brenner et al., 2007). CryoSat-2, launched in 2010, overcomes this problem by operating in a synthetic aperture interferometric mode over the margins of the ice sheets. In this mode, Doppler processing is applied to a burst of short (17.8-kHz frequency) radar pulses, which reduces the along-track (i.e., along the line of flight) resolution to approximately 400 m. Since the satellite is equipped with two receiving antennas, the across-track location of the echo can also be determined, based on phase difference of the received signal in the two antennas (Wingham et al., 2006). Unlike laser altimetry, radar altimetry is not affected by cloud cover, which allows continuous sampling of the ice sheets. The downside, however, is that at the Ku-band (13.575-GHz frequency) used by CryoSat-2, the radar wave may penetrate several meters into the firn, challenging the interpretation of the reflected waveform, depending on vertically changing firn properties. An exemplar of this point was the extreme melt event during the 2012 summer in the interior of Greenland. Prior to the melt, part of the radar signal was reflected from within the top firn layer. The ice layer created by surface meltwater refreezing subsequently acted as an efficient reflector, resulting in an apparent jump of the surface of almost 50 cm in the CryoSat-2 observations (Nilsson et al., 2015). Although this is an extreme case, slow changes in the structure of the firn layer may likewise bias altimetry-derived surface height changes; reducing these effects is an active field of research. On the other hand, this limitation can also be exploited to estimate the firn structure by combining radar observations, firn models, and microwave radiative transfer models (e.g., Adodo et al., 2018). The CryoSat-2 mission team is considering adjusting the satellite's orbit in the early 2020s so that its ground tracks will overlap once every ~2 days with those of ICESat-2. Since the penetration depth of laser in firn is an order of magnitude smaller than that of radar waves (Rémy & Parouty, 2009), this is expected to provide a wealth of information on the firn structure and how it changes in time.

2.1.9. Gravity Recovery and Climate Experiment and GRACE-Follow on

Since its launch in April 2002, the Gravity Recovery and Climate experiment (GRACE) has provided a novel tool for directly measuring mass variations of the ice sheets and other glaciated regions. The mission, which ended mid-2017, consisted of two identical satellites, circling the Earth in the same near polar orbital plane, but separated by a distance of about 200 km. Because of this separation, local variations in the gravitational field of the Earth affected the orbits of the two satellites slightly differently, hence changing the intersatellite range. This range and its rate of change were measured continuously at micrometer accuracy using a microwave radar link between the two satellites. The Earth's gravitation field and its temporal variations could be mapped at monthly—or even shorter—time intervals, and at a spatial resolution of 300–400 km (see Wouters et al., 2014, for an extensive introduction to GRACE).

Atmospheric (and partly also oceanic) signals are removed during processing of the GRACE data, so that at annual to decadal time scales, variations in the gravitational field are largely related to redistribution of mass at the Earth's surface and at greater depth (Wahr et al., 1998). Whereas initial studies mainly focused on land hydrology applications, it soon became clear that the GRACE satellites could also provide invaluable information on the state of the ice sheets. Velicogna and Wahr (2005) provided a first estimate of the MB of the GrIS, revealing a mass loss of about 75 Gt/year for 2002–2004. Follow-up studies confirmed this negative trend but reported numbers showed a substantial spread, roughly between 100 and 250 Gt/year (Luthcke et al., 2006; Velicogna & Wahr, 2006; Wouters et al., 2008). These estimates were based on short time spans and were therefore particularly sensitive to interannual variability in SMB, which can vary by several hundreds of Gt between years (Wouters et al., 2013, section 4). Similarly, early studies focusing on the AIS varied by a considerable amount, from −109 Gt/year for 2002–2007 (Sasgen et al., 2010) to −190 Gt/year for 2002–2008 (Chen et al., 2009). In this case, this was not only due to interannual variability in SMB but also because of differences in the correction for GIA, the ongoing redistribution of mantle material in response to past changes in ice loading. Such internal mass movement likewise induces a gravitational signal for which a correction must be applied, but early GIA models differed by several hundreds of Gt/year, depending on the Earth parameters used (Barletta et al., 2008). As longer data records became available and GIA estimates improved, trend estimates finally converged (See Figure 13 and section 4, which provide an update of Wouters et al., 2013).

The drawback of the GRACE observations is that they represent the total mass change. Validation of SMB models by means of GRACE data therefore always requires auxiliary data to account for solid ice

discharge. Van den Broeke, Bamber, et al. (2009) combined cumulative anomalies of SMB from the RACMO2 model and observed ice discharge ("input-output" method), and found a close match between those and the GRACE-derived GrIS MB record. This successful validation of the modeled SMB allowed for further partitioning of the 2000–2008 mass loss into SMB decrease and D increase, which was repeated and refined in follow-up studies (Enderlin et al., 2014; van den Broeke et al., 2016). Similarly good agreement was found at regional scales (Sasgen et al., 2012; Velicogna et al., 2014), except for across the northwest and southeast of the GrIS, with the latter attributed to a bias in the (now superseded) RACMO2.0 climate model (Noël et al., 2018). Considering shorter time scales, Vizcaíno et al. (2013) compared the GRACE data to validate the mean seasonal cycle in SMB in the Community Earth System Model and demonstrated a good agreement in both the overall timing and amplitude. Schlegel et al. (2016) used GRACE data to validate a historical run of the Ice Sheet System Model forced with SMB anomalies from three different regional climate models. Again, a good agreement was found in the seasonal cycle, this time also on regional scales, although discrepancies remained in the northwest and southeast. The overall good agreement was largely attributed to the direct contribution of the SMB forcing. Long-term trends, however, were significantly underestimated by the model, partly due to missing physical processes such as ice-ocean interactions.

In Antarctica, similarly good agreement on seasonal time scales was found between GRACE observations and SMB data from the RACMO2 model (van Wessem et al., 2014). In regions with large interannual variability in SMB and a relatively constant ice flux, the combination of GRACE with regional climate model output has been shown to be instrumental in revealing large scale anomalous SMB signals, such as the 2009–2011 extreme snowfall episode in Dronning Maud Land and SMB-driven mass loss events in Wilkes Land (see Glossary; Boening et al., 2012; Lenaerts et al., 2013; Mohajerani et al., 2018; Velicogna et al., 2014). Reconciling decadal mass loss, however, still remains challenging; in the latest Ice sheet Mass Balance Intercomparison Exercise 2 (Shepherd et al., 2018), budget closure between the input-output method and GRACE estimates was not obtained for Antarctica, with the exception of West Antarctica where mass loss is dominated by dynamic discharge (Shepherd et al., 2018). Remaining uncertainties in the GIA correction for GRACE (Martín-Español, King, et al., 2016; Martín-Español, Zammit-Mangion, et al., 2016), and in the estimates of ice discharge, to date limit the direct validation of secular SMB changes, in particular on regional scales. An interesting recent development, and the fusion of the use of altimetry and gravimetry, is the combination of several observational (altimetry, GRACE, GPS, and ice flow velocities) and model-based (SMB and firn compaction) data sets in a Bayesian framework, which allows the simultaneous estimation of SMB anomalies, ice dynamics, and GIA (Martín-Español, King, et al., 2016; Martín-Español, Zammit-Mangion, et al., 2016).

There are many factors that limit the application of GRACE to estimating or validating SMB fluctuations on shorter, monthly time scales. Shortcomings in the atmospheric and ocean models used in the processing of the GRACE data may cause significant errors in the GRACE derived time series. This is particularly true for Antarctica, where the models are rather poorly constrained and monthly errors can exceed 10 Gt (Hardy et al., 2017). Also, instrumental noise and the predominant sampling of the gravity field along the north-south direction (defined by the satellites' orbit) introduces additional high-frequency noise.

A follow-on mission (GRACE-FO) was launched on 22 May 2018. These satellites are a carbon copy of their predecessors but carry an experimental laser instrument in addition to the microwave ranging system to track the changes in distance between the satellites. This is expected to reduce the instrumental noise by some 20% (Flechtner et al., 2016). The spatial resolution of the observations will remain about the same (300–400 km) and hence will still not allow the isolation of local signals or the separation of signals occurring on the main ice sheet from those in its periphery (e.g., tundra or detached glaciers). To overcome these limitations requires a redesign of the mission concept, for example, with multiple satellite pairs flying in different orbits (Pail et al., 2015). Concept studies and funding negotiations are currently being carried out, and it is envisaged that such a mission will be launched in the mid-2020s, allowing a second leap forward in our understanding of the state of the ice sheets.

2.1.10. Precipitation Radar (CloudSat, MRR)

Recently, spaceborne, and ground-based precipitation radars have been used to estimate snowfall rates over the AIS (e.g., Boening et al., 2012; Palerme et al., 2014; Souverijns et al., 2018), where snowfall is by far the largest contributor to SMB. This technique is based on a relation between radar backscatter (Z) and snowfall

rate (S), the Z/S relation, which is determined using a priori estimates of snow particle size distribution, microphysical and scattering properties, all of which are spatially and temporally variable over the ice sheet (Wood et al., 2014). Since the radar systems used are initially designed to measure rainfall, dedicated algorithms had to be developed to enable snow particle detection (e.g., Gorodetskaya, van Lipzig, et al., 2014; Gorodetskaya, Tsukernik, et al., 2014; Kneifel et al., 2011). Snowfall rates derived by spaceborne radar originate from a cloud profiling radar aboard NASA's CloudSat (part of the A-Train constellation), and associated 2C-SNOW-PROFILE product (e.g., Palerme et al., 2014). This product shows a realistic snowfall climatology in comparison with ERA-Interim reanalysis but is not able to detect individual snowfall events (Souverijns et al., 2018) because of its sparse spatial coverage (as it covers repeated tracks that are spaced tens of kilometers apart) and poor temporal sampling (revisit time of 2–4 days).

2.2. Modeling Tools

Eisen et al. (2008) showed that AIS SMB maps based on guided interpolation of in situ SMB observations fail to reproduce the high-accumulation marginal zones of the ice sheet, as well as the coastal and inland blue ice areas, the only regions of the AIS (~1.7% coverage), where SMB is negative (Hui et al., 2014). For Greenland, the same is true for the wet southeastern ice sheet, which is almost devoid of observations yet home to the recently discovered perennial firn aquifers (Forster et al., 2014). That implies that we rely on modeling tools to reveal SMB in these areas. In this section we review traditional modeling techniques and discuss the recent developments in modeling SMB over ice sheets.

2.2.1. Statistical Downscaling

The lack of in situ observations in climatologically key areas in combination with insufficient resolution of SMB models has long hampered accurate ice sheet SMB estimates. Until the early 2000s, most estimates of ice sheet SMB were based either on idealized MB schemes or snowpack models using input from atmospheric general circulation models (GCMs; see Glossary) and/or atmospheric reanalysis (see Glossary) products, such as ERA-40 and ERA-Interim from the European Centre for Medium-Range Weather Forecasts (ECMWF). Hanna and Valdes (2001) and Hanna et al. (2002) assessed the quality of ERA-40 to determine the SMB of the GrIS. Bugnion and Stone (2002) used a snowpack model driven by ECMWF analyses to estimate GrIS SMB. Hanna et al. (2005) used ERA-40 in combination with a meltwater retention model (Janssens & Huybrechts, 2000) to retrieve annual accumulation, runoff, and SMB on a 5 × 5 km grid for the GrIS for 1958–2003. Bougamont et al. (2005) presented a SMB model for the GrIS for use in GCMs and tested it using ERA-40.

This statistical downscaling of the relatively coarse-gridded GCM fields, employing a typical 100- to 150-km resolution, to a scale that is required to the narrow GrIS ablation zone (tens of km) where most of the ablation occurs, or to narrow valleys in the AIS where precipitation gradients are largest, is a highly uncertain approach given the complex dynamics of the ice sheet atmospheric boundary layer (Denby et al., 2002) and the great variability in surface characteristics (albedo, roughness, etc.; Smeets & van den Broeke, 2008). Another shortcoming of many of the above methods is the simplified treatment of the SEB, using, for example, degree-day factors (see Glossary).

2.2.2. Dynamical Downscaling (RCM)

An approach that circumvents these problems is dynamical downscaling, that is, to use a high-resolution regional (atmospheric) climate model (RCM; see Glossary) forced at its boundaries with GCM or reanalysis data. This ensures a sufficiently high resolution over the ice sheet as well as an explicit, physically realistic calculation of all SMB components. A full interaction between the snow/ice surface and the atmosphere is achieved by coupling a realistic snow model to the atmosphere module. Almost two decades ago, regional climate models started to be used to hindcast the SMB of the AIS (Bromwich et al., 2004; van de Berg et al., 2006; Wacker et al., 2009) and GrIS (Box et al., 2004; Cassano et al., 2001; Dethloff et al., 2002; Fettweis et al., 2005). These studies have added significantly to our understanding of ice sheet SMB variability and the present-day contribution of the AIS and GrIS to global sea level change (van den Broeke et al., 2011), as well as offering insights into the role of large-scale circulation variability on the SMB of the GrIS (Fettweis et al., 2013) and the AIS (Marshall et al., 2017). The latest versions of these specialized RCMs show a high skill in simulating the contemporary SMB of the AIS (Agosta et al., 2018; van Wessem et al., 2018) and GrIS (Fettweis et al., 2017; Lucas-Picher et al., 2012; Noël et al., 2018), although important regional discrepancies remain (Hermann et al., 2018). RCMs can also be used in forecasting mode (i.e., driven by

atmospheric fields from a global weather forecasting model) for operational purposes, mainly for fieldwork planning. The Antarctic Mesoscale Prediction System (Bromwich et al., 2003; Bromwich et al., 2005; Powers et al., 2003, 2012) uses the Weather Research and Forecasting RCM with polar modification to provide a continuous 5-day forecast of Antarctic weather conditions, while also providing an archive to study past weather phenomena (Nigro et al., 2012; Speirs et al., 2010; Steinhoff et al., 2008; Wille et al., 2014).

2.2.3. Improving Existing RCMs

Recently, several SMB processes not previously included have been added to address remaining RCM caveats in simulating the SMB of the AIS and GrIS. These include drifting snow physics (Gallée et al., 2013; Lenaerts, van den Broeke, van Angelen, et al., 2012; Lenaerts, van den Broeke, van de Berg, et al., 2012; Lenaerts, van den Broeke, Déry, et al., 2012; Lenaerts, van den Broeke, Scarchilli, et al., 2012), sublimation of falling snow (Grazioli et al., 2017), and resolving the all-important albedo of snow and ice into multiple spectral bands (van Dalum et al., 2018). Further desired refinements have been identified, such as bio-albedo paramaterizations for the GrIS (Stibal et al., 2017; van den Broeke et al., 2017), representation of low-albedo/high-melt areas such as nunataks and blue ice areas in Antarctica (Lenaerts, Lhermitte, et al., 2017; Lenaerts, Ligtenberg, et al., 2017; Lenaerts, van Tricht, et al., 2017), and the horizontal meltwater routing in snow and firn (Bell et al., 2017; Kingslake et al., 2017).

2.2.4. Earth System Models (ESMs)

The great advantage of using ESMs (see Glossary) to simulate ice sheet SMB is the use of consistent physics across the globe, the possibility of interactive coupling of the atmosphere to the ocean, sea ice and ice sheets, and the relative simplicity of performing ensemble runs for parameter uncertainty studies or assessing the uncertainty in future climate projections (e.g., Kay et al., 2014). Glimpsing into the future with further increases in available computing resources, it is safe to say that at some point in time, RCMs will become redundant and ESMs will be the modeling tools of choice to simulate contemporary and predict future ice sheet SMB. However, most state-of-the-art ESMs suffer from two issues that currently preclude them from simulating a realistic ice sheet SMB. First, most ESMs do not include a sophisticated snow model that is required to represent snow processes and their interaction with the atmosphere. Second, typical ESM resolutions in the most recent Climate Model Intercomparison Project (Eyring et al., 2016; the results of which being released in 2019) of ~1 latitudinal degree are insufficient to resolve properly the SMB gradients along ice sheet margins. Recent work has focused on resolving both issues. To remedy the first issue, snow models in ESMs, typically designed to simulate seasonal snow (Krinner et al., 2018), have been progressively refined and tailored for application over the ice sheets (Cullather et al., 2014; van Kampenhout et al., 2017). To increase horizontal resolution, the pioneering study of Krinner and Genthon (1997) used a stretched-grid GCM to study the Antarctic climate and MB, at the time resulting in a typical resolution of 100–150 km. More recently, attempts have been made to apply ESMs at resolutions typical for RCMs. In particular, the potential of using variable-resolution in ESMs (Rhoades et al., 2015) to improve the representation of ice sheet SMB is currently being tested for the GrIS (van Kampenhout et al., 2018); using fixed, nested grids over the region of interest with resolutions up to 28 km, the regionalization added a factor 4 to the computational load. Additional ongoing ESM developments to improve ice sheet SMB, in line with those for RCMs, are focusing on remedying the high-latitude atmospheric biases, such as precipitation (Noël et al., 2015), surface based temperature inversion strength and resulting stability (Vignon et al., 2018), and clouds and their radiative effects (van Wessem et al., 2018).

2.2.5. New Atmospheric Reanalysis Products

Until recently, atmospheric reanalyses (see Glossary) shared many disadvantages with ESMs, that is, the absence of a sophisticated snow/firn model and low resolution. Moreover, (1) the relative scarcity of meteorological observations over the polar regions in general, and over ice sheets in particular, to assimilate in the reanalyses, and (2) the optimization of atmospheric parameterizations to perform well in midlatitude conditions, led to substantial biases in, for example, ice sheet clouds and radiation (Lenaerts, Lhermitte, et al., 2017; Lenaerts, Ligtenberg, et al., 2017; Lenaerts, van Tricht, et al., 2017; Miller et al., 2018), precipitation (Bromwich et al., 1998, 2012; Chen et al., 2011; Medley et al., 2013; Nicolas & Bromwich, 2011), (near-)surface temperature (Fréville et al., 2014; Jones & Lister, 2015; Lindsay et al., 2014; Screen & Simmonds, 2011), and turbulent heat exchange (Miller et al., 2018). Newly emerging reanalysis products will likely improve on many of these issues. For example, ECMWF's new reanalysis product ERA-5 combines unparalleled horizontal resolution (0.25°) with refined atmospheric physics and a revised snow scheme (Dutra et al., 2010).

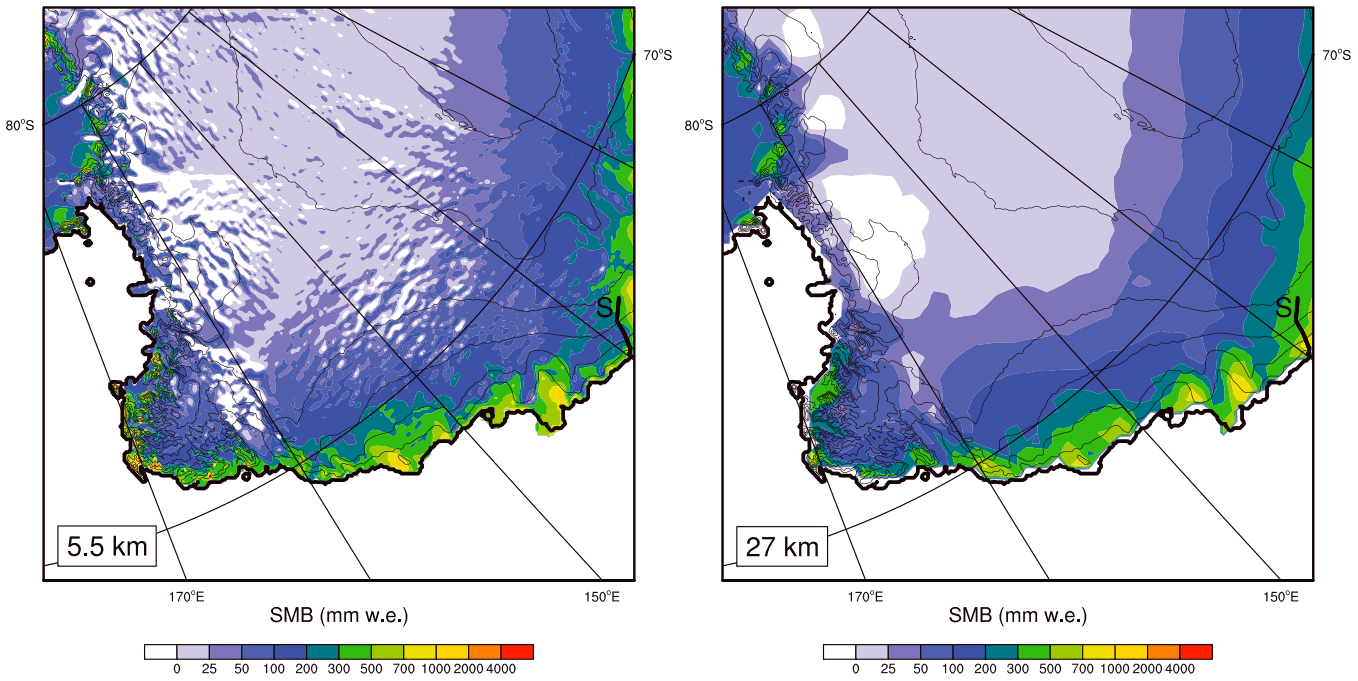

Figure 5. Surface mass balance in 2009 (mm w.e.) in RACMO2 at 5.5-km resolution (left) and at 27 km (right). Source: Lenaerts, van den Broeke, Scarchilli, et al. (2012). Sublimation-driven blue ice areas (in white, SMB < 0) are much more prevalent in the higher-resolution product.

2.2.6. Further Downscaling

Despite the recent exciting developments of RCMs and ESMs, dedicated models will always be required to simulate processes at the smallest scales (5 km and smaller). Multiple studies have shown that increasing the horizontal model resolution, either by dynamical and/or statistical downscaling, can significantly improve the representation of ice sheet SMB. This can be applied to the full range of models, for example, ESMs (Vizcaino, 2014), RCMs, large eddy simulations, and direct numerical simulations. For the GrIS, it has been shown that further statistical downscaling, for example, using elevation dependency, from the current state-of-the-art RCM resolution of ~5 to 1 km, remains necessary to properly resolve melt and runoff from low-lying tongues of the narrow outlet glaciers (Noël et al., 2018). This technique also enables the construction of high-resolution SMB fields over smaller ice masses, such as Greenland's peripheral ice caps (Noël et al., 2017). Another way to enhance RCM resolution is multiple nesting, in which one or more small spatial domains with higher horizontal grid resolution are embedded in a large spatial domain. For the AIS, double-nesting has been successfully applied to RACMO2.3, effectively enhancing resolution from 27 to 5.5 km, for the Antarctic Peninsula (van Wessem et al., 2016), Adélie Land, where the use of a higher resolution revealed sublimation-driven blue ice areas (Lenaerts, van den Broeke, van Angelen, et al., 2012; Lenaerts, van den Broeke, van de Berg, et al., 2012; Lenaerts, van den Broeke, Déry, et al., 2012; Lenaerts, van den Broeke, Scarchilli, et al., 2012, Figure 5), West Antarctica (Lenaerts, Ligtenberg, et al., 2017), and Dronning Maud Land (Lenaerts, Lhermitte, et al., 2017; Lenaerts et al., 2014). Further nesting is possible but requires computationally expensive, nonhydrostatic models (e.g., Mottram et al., 2017). An emerging approach for modeling interior ice sheet SMB at subkilometer resolution consists of employing sophisticated snow models that can resolve small-scale redistribution patterns resulting from blowing snow. These models are typically forced by atmospheric forcing that is statistically downscaled to the snow model resolution (e.g., Groot Zwaaftink et al., 2013).

3. Spatial Variability of Ice Sheet SMB

3.1. Ice Sheet-Wide Scale

Observational data sets are limited to a point-scale to regional-scale estimate of SMB, so we rely on RCMs to provide a continuous and gridded product of SMB for the full ice sheet. Here we use the output of the

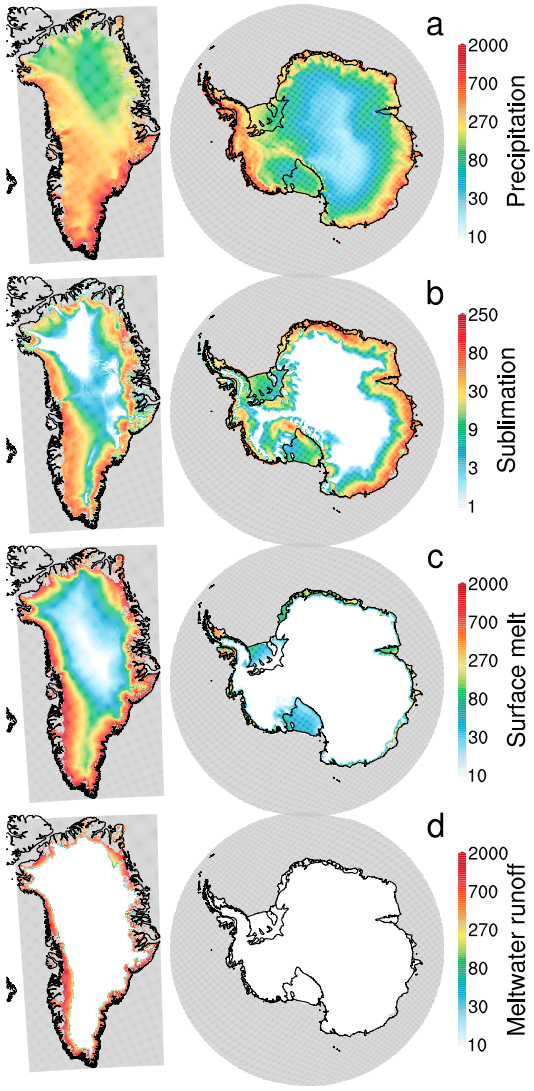

Figure 6. Annual mean (mm w.e./year, 1980–2015) surface mass balance (SMB) components from RACMO2 on the GrIS (left) and the AIS (right). (a) Precipitation; (b) sublimation (surface + drifting snow); (c) surface melt rate; (d) meltwater runoff.

RACMO2.3p2 (RACMO2 hereafter) model (Noël et al., 2018; van Wessem et al., 2018) to present a side-by-side comparison of spatial distribution of SMB and its components on Greenland and Antarctica. In our analysis, we mostly focus on the period 1980–2015, which is covered by RACMO2 as well as all the reanalysis products that are discussed in sections 4 and 5.

Precipitation varies strongly on ice sheets (Figure 6a). The general pattern is for precipitation to increase from the ice sheet interior to the margins, with values <20 mm w.e./year observed in the East Antarctic ice sheet interior, to >2000 mm w.e./year in the Antarctic Peninsula and southeast Greenland (Koenig et al., 2016; Miège et al., 2013). Due to its higher elevation and colder climate, the interior of the AIS is drier than that of the GrIS, which in the driest part in the northeast still receives about 50 mm w.e./year of precipitation. We find regional precipitation maxima in southwest, west, and northwest Greenland, and in the Amundsen and Bellingshausen coasts in West Antarctica (see Glossary), and locally along the East Antarctic coast, for example, on the windward side of Law Dome (van Ommen et al., 2004, see Glossary). All these regions are characterized by close proximity to the coast at relatively low latitudes, ensuring sufficient moisture supply, and the presence of large-scale, steep topography that is oriented perpendicular to the large-scale atmospheric flow. Low precipitation areas are found not only further away from the coast on the elevated inland ice sheet but also in coastal regions leeward of topography, for example, in the eastern Antarctic Peninsula, or west of Law Dome; owing to the foehn effect, these areas receive an order of magnitude less precipitation than the windward sides. Precipitation on ice sheets mainly falls as snow, rainfall being limited to the northernmost Antarctic ice shelves and lowermost (<500 m above sea level [a.s.l.]) areas of the GrIS. Most of the rain (not shown) falls in coastal south Greenland, where it amounts to approximately 10–20% of the total annual precipitation.

Total sublimation, defined as the sum of surface sublimation and drifting snow sublimation, is small (or even negative—implying riming) over the ice sheet interiors (Figure 6b). The highest sublimation rates (>50 mm w.e./year) are found in the escarpment zones, where strong katabatic winds and low near-surface relative humidity promote sublimation. Surface sublimation is most active in the GrIS ablation zone (outside of the melting season) and on low-lying Antarctic blue ice areas and ice shelves in summer, where absorption of solar radiation results in relatively high surface temperatures, enhancing near-surface vertical specific humidity gradients.

Surface melt rates over the GrIS are an order of magnitude greater than over the AIS (Figure 6c). Even the highest areas of Greenland (>3,000 m a.s.l.), experience surface melting in summer, for example in 2012, although that only occurs every few centuries (Nghiem et al., 2012). Melt rates exceed 2,000 mm w.e./year in the marginal ice sheet in the south and southwest and are between 1,000 and 2,000 mm w.e. in the northern ablation areas. In contrast, the vast majority of the grounded AIS does not experience any surface melting. The highest AIS melt rates (>400 mm w.e./year) are found on Antarctic Peninsula ice shelves (Larsen C, Wilkins, and George VI; see Glossary), while many of the smaller ice shelves fringing the coast of West and East Antarctica experience 50–200 mm w.e./year of melt. The large, southerly Ross and Ronne-Filchner Ice Shelves typically have melt amounts less than 100 mm w.e./year.

Runoff from the GrIS is spatially constrained to a narrow zone along the margins of the ice sheet (Figure 6d). High runoff rates (500–2,000 mm w.e./year) are found in the ablation zones below 1,500–2,000 m a.s.l., where there is no firn layer (only the winter snow layer) in which melt water can refreeze locally

(Figure 1). Other ways by which meltwater runoff to the ocean is delayed is by supraglacial (lakes) and englacial or subglacial storage (Chu, 2013; Palmer et al., 2013). Over Antarctica, nearly all the melt water that is produced at the surface refreezes in the firn, and runoff is deemed negligible as an ice sheet integrated mass loss term (Lenaerts, van den Broeke, van de Berg, et al., 2012). Nevertheless, runoff can be significant locally: Field and remote sensing studies indicate that extensive hydrological systems exist locally on Antarctic ice shelves (Bell et al., 2017) and that meltwater storage inside Antarctic ice shelves is more extensive than previously assumed (Lenaerts, Lhermitte, et al., 2017).

Snow divergence/convergence resulting from drifting snow transport leads to redistribution of accumulated snow through the interaction of surface topography and wind patterns. This leads to blowing snow erosion in exposed, windy areas and deposition in sheltered, calmer locations (Figure 5). Although a significant component on the local scale (see below), it is commonly believed that blowing snow redistribution does not significantly contribute to ice sheet-integrated SMB (Lenaerts, van den Broeke, van de Berg, et al., 2012; Palm et al., 2011, 2017). The net effect of erosion and deposition largely cancels out if a large area is considered, and it is assumed that most of the blowing snow volume sublimates along the way (Palm et al., 2017).

The above analysis is based on output of an RCM (RACMO2), which provides well-evaluated, high-resolution, gridded, and temporally continuous estimates of each of the individual SMB components on both ice sheets (1979 onward for AIS and 1958 onward for GrIS). Potentially alternative products for mapping ice sheet SMB are atmospheric reanalyses. However, as discussed in section 2.2.1, these models often lack a dedicated snow model to properly represent the liquid water balance (Figure 2; see Glossary) and snow and ice albedo. The only two SMB components that can be compared amongst different reanalysis products are precipitation and evaporation (sublimation), the difference of which is commonly known as P−E (precipitation minus evaporation, or accumulation, assuming that sublimation equals evaporation). Figure 7 shows that the 1980–2015 mean P−E patterns (supplied as supplementary data sets to this paper) are broadly consistent among the different reanalyses (MERRA-2, ERA-Interim, and CFSR) and regional climate models (RACMO2, MARv3). However, a few differences stand out:

1. the higher spatial detail in regional climate models (RACMO2 and MARv3 at 1- to 35-km resolution) relative to the lower resolution products (MERRA-2 at 0.5° × 0.625° resolution, ERA-Interim at 0.75° resolution, and CFSR at 0.5° resolution), which is especially evident on the GrIS in RACMO2.;
2. The generally lower P−E values in ERA-Interim, and to a lesser degree CFSR, relative to the other products. This is especially evident in interior Antarctica (where ERA-Interim P−E is <10 mm w.e./year in a very large region), but also over northern Greenland. Whereas ERA-Interim is generally considered to be the best performing reanalysis product over high-latitude regions, especially Antarctica (Nicolas & Bromwich, 2011), recent work has highlighted that the low P−E values in ERA-Interim are unrealistic (van Wessem et al., 2014) and that MERRA-2 shows improved agreement with a selection of Antarctic ice cores (Medley & Thomas, 2019).

3.2. Regional Variability (10–100 km)

The large spatial gradients in all SSMB components near the ice sheet periphery, in particular precipitation (AIS and GrIS) and runoff (GrIS only), lead to extreme SSMB gradients. In situ observations in these areas are therefore most useful if performed along transects. An example in Figure 8 shows a 20-year semicontinuous record of SMB (derived from stakes) along the K-transect in Southwest Greenland (which is currently still updated). The multiannual mean SSMB increases from −4 m w.e./year in the low ablation zone, near the glacier terminus at approximately 350 m a.s.l., to near zero (i.e., close to the equilibrium line) at around 1,500 m a.s.l., over a horizontal distance of only ~150 km. These large spatial SSMB gradients require the use of high horizontal resolution models and/or postprocessing of the model output using statistical downscaling methods (see section 2.2.6).

3.3. Subgrid Scale Variability (<10 km)

On the local scale (distance of meters to kilometers), spatial SSMB variability is largely governed by small-scale variations in the local surface topography and the associated patterns of snow accumulation (during snowfall), blowing snow redistribution (during windy conditions), and heterogeneous snow and ice melting. Consequently, SSMB can vary by up to an order of magnitude over relatively short distances. Emerging

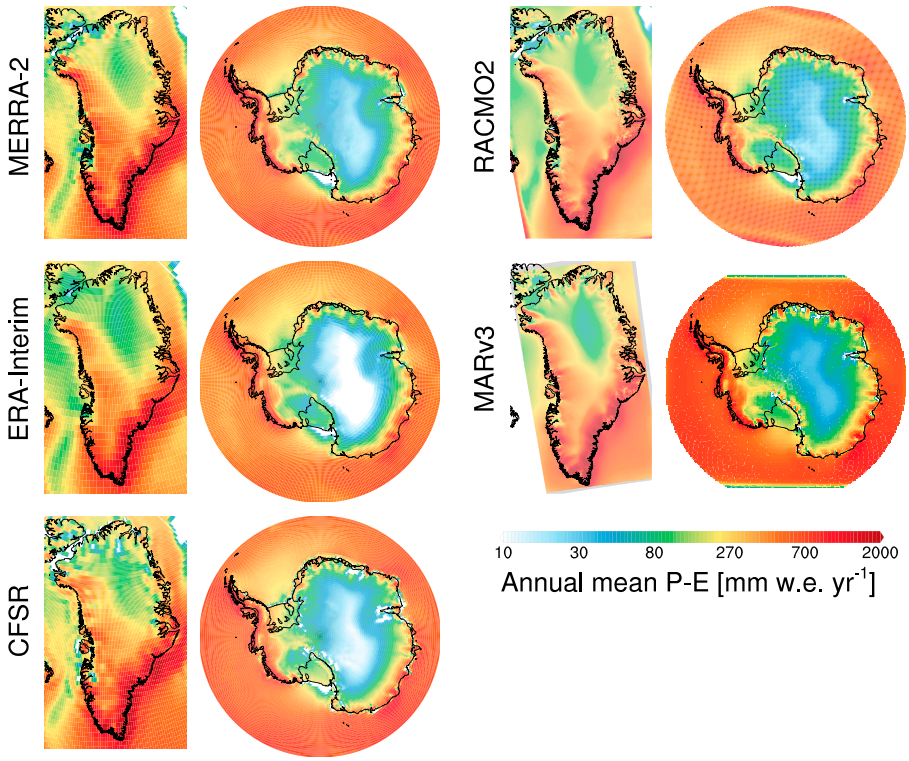

Figure 7. Annual mean P−E (mm w.e./year, 1980–2015) surface mass balance components from RACMO2 on the GrIS (left) and the AIS (right) according to atmospheric reanalyses (MERRA-2, ERA-Interim, CFSR), and regional atmospheric climate models (RACMO2 and MARv3).

SSMB measuring techniques, such as snow radar, and laser and SAR radar altimetry (see section 2.1) enable the mapping of these large gradients. An example is shown in Figure 9, which shows a snow radar transect on Pine Island Glacier (West Antarctica; see Figure 16) from the 2016 OIB airborne mission. The radar profile shows very large horizontal variability in the depth of the reflectors, indicative of large SSMB gradients.

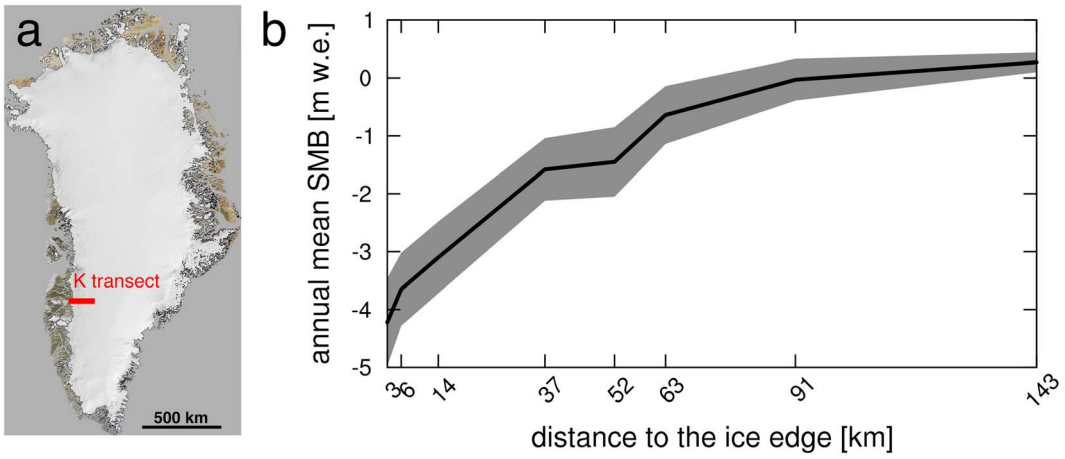

Figure 8. (b) Mean annual (1990–2011) surface mass balance along the K-transect in Southwest Greenland). The location of the transect is shown in (a), which is a figure adapted from Kargel et al. (2012). Data source: van de Wal et al. (2012).

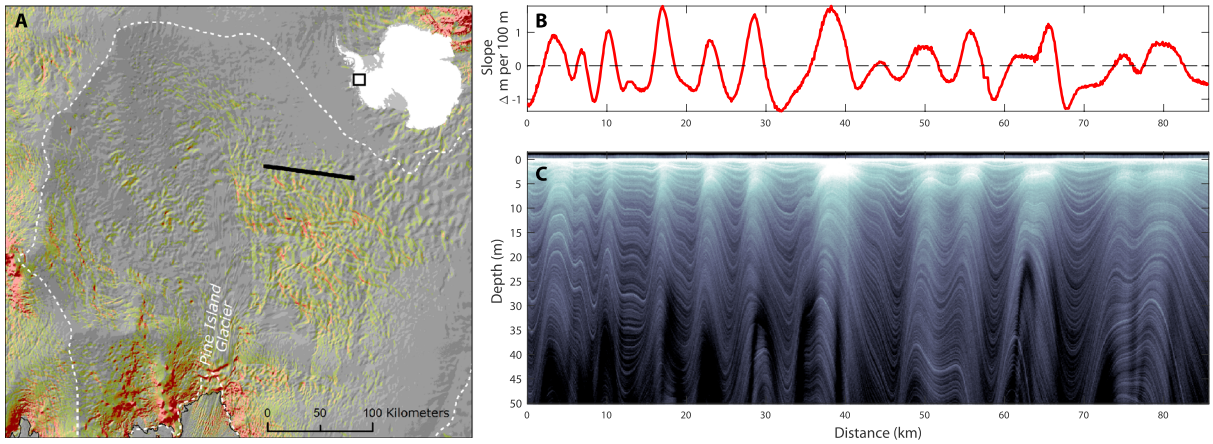

Figure 9. (b) Operation IceBridge surface slope (in units vertical meters per 100 horizontal meters, or %; derived from the Airborne Topographic Mapper) and (c) firn stratigraphy (as detected by Operation IceBridge's snow radar) along a transect on upper Pine Island Glacier (location shown in a), collected on 9 November 2016.

The alternating patterns between high and low SSMB are clearly linked to variations in slope. Near-zero SSMB values are generally found over concave areas (near the peaks in slope in Figure 9b), where exposed terrain limits accumulation of fresh snow and enhances wind-driven snow erosion. Highest SSMB values, in turn, are found in places where slopes are convex (close to the valleys in the slope shown in Figure 9b), providing wind sheltering and promoting snow accumulation and drifting snow deposition. Similarly alternating SMB patterns, driven by variations in surface topography, are found all over the AIS: around megadunes in interior East AIS (Fahnestock et al., 2000; Frezzotti et al., 2002, Figure 5), wind scour zones (Das et al., 2013, 2015; Scambos et al., 2012), on ice shelves, where the surface imprint of basal channels controls SMB patterns (Drews, 2015), and coastal ice rises (King et al., 2004; Lenaerts et al., 2014; Matsuoka et al., 2015).

4. Temporal Variability and Trends in Ice Sheet SMB

Driven by natural variability on time scales that range from subdaily (turbulence, daily cycle), interdaily (i.e., synoptic weather systems), subannual (seasonal cycle) to interannual (interannual to decadal), ice sheet SMB is highly variable across a spectrum of temporal scales. Precipitation over ice sheets is generated primarily by synoptic weather systems, whereas (surface) temperature variations on subdaily to seasonal time scales control sublimation, surface melt, and runoff. Moreover, ice sheet SMB exhibits long-term changes (trends) that follow from external forcing, in particular human-induced increase of atmospheric greenhouse gasses and subsequent atmospheric warming. Here we review the dominant modes of temporal variability in ice sheet SMB and present recent trends and potential drivers.

4.1. Interannual Variability

Ice sheet-integrated SMB varies strongly on interannual time scales (Figure 10). During 1958–2017, modeled GrIS SMB varied from ~100 to ~700 Gt/year, with a standard deviation of ~120 Gt/year, that is, ~32% of the mean. This strong variability in GrIS SMB is a combined effect of variations in precipitation and runoff, which tend to be anticorrelated (fresh snow limits melt through high albedo), enhancing SMB variability. The marked post-1995 decrease in GrIS SMB is driven mainly by increased meltwater runoff, an effect of increasing summer temperatures resulting from persistent anomalies in large-scale atmospheric circulation (Delhasse et al., 2018; Fettweis et al., 2013). In the most recent years (2017 and 2018), the circulation pattern became more zonal and SMB returned to pre-1995 values. Although the mean (grounded) AIS SMB is almost six times higher than the GrIS SMB (~2,150 vs. ~365 Gt/year), its absolute interannual variability is actually smaller (~100 Gt/year, or ~5% of the mean). This can be explained by (1) only precipitation variability contributing to AIS SMB variability, in the general absence of surface runoff, and sublimation being about ten

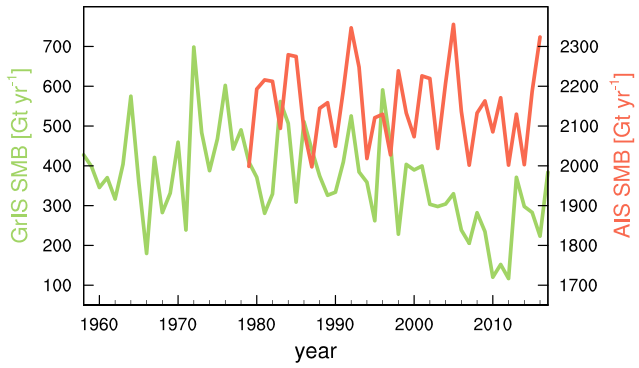

Figure 10. Annual ice sheet integrated surface mass balance (SMB) from RACMO2 for the Greenland ice sheet (GrIS; left, green axis, from 1958 to 2017) and for the Antarctic ice sheet (AIS; red, right axis, from 1979 to 2016). Note that the left and right axes differ, but the vertical extent is the same.

times smaller and with low interannual variability, and (2) a larger surface area of the AIS, where negative precipitation anomalies in some regions are compensated by positive anomalies elsewhere (Fyke et al., 2017).

4.2. Seasonal Variability

Owing to their high-latitude positions and consequent large seasonal fluctuations in insolation, the climates of the ice sheets are characterized by strong seasonal cycles, although this is partly offset by the high surface albedo, which reduces the absorption of solar radiation at the surface. Figure 11 shows that all (modeled) GrIS and AIS SMB components vary with the seasons. Precipitation shows a maximum in early fall (August–September) for the GrIS and early winter for AIS (March–May), and a minimum in summer. In contrast, melt, runoff, and sublimation peak in summer on both ice sheets, driven by higher insolation and ambient temperatures. While AIS melt is limited to the summer months (December and January), and runoff is negligible, the GrIS melt season starts already in May and usually does not end before early September. The onset of runoff is delayed with respect to melt, since the first batch of meltwater refreezes in the cold winter snow. Sublimation is active throughout the year on the AIS, indicative of an active drifting snow climate and the associated sublimation, and is comparable in magnitude to melt in summer, when surface sublimation dominates. The largest mass flux in all months of the year is AIS precipitation, exceeding peak GrIS surface meltwater production in July.

4.3. Short-Term Trends (1980–2015)

As mentioned in section 2.2.1, atmospheric reanalyses do not correctly represent ice sheet meltwater processes, which limits their use to analyze SMB trends to accumulation (P−E). Comparing trends in P−E (Figure 12) highlights significant differences in magnitude and even sign, in contrast with their comparable P−E climatology (Figure 7). For instance, MERRA-2 shows a negative P−E trend over northern Greenland, which is not present in ERA-Interim but appears in CFSR, although as part of a negative P−E trend over a much larger region. ERA-Interim shows a significant P−E increase over central Greenland, which is not confirmed by MERRA-2 or CFSR. Over Antarctica, the reanalyses show important differences but agree on negative P−E trends over Wilkes Land and the western Ross Ice Shelf. As both RACMO2 and MARv3 use ERA-Interim for lateral boundary and surface ocean forcing, their trends broadly agree with those of ERA-Interim (Figure 12). This result suggests that the choice of lateral forcing largely determines SMB trends in RCMs. The large disagreement among what are considered to be state-of-the-art atmospheric reanalysis products indicates that modeled ice sheet P−E trends, especially those over the AIS, are associated with large uncertainties, and should be used with caution.

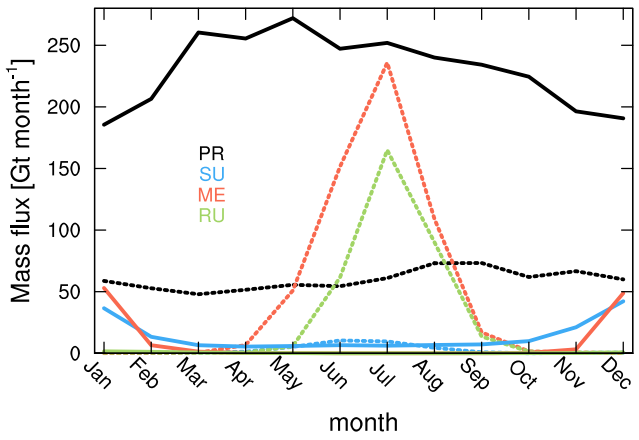

Figure 11. Seasonal cycle of surface mass balance components (in units Gt per month, including surface melt) according to RACMO2 for the Greenland ice sheet (dashed, 1958–2017 mean) and the Antarctic ice sheet (solid, 1979–2016 mean). PR = precipitation; SU = sublimation; ME = surface melt; RU = meltwater runoff.

RCM results show that AIS-integrated SMB has not significantly changed over the period 1980–2015 (Figure 10), and that trends in other SMB components are negligible (not shown). Regional trends, in the absence of significant meltwater runoff, are driven by P−E changes (particularly snowfall). In contrast, the recent GrIS SMB decrease (Figure 10) is dominated by increased runoff (van Angelen et al., 2014; van den Broeke et al., 2016). We use SMB anomalies from RACMO2 and MB anomalies from GRACE (Figure 13) to quantify the contribution of SMB to ice sheet mass loss. From summer 2003 to summer 2016, the GrIS lost more than 4,000 Gt of mass (average MB = −290 ± 19 Gt/year; where the 2-sigma uncertainty accounts for the formal error of the fit and uncertainties in the GIA correction). Most of this mass loss (~63%) can be attributed to a decrease in SMB over the same period (−182 ± 45 Gt/year; mean +/- 2-sigma uncertainty of best linear trend of SMB anomaly in Figure 13). Note that the GrIS seasonal mass amplitude is higher in GRACE than in

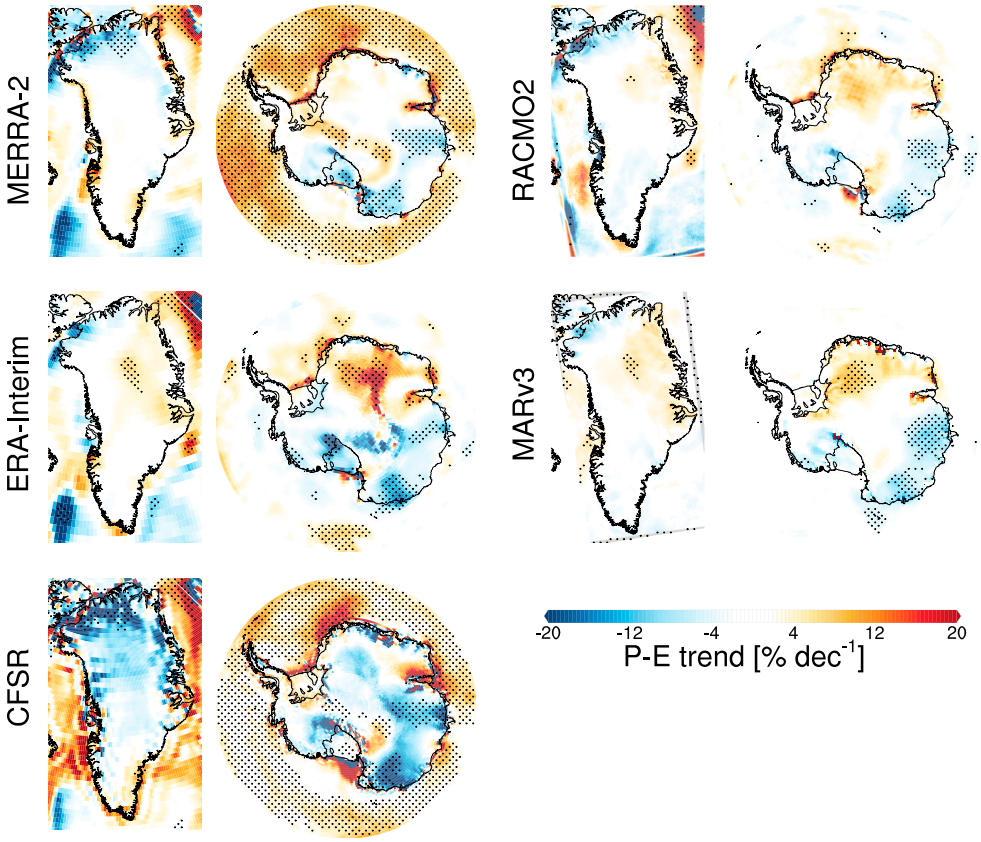

Figure 12. Relative linear P−E trend (in % per decade) over 1980–2015 on the Greenland ice sheet (left) and Antarctic ice sheet (right), according to atmospheric reanalysis products (MERRA-2, ERA-Interim, and CFSR), and regional climate models (RACMO2 and MARv3). Stippled areas indicate that the linear trend is significant at the 95% level.

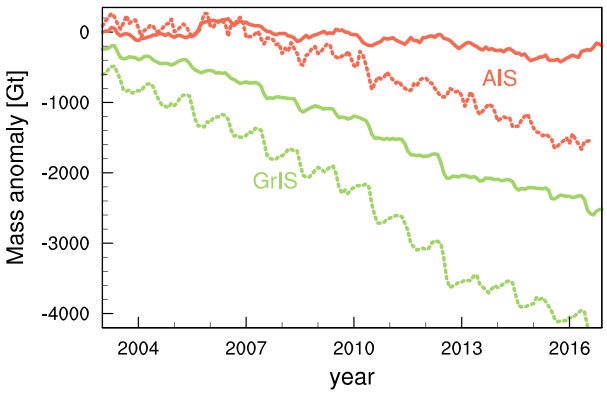

Figure 13. Surface mass balance anomalies over the period 2003–2016 (solid, taken to be the cumulative anomalies relative to a base period, that is, 1960–1990 for the Greenland ice sheet (GrIS), and 1979–2002 for the Antarctic ice sheet (AIS), as in van den Broeke, Bamber, et al. (2009), van den Broeke, König-Langlo, et al. (2009), van den Broeke, Smeets, et al. (2009), and ice sheet mass anomalies derived from Gravity Recovery and Climate experiment (dashed, update from Wouters et al., 2013) for the GrIS (green) and AIS (red).

RACMO2, since the former includes the signal of seasonal snow buildup (fall-winter) and melt (spring) on the tundra surrounding the GrIS, which GRACE cannot separate from ice sheet mass changes. In contrast, AIS mass loss over the same period (average MB = −147 ± 6 Gt/year) is only for a small part (~22%) explained by SMB (−32 ± 4 Gt/yr), confirming that recent AIS mass loss is predominantly driven by enhanced ice discharge (Shepherd et al., 2018). Higher-frequency variability in AIS MB as measured by GRACE can be attributed to SMB (snowfall) anomalies; for instance, the increase in AIS mass during 2005 coincides with a positive SMB anomaly in that year. Similarly, the leveling off of AIS mass loss in 2008, and again in 2010–2011, coincide with periods of high AIS SMB. These snowfall anomalies are even more clearly detectable on a regional scale. In particular, recent high snowfall events in 2009 and 2011 in Dronning Maud Land, East Antarctica (Lenaerts et al., 2013), were detected by GRACE and CloudSat (Boening et al., 2012), as well as laser and radar altimetry (Shepherd et al., 2012).

4.4. Long-Term Trends

Reanalyses and other model products that depend on them (such as RCMs) typically go back only to when satellite data were assimilated

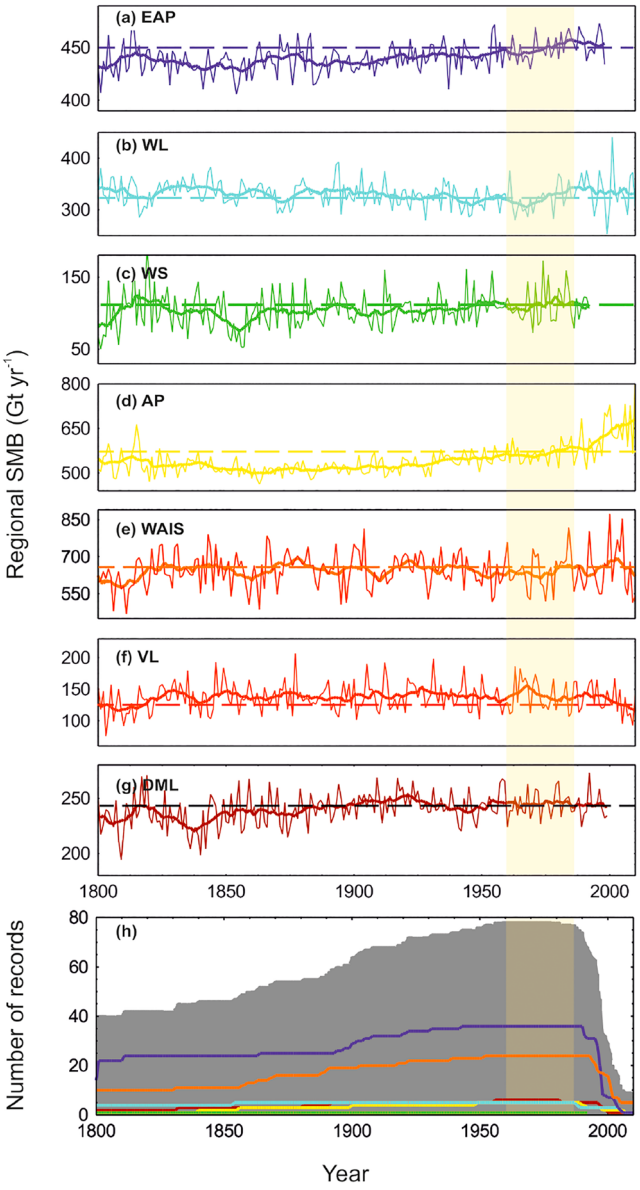

Figure 14. Regional surface mass balance composites (1800–2010) shown as annual averages (thin lines) and 10-year running means (thick lines) for (a–g) the East Antarctic Plateau (EAP, dark blue); Wilkes Land coast (WL, cyan), Weddell Sea coast (WS, green), Antarctic Peninsula (AP, yellow), West Antarctic Ice Sheet (WAIS, orange), Victoria Land (VL, red), and Dronning Maud Land (DML, brown). Panel (h) represents the total number of records (solid grey) and the number of records by region. See Figure 16 for the location of the regions on the Antarctic ice sheet. Source: Thomas et al. (2017).

into the atmospheric products (around 1979). The recent release of a few century-long reanalyses is promising for evaluation of long-term changes. However, large spurious jumps in atmospheric pressure when additional data sets were assimilated, that is, around the International Geophysical Year (1957/1958) in the Arctic, and in 1979 around the AIS, suggest that they require further improvement before they are of sufficient quality for robust trend analysis (Schneider & Fogt, 2018). Therefore, ice core records are of immeasurable importance for contextualizing the satellite-era time series in a historical sense for assessment of natural variability (Steig & Neff, 2018; Trusel et al., 2018).

Ice core records are typically synthesized in two manners: (1) by weighted or unweighted averaging by region (Frezzotti et al., 2013; Thomas et al., 2017) or (2) by spatiotemporal reconstruction (Medley & Thomas, 2019; Monaghan et al., 2006). The basis of the former is that there is a coherent regional signal that will emerge when enough records are averaged together, minimizing the impact of glaciological "noise." The later uses the same principle, but derives the spatial coherence signal in SMB from atmospheric models instead from the ice core records themselves. A gridded reconstruction is next built by weighted averaging based on the model coherence patterns. In reality, the convolution of wind anomalies on the local topography controls the spatial pattern of precipitation, which means that nearby locations might not actual share a common signal. Thus, the additional coherence information provided by the atmospheric models improves the integrity of the reconstruction. Synthesis of several ice cores provides an invaluable tool for evaluation of trends within atmospheric reanalyses and RCMs.

Because there are large regions of Greenland where SSMB < 0, ice sheet-wide reconstructions of accumulation are more challenging and are limited to the accumulation zone. The Program for Arctic Regional Climate Assessment produced several decadal records of accumulation change over the GrIS (Bales, McConnell, et al., 2001; Bales, Mosley-Thompson, et al., 2001; Bales et al., 2009; Mosley-Thompson et al., 2001)

While studies using Antarctic ice core compilations mutually agree that additional accumulation records from Antarctica are desperately needed, they also have a few commonalities. Specifically, several agree that recent (post-1801) Antarctic-wide accumulation has increased significantly, especially over the Antarctic Peninsula and portions of East Antarctica (Figure 14; Frezzotti et al., 2013; Medley & Thomas, 2018; Thomas et al., 2017). While Monaghan et al. (2006) found an insignificant negative trend since 1957, the combination of a short trend interval with use of ERA-40 for the modern era makes trend detection challenging.

Medley and Thomas (2019) determined that the SAM plays a significant role in recent (post-1957) accumulation trends; however, the positive trend in SAM index actually reduced net snow accumulation over Antarctica. Thus, the actual driver of the precipitation increase remains uncertain. Medley and Thomas (2019) suggest that the temperature trends required to generate the observed increases are similar to observations, indicating that thermodynamical forcing cannot be eliminated as a driver of recent precipitation increases. Additional work by Lenaerts et al. (2018) found that the signature of ozone depletion on Antarctic-wide precipitation is remarkably similar to the Medley and Thomas (2019) reconstructed accumulation increase. While the ultimate mechanistic link between ozone depletion and increases in Antarctic precipitation has not been

established as of yet, the work of Lenaerts et al. (2018) suggests that ozone depletion might have also played an important role in Antarctic-wide SMB.

5. Future Ice Sheet SMB: Projections, Feedbacks, Uncertainties

With ongoing global warming and polar amplification, ice sheet SMB will inevitably continue to change. For the GrIS, despite large differences between models and scenarios, all future projections agree that increased runoff will dominate the future decrease of GrIS SMB (Figure 15), with the largest increases in runoff projected to occur in the strongest warming scenarios (Fettweis et al., 2008; Mottram et al., 2017; Rae et al., 2012; van Angelen et al., 2014), confirming the high sensitivity of GrIS SMB to atmospheric warming. An increase in snowfall can partly mitigate the higher runoff, but this signal is projected to be small (Rae et al., 2012). SMB changes will likely continue to dominate future GrIS mass loss, even more so when currently marine-terminating glaciers, apart from those sitting on deeply incised channels (Morlighem et al., 2017), retreat onto land and GrIS solid ice discharge is reduced (Goelzer et al., 2013; Vizcaino et al., 2015). An important aspect of future GrIS SMB, especially beyond 2100, is the shrinking ice sheet geometry, in which the ice sheet lowers and retreats; to resolve these effects requires fully coupled dynamical ice sheet models (Vizcaino, 2014). GrIS SMB decrease is associated with multiple positive feedbacks that can further amplify GrIS mass loss: The increase of ice-free land will enhance summer warming, favoring barrier wind effects (van den Broeke & Gallée, 1996), increasing the heat to melt the retreating ice sheet. The lowering ice sheet surface will experience higher ambient temperatures, further increasing melt. A retreating ice sheet increases its distance to sea, lowering precipitation, which decreases SMB. More precipitation will fall as rain, which saturates the firn layer and runs off when it falls on bare ice, reducing the negative snowfall-albedo affect (Noël et al., 2015). Several of these processes are discussed in more detail below.

Pore Space Loss in the Firn. Currently, almost half of the meltwater produced at the snow surface of the GrIS is refrozen and stored in the firn (Harper et al., 2012; Noël et al., 2017). However, as more liquid water enters the firn layer from melt and rain, this pore space is progressively lost while at the same time additional latent heat by refreezing warms up the firn, further enhancing densification and reducing pore space. As a result, the GrIS firn layer is expected to lose its buffering capacity, an effect that has been projected to become significant as early as the end of the 21st century (van Angelen et al., 2013) and that has already occurred in Greenland's smaller ice caps (Noël et al., 2017). Without this refreezing, all meltwater produced at the surface—even if temporarily stored in the firn by capillary forces—runs off into the ocean, enhancing the GrIS contribution to sea level rise.

Melt-Albedo Feedback. When snow melts, the powerful snowmelt-albedo feedback kicks in. Melt water enters the snow and grains grow rapidly, reducing broadband surface albedo (from ~0.85 for clean fresh snow to ~0.7 for clean wet snow, i.e., essentially doubling net shortwave energy at the surface), which further promotes melting. If the entire winter snowpack is melted, ice is exposed with a surface albedo that is even lower, ranging from 0.55 for clean ice to much lower values determined by the presence of impurities. The "dark zone" in West Greenland, where dust outcropping and biological activity (Stibal et al., 2017) explain a very low (<0.3) ice albedo, will likely progress inward and upward as the ablation area grows, and the presence of impurities might increase, as the ice melts and warms and more water is available (Greuell, 2000).

Melt-Elevation Feedback. As surface ablation increases, surface elevation decreases, exposing the ice sheet to higher ambient temperatures, further enhancing ablation. Although this effect is typically assumed to be small on short temporal scales, and not considered in most projections, it is suggested to enhance GrIS SMB decrease with ~5% at the end of this century, becoming ever more important afterward (Edwards et al., 2014).

Tundra-Ice Sheet Interaction. As more dark tundra surface is exposed during summer through the retreat of peripheral glaciers and ice caps and a shortening of the snow-covered season, more convection will occur, heating the tundra atmosphere; part of this heat may be transferred to the neighboring ice, enhancing melting.

The above feedbacks are typically not fully captured in low-resolution model projections, enhancing the uncertainties associated with these projections. As discussed in section 2.2.5, even the latest generation of ESMs exhibits substantial biases in representing the Arctic atmosphere, ice sheet surface processes,

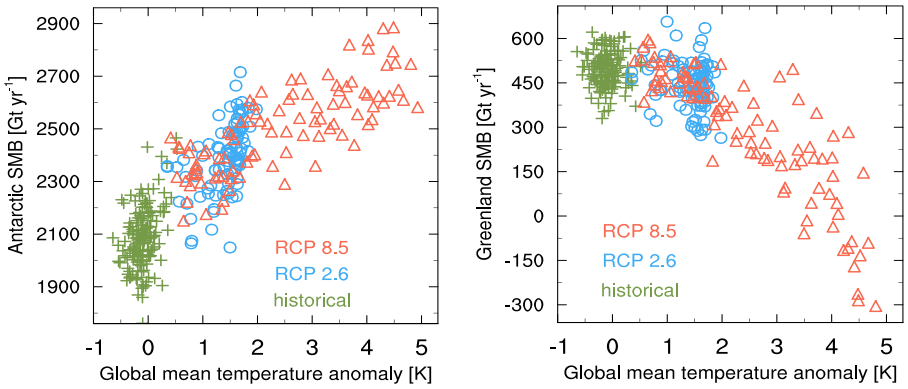

Figure 15. Antarctic ice sheet (left) and Greenland ice sheet (right) surface mass balance (SMB; each point in the plots represents an annual, ice sheet-integrated SMB) in the CMIP5 ESM CESM1-CAM5 (Lenaerts et al., 2015; Lenaerts et al., 2016) in the historical period (1850–2005, green), and two future climate change scenarios (2006–2099) from IPCC AR5: the strong mitigation scenario RCP2.6 (blue), and the high-emission scenario RCP8.5 (red).

and/or ocean and sea ice conditions. For now, RCMs will resolve these features better, but their results remain strongly dependent on the choice of the GCM/ESM forcing (Fettweis et al., 2013).

A tipping point in GrIS MB is sometimes defined as the moment at which GrIS SMB becomes negative, making MB definitively negative (Figure 2). Climate model predictions indicate that this threshold is reached at a global temperature increase of ~2 °C relative to the preindustrial climate (Robinson et al., 2012), although the above-mentioned positive feedbacks might accelerate that (Pattyn et al., 2018). Depending on the scenario, this threshold might be reached as early as the 2030s (in high-emission scenarios such as RCP8.5) or will not be reached at all (in low-emission scenarios, which are the target of the 2015 Paris Agreement and which would limit global mean temperature rise to well below 2 °C above preindustrial levels).

In sharp contrast with the GrIS, future AIS SMB is expected to increase initially in response to atmospheric warming (Figure 15) as a result of enhanced snowfall, while runoff remains small. SMB is predicted to increase at a rate of ~100 Gt/year per degree of (near-surface AIS) warming (Ligtenberg et al., 2013) by the mechanism of enhanced water vapor concentration in a warmer atmosphere. Additionally, changes in atmospheric dynamics, in turn driven by global warming, stratospheric ozone recovery, and/or natural variability, have recently been suggested to influence Antarctic SMB trends (Lenaerts et al., 2018; Medley & Thomas, 2019). Finally, changes in cloud phase and structure over Antarctica, sea ice decline, and ocean surface warming have been suggested to control AIS SMB into the future (Lenaerts et al., 2016). The projected Antarctic SMB increase is expected to mitigate some fraction of the currently ongoing dynamic mass loss in West Antarctica, which is about 200 Gt/year (Gardner et al., 2017; Shepherd et al., 2018). While the consensus is that dynamic losses will dominate future AIS MB, especially in marine sectors of the ice sheet in West Antarctica, the Antarctic Peninsula, and some portions of East Antarctica, some other parts of the AIS are likely to experience mass gain by enhanced snowfall, as long as surface runoff remains small (Winkelmann et al., 2012).

Other AIS SMB components, which are at least an order of magnitude smaller than snowfall, will likely continue to play a minor role in future SMB changes as long as the warming remains modest. A notable exception is the potential indirect role of increased rainfall and surface melt on controlling the stability of Antarctic ice shelves, and thereby the stability of the overall AIS. Similar to the GrIS, firn on AIS ice shelves can lose its meltwater buffering capacity through enhanced meltwater refreezing, latent heat release, and compaction. The water starts ponding on the surface and/or collects in crevasses. Eventually, the water finds its way down, as it exerts a downward or tensile pressure that exceeds that of ice, and ultimately reaches the ice shelf bottom, leading to rapid and catastrophic ice shelf disintegration (Banwell & Macayeal, 2015). This ice shelf hydrofracture mechanism has so far only been observed in the northernmost parts of the Antarctic Peninsula (Scambos et al., 2003 but might expand to other AIS regions in a warmer climate.

6. Conclusions and Recommendations

In this paper, we have reviewed the current state of knowledge of ice sheet SMB in Greenland and Antarctica. Traditional observational methods, which are convenient and cheap but carry relatively large uncertainties and often provide only a single-point SMB measurement, are complemented by novel techniques, such as airborne and satellite radar and laser, and GPS. Although these new techniques provide more precise observations and give us insight in the spatial variability in SMB, they all measure snow depth or surface height changes, requiring knowledge of snow density (with the exception of cosmic ray neutron detection). Therefore, the development of instrumentation to measure snow density precisely over large areas is urgently needed. Cosmic ray counters, which measure snow water equivalent directly and thereby circumvent the need for density observations, have the potential to revolutionize the field of SMB observations into the future.

These new observational techniques have revealed previously unknown large spatial variability in ice sheet SMB, superimposed on the large-scale gradients in SMB from the coast to the interior, both on the GrIS—transitioning from multiple-meter ice ablation to net snow accumulation over less than 100-km distance—and the AIS—where high-precipitation regions coexist with blue ice areas along the coasts. On smaller scales (<1 km), SMB varies considerably as well, driven by surface topography undulations and consequent wind-driven snow redistribution, which challenges the spatial representativeness of stake and firn/ice core records. This small-scale variability is not represented by RCMs, which currently operate at horizontal resolutions of typically 5 km (full GrIS and local AIS) to 25 km (full AIS). Because small-scale snow redistribution does not greatly impact the integrated SMB of a larger area, multiple RCMs now properly simulate SMB on scales of the entire ice sheet down to individual glacier drainage basins. Improved RCM performance was mainly achieved by (1) enhancing the horizontal resolution, including statistical downscaling; (2) including additional (snow) physical processes to represent all SMB components; and (3) the availability of observational datasets to enable detailed model evaluation, in particular GRACE and snow radar.

Further enhancement of horizontal resolution in RCMs will require using nonhydrostatic atmospheric models (e.g., Weather Research and Forecasting (WRF) model, HARMONIE) and/or continued development of statistical downscaling. In tandem, improved simulation of ice sheet SMB requires further development of (high-resolution) atmospheric reanalyses and ESMs, with special emphasis on atmospheric processes (clouds, precipitation, radiation, and turbulence); snow-atmosphere coupling; snow hydrology; snow and ice albedo; SMB downscaling; and, for ESMs in particular, coupling between SMB and ice sheet dynamics. In the not-too-distant future, rapidly increasing computational power will enable us to operate ESMs at horizontal resolutions similar to current RCMs, enabling a direct and fully coupled global framework to assess ice sheet SMB. This should not prevent continuation of model/observational efforts to understand and model small-scale SMB variability (and its driving processes), such as refining statistical downscaling of SMB, developing models of heterogeneous water percolation in firn, and simulating wind-driven processes.

Recent SMB trends strongly differ between the GrIS and the AIS. GrIS SMB has decreased significantly since the mid-1990s, dominating GrIS mass loss since then although a return to pre-1990 values occurred in 2017 and 2018. We expect melt and runoff from the GrIS to increase further under sustained global warming, the degree of which strongly depends on model formulations, climate change scenario, and the potential impact of positive feedbacks associated with GrIS SMB decline. In contrast, recent AIS SMB trends remain relatively poorly constrained, since atmospheric reanalyses differ substantially. Ice core records suggest that AIS SMB has been increasing since the start of the 20th century; however, it remains unclear whether the increase is driven by thermodynamics, atmospheric dynamics, or both, which suggests that our ability to assess future projections over the AIS is limited.

By dominating GrIS mass loss through increased runoff and partly mitigating dynamic AIS mass loss by increased snowfall, the future evolution of ice sheet SMB will continue to play a pivotal role in ice sheet mass changes and associated changes in sea level. Ice sheet SMB also influences past, present, and future ice sheet mass change by controlling ice sheet dynamical processes, such as basal hydrology, fjord circulation by basal runoff and determining meltwater input for Antarctic ice shelf hydrofracture and ice cliff instability (DeConto & Pollard, 2016; Edwards et al., 2019).

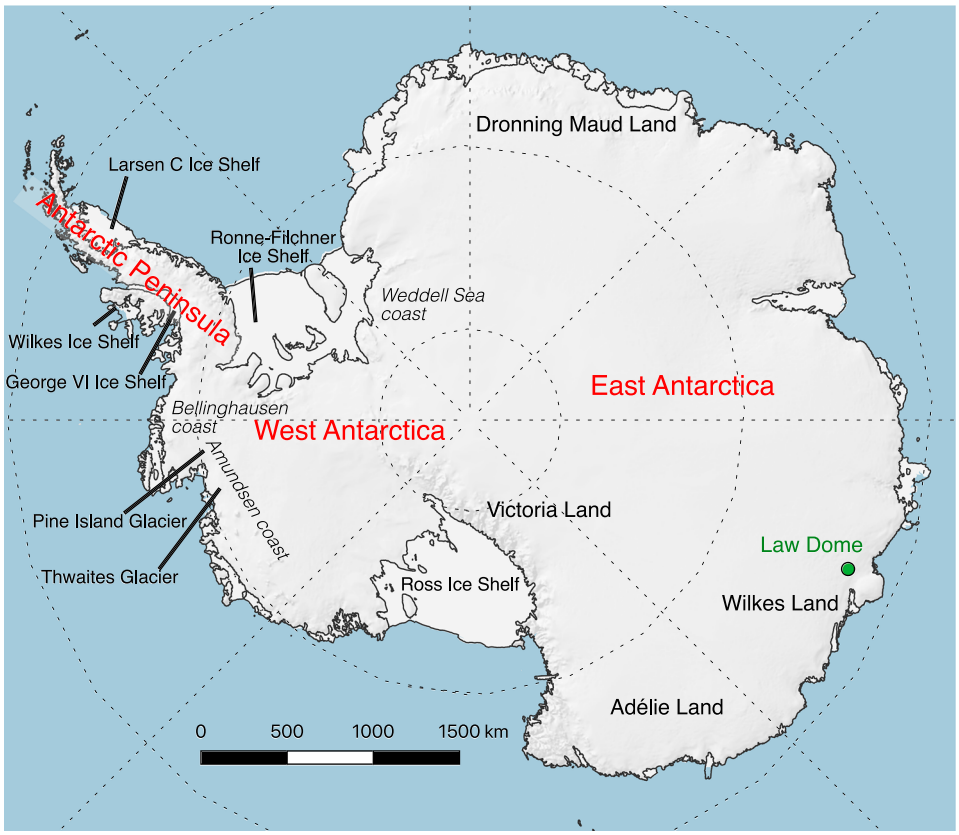

Figure 16. Overview map of the Antarctic Ice Sheet with geographical names used throughout this paper highlighted.

Glossary

Antarctic geographical names

Figure 16 shows an overview map of the Antarctic Ice Sheet, with names of regions, ice shelves, glaciers, and locations that are names in this review paper indicated on the map.

Mass balance (MB, Figure 2): the rate of change of mass (M) of (in the context of this paper) an ice sheet with respect to time (t), or dM/dt. Mass balance is negative when an ice sheet loses mass in time and is positive when it gains mass in time. Units are [units mass] per [units time]; in the context of ice sheet mass balance typically expressed as Gt ($=10^{12}$ kg) per year.

Accumulation area or zone: the group of locations where, over the course of one hydrological or calendar year (depending on the definition), SSMB is positive.

Ablation area or zone: the group of locations where, over the course of one hydrological or calendar year (depending on the definition), SSMB is negative.

Equilibrium line: the line of locations where, over the course of one hydrological or calendar year (depending on the definition), SSMB is zero. The equilibrium line constitutes the boundary between accumulation and ablation areas or zones.

Accumulation: although sometimes used as a synonym for SMB, it is not the same. Accumulation is the difference between PR and SU (PR-SU), that is, SMB without accounting for mass changes by meltwater runoff. Accumulation is identical to SMB at locations where there is no surface melt, or where all the surface meltwater locally refreezes in the snowpack.

Ablation:	a term used to refer to a negative SSMB over some amount of time.
Surface energy balance (SEB, Figure 2):	the balance of radiative (shortwave and longwave) fluxes (RAD), turbulent (sensible and latent) fluxes (TURB), and ground heat flux (GHF) at the ice sheet surface (units Watts per square meter ($W\ m^{-2}$)
Liquid water balance (LWB, Figure 2):	the balance of processes adding to and removing liquid water from the ice sheet surface and firn (units (Gt/year)
Strain Correction:	Densification dominates the vertical strain experienced in the upper firn column. SMB measurements must account for layer thinning within the column as well as longitudinal stretching of the firn and ice due to variations in ice flow; this imparts an additional strain that accumulates with depth (i.e., over time). Therefore, in situ measurements of SMB must correct for the loss of mass via lateral stretching in regions experiencing high longitudinal strain rates or for longer-term historical measurements (>10s/year). The SMB correction is typically used on firn/ice core or ground-penetrating radar measurements.
Degree-day factor:	a factor relating accumulated positive air temperatures (exceeding the melting point) to surface melt. Although this is an efficient method to calculate surface melt (and resulting runoff, if combined with a retention scheme) since it only requires (hourly) temperature data, it is prone to large uncertainties due to variations in surface characteristics (albedo, etc.).
Atmospheric reanalysis:	Atmospheric reanalysis products are essentially GCMs/ESMs assimilated with atmospheric observations to obtain a "reanalysis" of the global atmosphere, including that at the high latitudes.
Regional climate model (RCM):	an atmospheric model with a limited-area domain (i.e., spanning a part of the globe, for example, the Greenland or Antarctic Ice Sheet and surrounding oceans), driven by vertical atmospheric profiles at its lateral boundaries and (commonly) the top of the troposphere, and sea-ice extent and sea-surface temperatures at its ocean surface boundary taken from a global data set (which is either an atmospheric reanalysis data set, or a GCM/ESM; see below for definition). Currently, RCMs are typically employed at horizontal resolutions of 5–35 km. For application on ice sheets, RCMs are coupled to a sophisticated snow model that uses the RCM atmospheric input to simulate snow and firn processes.
General circulation model (GCM):	a modeling framework that couples a global atmospheric, ocean/sea ice, and land model. A GCM only requires input of solar irradiance, concentrations of atmospheric greenhouse gases and aerosols, and land use and generates its internal climatology, which can also respond to changes in any of the above-mentioned inputs (e.g., atmospheric CO_2 concentrations). Currently, GCMs are employed at horizontal resolutions of 1 to 2.5°.
Earth System Model (ESM):	a modeling framework that is an extension of that of a GCM, where ESMs also include models of the biogeochemistry of the ocean and land (carbon cycle, nutrient cycle, etc.), atmospheric chemistry, and dynamic ice sheets. With the additional processes included, ESMs are able to internally calculate atmospheric CO2 concentrations and aerosols and require only input of carbon into the natural system. Currently, ESMs are employed at horizontal resolutions of ~1°, but higher-resolution ESM results (0.25°) will become available within the framework of the upcoming CMIP6 effort.

Acknowledgments
We are extremely grateful to Marlo Garnsworthy (http://www.wordybirdstudio.com) for sharing her illustrating talents with us, which led to the creation of Figure 1 of this paper. We thank Operation IceBridge for the data collection and processing and the National Snow and Ice Data Center (NSIDC) for IceBridge data distribution. OIB data are available on the NSIDC Operation IceBridge Data Portal (https://nsidc.org/icebridge/portal/). Atmospheric reanalysis data sets are available on online data servers. ERA-Interim is available on ECMWF (https://apps.ecmwf.int/datasets/), MERRA-2 can be retrieved on MDISC (https://disc.gsfc.nasa.gov), and CFSR via NCAR (https://rda.ucar.edu/datasets/ds093.1/). The 1980–2015 annual P−E from these three reanalyses are made available as supplementary data sets. RACMO2 output is feely available upon request to Michiel van den Broeke (m.r.vandenbroeke@uu.nl). MARv3 output can be downloaded via FTP (ftp.climato.be/fettweis/). J. T. M. Lenaerts acknowledges support from the National Aeronatics and Space Administration (NASA), Grants 80NSSC18K0201 (ROSES-2016: studies with ICESat-2 and CryoSat-2) and 80NSSC17K0565 (NASA Sea Level Team 2017–2020). B. Medley acknowledges support from the ICESat-2 Project Science Office. B. Wouters was supported by NWO VIDI Grant 016.Vidi.171.065.

References

Adodo, F. I., Remy, F., & Picard, G. (2018). Seasonal variations of the backscattering coefficient measured by radar altimeters over the Antarctic Ice Sheet. *The Cryosphere*, *12*(5), 1767–1778. https://doi.org/10.5194/tc-12-1767-2018

Agosta, C., Amory, C., Kittel, C., Orsi, A., Favier, V., Gallée, H., et al. (2018). Estimation of the Antarctic surface mass balance using MAR (1979-2015) and identification of dominant processes. *The Cryosphere Discussions*, 1–22. https://doi.org/10.5194/tc-2018-76

Alley, R., Clark, P., Huybrechts, P., & Joughin, I. (2005). Ice-sheet and sea-level changes. *Science*, *310*(5747), 456–460. https://doi.org/10.1126/science.1114613

Alley, R. B., Shuman, C. A., Meese, D. A., Gow, A. J., Taylor, K. C., Cuffey, K. M., et al. (1997). Visual-stratigraphic dating of the GISP2 ice core: Basis, reproducibility, and application. *Journal of Geophysical Research*, *102*(C12), 26,367–26,381. https://doi.org/10.1029/96JC03837

Anschutz, H., Eisen, O., Oerter, H., Steinhage, D., & Scheinert, M. (2007). Investigating small-scale variations of the recent accumulation rate in coastal Dronning Maud Land, East Antarctica. *Annals of Glaciology*, *46*, 14–21. https://doi.org/10.3189/172756407782871756

Anschutz, H., Steinhage, D., Eisen, O., Oerter, H., Horwath, M., & Ruth, U. (2008). Small-scale spatio-temporal characteristics of accumulation rates in western Dronning Maud Land, Antarctica. *Journal of Glaciology*, *54*(185), 315–323. https://doi.org/10.3189/002214308784886243

Appenzeller, C., Schwander, J., Sommer, S., & Stocker, T. F. (1998). The North Atlantic Oscillation and its imprint on precipitation and ice accumulation in Greenland. *Geophysical Research Letters*, *25*(11), 1939–1942. https://doi.org/10.1029/98GL01227

Arcone, S. A., Spikes, V. B., & Hamilton, G. S. (2005). Phase structure of radar stratigraphic horizons within Antarctic firn. *Annals of Glaciology*, *41*(1), 10–16. https://doi.org/10.3189/172756405781813267

Arthern, R. J., Vaughan, D. G., Rankin, A. M., Mulvaney, R., & Thomas, E. R. (2010). In situ measurements of Antarctic snow compaction compared with predictions of models. *Journal of Geophysical Research*, 115, F03011. https://doi.org/10.1029/2009JF001306

Arthern, R. J., & Wingham, D. J. (1998). The natural fluctuations of firn densification and their effect on the geodetic determination of ice sheet mass balance. *Climatic Change*, *40*(3–4), 605–624. https://doi.org/10.1023/A:1005320713306

Bales, R. C., Guo, Q., Shen, D., McConnell, J. R., du, G., Burkhart, J. F., et al. (2009). Annual accumulation for Greenland updated using ice core data developed during 2000–2006 and analysis of daily coastal meteorological data. *Journal of Geophysical Research*, *114*, D06116. https://doi.org/10.1029/2008JD011208

Bales, R. C., McConnell, J. R., Mosley-Thompson, E., & Lamorey, G. (2001). Accumulation map for the Greenland Ice Sheet: 1971-1990. *Geophysical Research Letters*, *28*(15), 2967–2970. https://doi.org/10.1029/2000GL012052

Bales, R. C., Mosley-Thompson, E., & McConnell, J. R. (2001). Variability of accumulation in northwest Greenland over the past 250 years. *Geophysical Research Letters*, *28*(14), 2679–2682. https://doi.org/10.1029/2000GL011634

Banta, J. R., McConnell, J. R., Frey, M. M., Bales, R. C., & Taylor, K. (2008). Spatial and temporal variability in snow accumulation at the West Antarctic Ice Sheet Divide over recent centuries. *Journal of Geophysical Research*, *113*, D23102. https://doi.org/10.1029/2008JD010235

Banwell, A. F., & Macayeal, D. R. (2015). Ice-shelf fracture due to viscoelastic flexure stress induced by fill/drain cycles of supraglacial lakes. *Antarctic Science*, *27*(06), 587–597. https://doi.org/10.1017/S0954102015000292

Barletta, V. R., Sabadini, R., & Bordoni, A. (2008). Isolating the PGR signal in the GRACE data: Impact on mass balance estimates in Antarctica and Greenland. *Geophysical Journal International*, *172*(1), 18–30. https://doi.org/10.1111/j.1365-246X.2007.03630.x

Bell, R. E., Chu, W., Kingslake, J., Das, I., Tedesco, M., Tinto, K. J., et al. (2017). Antarctic ice shelf potentially stabilized by export of meltwater in surface river. *Nature*, *544*(7650), 344–348. https://doi.org/10.1038/nature22048

Benson, C. S. (1962). Stratigraphic studies in the snow and firn of the Greenland ice sheet. Cold Regions Research and Engineering Lab, No. RR70.

Berdahl, M., Rennermalm, A., Hammann, A., Mioduszweski, J., Hameed, S., Tedesco, M., et al. (2018). Southeast Greenland winter precipitation strongly linked to the Icelandic low Position. *Journal of Climate*, *31*(11), 4483–4500. https://doi.org/10.1175/JCLI-D-17-0622.1

Bintanja, R. (1998). The contribution of snowdrift sublimation to the surface mass balance of Antarctica. *Annals of Glaciology*, *27*, 251–259.

Bintanja, R. (2000). Snowdrift suspension and atmospheric turbulence. Part 1: Theoretical background and model description. *Boundary-Layer Meteorology*, *95*(3), 343–368.

Bintanja, R. (2001). Modelling snowdrift sublimation and its effect on the moisture budget of the atmospheric boundary layer. *Tellus Series A: Dynamic Meteorology and Oceanography*, *53*(2), 215–232.

Bintanja, R., & van den Broeke, M. R. (1995). The surface energy balance of Antarctic snow and blue ice. *Journal of Applied Meteorology and Climatology*, *34*(4), 902–926.

Black, H. P., & Budd, W. (1964). Accumulation in the region of Wilkes, Wilkes Land, Antarctica. *Journal of Glaciology*, *5*(37), 3–15.

Boening, C., Lebsock, M., Landerer, F., & Stephens, G. (2012). Snowfall-driven mass change on the East Antarctic ice sheet. *Geophysical Research Letters*, *39*, L21501. https://doi.org/10.1029/2012GL053316

Bougamont, M., Bamber, J. L., & Greuell, W. (2005). A surface mass balance model for the Greenland Ice Sheet. *Journal of Geophysical Research*, *110*, F04018. https://doi.org/10.1029/2005JF000348

Box, J. E., Bromwich, D. H., & Bai, L. S. (2004). Greenland ice sheet surface mass balance 1991-2000: Application of Polar MM5 mesoscale model and in situ data. *Journal of Geophysical Research*, *109*, D16105. https://doi.org/10.1029/2003JD004451

Box, J. E., & Steffen, K. (2001). Sublimation on the Greenland ice sheet from automated weather station observations. *Journal of Geophysical Research*, *106*(D24), 33,965–33,981. https://doi.org/10.1029/2001JD900219

Braithwaite, R. J. (1995). Positive degree-day factors for ablation on the Greenland ice sheet studied by energy-balance modelling. *Journal of Glaciology*, *41*(137), 153–160.

Brandt, R. E., & Warren, S. G. (1993). Solar-heating rates and temperature profiles in Antarctic snow and ice. *Journal of Glaciology*, *39*(131), 99–110. https://doi.org/10.3189/S0022143000015756

Brenner, A. C., DiMarzio, J. P., & Zwally, H. J. (2007). Precision and accuracy of satellite radar and laser altimeter data over the continental ice sheets. *IEEE Transactions on Geoscience and Remote Sensing*, *45*(2), 321–331. https://doi.org/10.1109/TGRS.2006.887172

Bromwich, D. H. (1988). Snowfall in high southern latitudes. *Reviews of Geophysics*, *26*(1), 149–168. https://doi.org/10.1029/RG026i001p00149

Bromwich, D. H., Chen, Q., Li, Y., & Cullather, R. I. (1999). Precipitation over Greenland and its relation to the North Atlantic Oscillation. *Journal of Geophysical Research*, *104*(D18), 22,103–22,115. https://doi.org/10.1029/1999JD900373

Bromwich, D. H., Cullather, R. I., & van Woert, M. L. (1998). Antarctic precipitation and its contribution to the global sea-level budget. *Annals of Glaciology*, *27*, 220–226.
Bromwich, D. H., Du, Y., Hines, K. M., Bromwich, D. H., Du, Y., & Hines, K. M. (1996). Wintertime surface winds over the Greenland Ice Sheet. *Monthly Weather Review*, *124*(9), 1941–1947. https://doi.org/10.1175/1520-0493(1996)124<1941:WSWOTG>2.0.CO;2
Bromwich, D. H., Guo, Z., Bai, L., & Shen, Q. (2004). Modeled Antarctic precipitation. Part I: Spatial and temporal variability. *Journal of Climate*, *17*(3), 427–447.
Bromwich, D. H., Monaghan, A. J., Manning, K. W., & Powers, J. G. (2005). Real-Time Forecasting for the Antarctic: An evaluation of the Antarctic Mesoscale Prediction System (AMPS)*. *Monthly Weather Review*. https://doi.org/10.1175/MWR-2881.1
Bromwich, D. H., Monaghan, A. J., Powers, J. G., Cassano, J. J., Wei, H. L., Kuo, Y. H., & Pellegrini, A. (2003). Antarctic Mesoscale Prediction system (AMPS): A case study from the 2000–01 field season. *Monthly Weather Review*, *131*(2), 412–434.
Bromwich, D. H., Nicolas, J. P., Hines, K. M., Kay, J. E., Key, E. L., Lazzara, M. A., et al. (2012). Tropospheric clouds in Antarctica. *Reviews of Geophysics*, *50*, RG1004. https://doi.org/10.1029/2011RG000363
Bromwich, D. H., Parish, T. R., & Zorman, C. A. (1990). The confluence zone of the intense katabatic winds at Terra Nova Bay, Antarctica, as derived from airborne sastrugi surveys and mesoscale numerical modeling. *Journal of Geophysical Research*, *95*(D5), 5495–5509. https://doi.org/10.1029/JD095iD05p05495
Bugnion, V., & Stone, P. H. (2002). Snowpack model estimates of the mass balance of the Greenland ice sheet and its changes over the twentyfirst century. *Climate Dynamics*, *20*(1), 87–106. https://doi.org/10.1007/s00382-002-0240-1
Carsey, F. D. (1980). Microwave observation of the Weddell Polynya. *Monthly Weather Review*, *108*(12), 2032–2044. https://doi.org/10.1175/1520-0493(1980)108<2032:MOOTWP>2.0.CO;2
Cassano, J. J., Box, J. E., Bromwich, D. H., Li, L., & Steffen, K. (2001). Evaluation of Polar MM5 simulations of Greenland's atmospheric circulation. *Journal of Geophysical Research*, *106*(D24), 33,867–33,889. https://doi.org/10.1029/2001JD900044
Chandler, D. M., Wadham, J. L., Lis, G. P., Cowton, T., Sole, A., Bartholomew, I., et al. (2013). Evolution of the subglacial drainage system beneath the Greenland Ice Sheet revealed by tracers. *Nature Geoscience*, *6*(3), 195–198. https://doi.org/10.1038/ngeo1737
Chen, J. L., Wilson, C. R., Blankenship, D., & Tapley, B. D. (2009). Accelerated Antarctic ice loss from satellite gravity measurements. *Nature Geoscience*, *2*(12), 859–862. https://doi.org/10.1038/ngeo694
Chen, L., Johannessen, O. M., Wang, H., & Ohmura, A. (2011). Accumulation over the Greenland Ice Sheet as represented in reanalysis data. *Advances in Atmospheric Sciences*, *28*(5), 1030–1038. https://doi.org/10.1007/s00376-010-0150-9
Chen, Q., Bromwich, D. H., & Bai, L. (1997). Precipitation over Greenland retrieved by a dynamic method and its relation to cyclonic activity. *Journal of Climate*, *10*(5), 839–870. https://doi.org/10.1175/1520-0442(1997)010<0839:POGRBA>2.0.CO;2
Chen, T., Rossow, W. B., & Zhang, Y. (2000). Radiative effects of cloud-type variations. *Journal of Climate*, *13*(1), 264–286. https://doi.org/10.1175/1520-0442(2000)013<0264:REOCTV>2.0.CO;2
Chu, V. W. (2013). Greenland ice sheet hydrology: A review. *Progress in Physical Geography: Earth and Environment*, *38*(1), 19–54. https://doi.org/10.1177/0309133313507075
Church, J. A., Clark, P. U., Cazenave, A., Gregory, J. M., Jevrejeva, S., Levermann, A., et al. (2013). Sea level change. In T. F. Stocker, et al. (Eds.). *Climate Change 2013: The Physical Science Basis. Contribution of Working Group I to the Fifth Assessment Report of the Intergovernmental Panel on Climate Change.* Cambridge, United Kingdom and New York, NY, USA: Cambridge University Press.
Cogley, J. G., Hock, R., Rasmussen, L. A., Arendt, A. A., Bauder, A., Braithwaite, R. J., et al. (2011). Glossary of glacier mass balance and related terms. *Arctic, Antarctic, and Alpine Research*, *44*(2), 256–258.
Cole-Dai, J., Mosley-Thompson, E., Wight, S. P., & Thompson, L. G. (2000). A 4100-year record of explosive volcanism from an East Antarctica ice core. *Journal of Geophysical Research*, *105*(D19), 24,431–24,441. https://doi.org/10.1029/2000JD900254
Cooper, M. G., Smith, L. C., Rennermalm, A. K., Miège, C., Pitcher, L. H., Ryan, J. C., et al. (2018). Meltwater storage in low-density near-surface bare ice in the Greenland ice sheet ablation zone. *The Cryosphere*, *12*(3), 955–970. https://doi.org/10.5194/tc-12-955-2018
Csatho, B. M., Schenk, A. F., van der Veen, C. J., Babonis, G., Duncan, K., Rezvanbehbahani, S., et al. (2014). Laser altimetry reveals complex pattern of Greenland Ice Sheet dynamics. *Proceedings of the National Academy of Sciences of the United States of America*, *111*(52), 18,478–18,483. https://doi.org/10.1073/pnas.1411680112
Cullather, R. I., Nowicki, S. M. J., Zhao, B., & Suarez, M. J. (2014). Evaluation of the surface representation of the Greenland Ice sheet in a general circulation model. *Journal of Climate*, *27*(13), 4835–4856. https://doi.org/10.1175/JCLI-D-13-00635.1
Curry, J. A., Schramm, J. L., & Ebert, E. E. (1993). Impact of clouds on the surface radiation balance of the Arctic Ocean. *Meteorology and Atmospheric Physics*, *51*(3–4), 197–217. https://doi.org/10.1007/BF01030494
Dansgaard, W., & Johnsen, S. J. (1969). A flow model and a time scale for the ice core from Camp Century, Greenland. *Journal of Glaciology*, *8*, 215–223.
Das, I., Bell, R. E., Scambos, T. A., Wolovick, M., Creyts, T. T., Studinger, M., et al. (2013). Influence of persistent wind scour on the surface mass balance of Antarctica. *Nature Geoscience*, *6*(5), 367–371. https://doi.org/10.1038/ngeo1766
Das, I., Scambos, T. A., Koenig, L. S., van den Broeke, M. R., & Lenaerts, J. T. M. (2015). Extreme wind-ice interaction over Recovery Ice Stream, East Antarctica. *Geophysical Research Letters*, *42*, 8064–8071. https://doi.org/10.1002/2015GL065544
Davis, C. H., Li, Y., McConnell, J. R., Frey, M. M., & Hanna, E. (2005). Snowfall-driven growth in East Antarctic Ice Sheet mitigates recent sea-level rise. *Science*, *308*, 1898–1901.
Day, J. J., Bamber, J. L., & Valdes, P. J. (2013). The Greenland Ice Sheet's surface mass balance in a seasonally sea ice-free Arctic. *Journal of Geophysical Research: Earth Surface*, *118*, 1533–1544. https://doi.org/10.1002/jgrf.20112
DeConto, R. M., & Pollard, D. (2016). Contribution of Antarctica to past and future sea-level rise. *Nature*, *531*(7596), 591–597. https://doi.org/10.1038/nature17145
de la Peña, S., Howat, I. M., Nienow, P. W., van den Broeke, M. R., Mosley-Thompson, E., Price, S. F., et al. (2015). Changes in the firn structure of the western Greenland Ice Sheet caused by recent warming. *The Cryosphere*, *9*(3), 1203–1211. https://doi.org/10.5194/tc-9-1203-2015
Delaygue, G., Masson, V., Jouzel, J., Koster, R. D., & Healy, R. J. (2000). The origin of Antarctic precipitation: A modelling approach. *Tellus Series B: Chemical and Physical Meteorology*, *52*(1), 19–36. https://doi.org/10.3402/tellusb.v52i1.16079
Delhasse, A., Fettweis, X., Kittel, C., Amory, C., & Agosta, C. (2018). Brief communication: Impact of the recent atmospheric circulation change in summer on the future surface mass balance of the Greenland Ice Sheet. *The Cryosphere*, *12*(11), 3409–3418. https://doi.org/10.5194/tc-12-3409-2018
Denby, B., Greuell, W., & Oerlemans, J. (2002). Simulating the Greenland atmospheric boundary layer Part I: Model description and validation. *Tellus Series A: Dynamic Meteorology and Oceanography*, *54*(5), 512–528.
Depoorter, M. A., Bamber, J. L., Griggs, J. A., Lenaerts, J. T. M., Ligtenberg, S. R. M., van den Broeke, M. R., & Moholdt, G. (2013). Calving fluxes and basal melt rates of Antarctic ice shelves. *Nature*, *502*(7469), 89–92. https://doi.org/10.1038/nature12567

Déry, S. J., Taylor, P. A., & Xiao, J. (1998). The thermodynamic effects of sublimating, blowing snow in the atmospheric boundary layer. *Boundary-Layer Meteorology*, *89*(2), 251–283. https://doi.org/10.1023/A:1001712111718

Deser, C., Tomas, R., Alexander, M., & Lawrence, D. (2010). The seasonal atmospheric response to projected Arctic Sea ice loss in the late twenty-first century. *Journal of Climate*, *23*(2), 333–351. https://doi.org/10.1175/2009JCLI3053.1

Dethloff, K., Schwager, M., Christensen, J. H., Kiilsholm, S., Rinke, A., Dorn, W., et al. (2002). Recent greenland accumulation estimated from regional climate model simulations and ice core analysis. *Journal of Climate*, *15*(19), 2821–2832. https://doi.org/10.1175/1520-0442(2002)015<2821:RGAEFR>2.0.CO;2

Dibb, J. E., & Fahnestock, M. (2004). Snow accumulation, surface height change, and firn densification at Summit, Greenland: Insights from 2 years of in situ observation. *Journal of Geophysical Research*, 109, D24113. https://doi.org/10.1029/2003JD004300

Ding, Q., Wallace, J. M., Battisti, D. S., Steig, E. J., Gallant, A. J. E., Kim, H. J., & Geng, L. (2014). Tropical forcing of the recent rapid Arctic warming in northeastern Canada and Greenland. *Nature*, *509*(7499), 209–212. https://doi.org/10.1038/nature13260

Doyle, J. D., & Shapiro, M. A. (1999). Flow response to large-scale topography: The Greenland tip jet. *Tellus Series A: Dynamic Meteorology and Oceanography*, *51*(5), 728–748. https://doi.org/10.3402/tellusa.v51i5.14471

Drews, R. (2015). Evolution of ice-shelf channels in Antarctic ice shelves. *The Cryosphere*, *9*(3), 1169–1181. https://doi.org/10.5194/tc-9-1169-2015

Dumont, M., Brun, E., Picard, G., Michou, M., Libois, Q., Petit, J. R., et al. (2014). Contribution of light-absorbing impurities in snow to Greenland's darkening since 2009. *Nature Geoscience*, *7*(7), 509–512. https://doi.org/10.1038/ngeo2180

Dutra, E., Balsamo, G., Viterbo, P., Miranda, P. M. A., Beljaars, A., Schär, C., & Elder, K. (2010). An improved snow scheme for the ECMWF land surface model: Description and offline validation. *Journal of Hydrometeorology*, *11*(4), 899–916. https://doi.org/10.1175/2010JHM1249.1

Edwards, T. L., Brandon, M. A., Durand, G., Edwards, N. R., Golledge, N. R., Holden, P. B., et al. (2019). Revisiting Antarctic ice loss due to marine ice-cliff instability. *Nature*, *566*(7742), 58–64. https://doi.org/10.1038/s41586-019-0901-4

Edwards, T. L., Fettweis, X., Gagliardini, O., Gillet-Chaulet, F., Goelzer, H., Gregory, J. M., et al. (2014). Effect of uncertainty in surface mass balance-elevation feedback on projections of the future sea level contribution of the Greenland ice sheet. *The Cryosphere*, *8*(1), 195–208. https://doi.org/10.5194/tc-8-195-2014

Eisen, O., Frezzotti, M., Genthon, C., Isaksson, E., Magand, O., van den Broeke, M. R., et al. (2008). Ground-based measurements of spatial and temporal variability of snow accumulation in East Antarctica. *Reviews of Geophysics*, *46*, RG2001. https://doi.org/10.1029/2006RG000218

Eisen, O., Rack, W., Nixdorf, U., & Wilhelms, F. (2005). Characteristics of accumulation around the EPICA deep-drilling site in Dronning Maud Land, Antarctica. *Annals of Glaciology*, *41*, 41–46.

Elvidge, A. D., Renfrew, I. A., King, J. C., Orr, A., Lachlan-Cope, T. A., Weeks, M., & Gray, S. L. (2015). Foehn jets over the Larsen C Ice Shelf, Antarctica. *Quarterly Journal of the Royal Meteorological Society*, *141*(688), 698–713. https://doi.org/10.1002/qj.2382

Enderlin, E. M., Howat, I. M., Jeong, S., Noh, M. J., van Angelen, J. H., & van den Broeke, M. R. (2014). An improved mass budget for the Greenland ice sheet. *Geophysical Research Letters*, *41*, 866–872. https://doi.org/10.1002/2013GL059010

Essery, R., Li, L., & Pomeroy, J. (1999). A distributed model of blowing snow over complex terrain. *Hydrological Processes*, *13*(14-15), 2423–2438. https://doi.org/10.1002/(SICI)1099-1085(199910)13:14/15<2423::AID-HYP853>3.0.CO;2-U

Ettema, J., van den Broeke, M. R., van Meijgaard, E., van de Berg, W. J., Bamber, J. L., Box, J. E., & Bales, R. C. (2009). Higher surface mass balance of the Greenland ice sheet revealed by high-resolution climate modeling. *Geophysical Research Letters*, *36*, L12501. https://doi.org/10.1029/2009GL038110

Eyring, V., Bony, S., Meehl, G. A., Senior, C. A., Stevens, B., Stouffer, R. J., & Taylor, K. E. (2016). Overview of the Coupled Model Intercomparison Project Phase 6 (CMIP6) experimental design and organization. *Geoscientific Model Development*, *9*(5), 1937–1958. https://doi.org/10.5194/gmd-9-1937-2016

Fahnestock, M. A., Scambos, T. A., Shuman, C. A., Arthern, R. J., Winebrenner, D. P., & Kwok, R. (2000). Snow megadune fields on the East Antarctic Plateau: Extreme atmosphere-ice interaction. *Geophysical Research Letters*, *27*(22), 3719–3722. https://doi.org/10.1029/1999GL011248

Fausto, R. S., van As, D., Box, J. E., Colgan, W., Langen, P. L., & Mottram, R. H. (2016). The implication of nonradiative energy fluxes dominating Greenland ice sheet exceptional ablation area surface melt in 2012. *Geophysical Research Letters*, *43*, 2649–2658. https://doi.org/10.1002/2016GL067720

Fettweis, X., Box, J. E., Agosta, C., Amory, C., Kittel, C., Lang, C., et al. (2017). Reconstructions of the 1900–2015 Greenland ice sheet surface mass balance using the regional climate MAR model. *The Cryosphere*, *11*(2), 1015–1033. https://doi.org/10.5194/tc-11-1015-2017

Fettweis, X., Franco, B., Tedesco, M., van Angelen, J. H. H., Lenaerts, J. T. M., van den Broeke, M. R. R., & Gallée, H. (2012). Estimating the Greenland ice sheet surface mass balance contribution to future sea level rise using the regional atmospheric climate model MAR. *The Cryosphere*, *7*(2), 469–489. https://doi.org/10.5194/tc-7-469-2013

Fettweis, X., Gallée, H., Lefebre, F., & van Ypersele, J. P. (2005). Greenland surface mass balance simulated by a regional climate model and comparison with satellite-derived data in 1990-1991. *Climate Dynamics*, *24*(6), 623–640. https://doi.org/10.1007/s00382-005-0010-y

Fettweis, X., Hanna, E., Gallée, H., Huybrechts, P., & Erpicum, M. (2008). Estimation of the Greenland ice sheet surface mass balance for the 20th and 21st centuries. *The Cryosphere*, *2*(2), 117–129. https://doi.org/10.5194/tc-2-117-2008

Fettweis, X., Hanna, E., Lang, C., Belleflamme, A., Erpicum, M., & Gallée, H. (2013). Brief communication: Important role of the mid-tropospheric atmospheric circulation in the recent surface melt increase over the Greenland ice sheet. *The Cryosphere*, *7*(1), 241–248. https://doi.org/10.5194/tc-7-241-2013

Pattyn, F., Ritz, C., Hanna, E., Asay-Davis, X., DeConto, R., Durand, G., et al. (2018). The Greenland and Antarctic ice sheets under 1.5 °C global warming. *Nature Climate Change*, *8*(12), 1053–1061. https://doi.org/10.1038/s41558-018-0305-8

Fisher, D. A., Reeh, N., & Clausen, H. B. (1985). Stratigraphic noise in time series derived from ice cores. *Annals of Glaciology*, *7*, 76–83.

Flanner, M. G., & Zender, C. S. (2006). Linking snowpack microphysics and albedo evolution. *Journal of Geophysical Research*, *111*, D12208. https://doi.org/10.1029/2005JD006834

Flechtner, F., Neumayer, K.-H., Dahle, C., Dobslaw, H., Fagiolini, E., Raimondo, J.-C., & Güntner, A. (2016). What can be expected from the GRACE-FO laser ranging interferometer for earth science applications? *Surveys in Geophysics*, *37*(2), 453–470. https://doi.org/10.1007/s10712-015-9338-y

Forster, R. R., Box, J. E., van den Broeke, M. R., Miège, C., Burgess, E. W., van Angelen, J. H., et al. (2014). Extensive liquid meltwater storage in firn within the Greenland ice sheet. *Nature Geoscience*, *7*(2), 95–98. https://doi.org/10.1038/ngeo2043

Fréville, H., Brun, E., Picard, G., Tatarinova, N., Arnaud, L., Lanconelli, C., et al. (2014). Using MODIS land surface temperatures and the Crocus snow model to understand the warm bias of ERA-Interim reanalyses at the surface in Antarctica. *The Cryosphere*, *8*(4), 1361–1373. https://doi.org/10.5194/tc-8-1361-2014

Frezzotti, M., Gandolfi, S., & Urbini, S. (2002). Snow megadunes in Antarctica: Sedimentary structure and genesis. *Journal of Geophysical Research*, *107*(D18), 4344. https://doi.org/10.1029/2001JD000673

Frezzotti, M., Pourchet, M., Flora, O., Gandolfi, S., Gay, M., Urbini, S., et al. (2005). Spatial and temporal variability of snow accumulation in East Antarctica from traverse data. *Journal of Glaciology*, *51*(172), 113–124. https://doi.org/10.3189/172756505781829502

Frezzotti, M., Scarchilli, C., Becagli, S., Proposito, M., & Urbini, S. (2013). A synthesis of the Antarctic surface mass balance during the last 800 yr. *The Cryosphere*, *7*(1), 303–319. https://doi.org/10.5194/tc-7-303-2013

Frezzotti, M., Urbini, S., Proposito, M., Scarchilli, C., & Gandolfi, S. (2007). Spatial and temporal variability of surface mass balance near Talos Dome, East Antarctica. *Journal of Geophysical Research*, *112*, F02032. https://doi.org/10.1029/2006JF000638

Fyke, J., Lenaerts, J. T. M., & Wang, H. (2017). Basin-scale heterogeneity in Antarctic precipitation and its impact on surface mass variability. *The Cryosphere*, *11*(6). https://doi.org/10.5194/tc-11-2595-2017

Gallée, H., Schayes, G., Gallée, H., & Schayes, G. (1994). Development of a three-dimensional meso-γ primitive equation model: Katabatic winds simulation in the area of Terra Nova Bay, Antarctica. *Monthly Weather Review*, *122*(4), 671–685. https://doi.org/10.1175/1520-0493(1994)122<0671:DOATDM>2.0.CO;2

Gallée, H., Trouvilliez, A., Agosta, C., Genthon, C., Favier, V., & Naaim-Bouvet, F. (2013). Transport of snow by the wind: A comparison between observations in Adélie Land, Antarctica, and Simulations Made with the Regional Climate Model MAR. *Boundary-Layer Meteorology*, *146*(1), 133–147. https://doi.org/10.1007/s10546-012-9764-z

Gardner, A. S., Moholdt, G., Scambos, T., Fahnstock, M., Ligtenberg, S., van den Broeke, M., & Nilsson, J. (2017). Increased West Antarctic ice discharge and East Antarctic stability over the last seven years. *The Cryosphere Discussions*, 1–39. https://doi.org/10.5194/tc-2017-75

Gerland, S., Oerter, H., Kipfstuhl, J., Wilhelms, F., Miller, H., & Miners, W. D. (1999). Density log of a 181 m long ice core from Berkner Island, Antarctica. *Annals of Glaciology*, *29*, 215–219. https://doi.org/10.3189/172756499781821427

Goelzer, H., Huybrechts, P., Fürst, J. J., Nick, F. M., Andersen, M. L., Edwards, T. L., et al. (2013). Sensitivity of Greenland ice sheet projections to model formulations. *Journal of Glaciology*, *59*(216), 733–749. https://doi.org/10.3189/2013JoG12J182

Gorodetskaya, I., van Lipzig, N. P. M., Kneifel, S., Tricht, K. van, Schween, J. H., & Crewell, S. (2014). Cloud and precipitation properties from ground-based remote sensing in East Antarctica.

Gorodetskaya, I. V., Tsukernik, M., Claes, K., Ralph, M. F., Neff, W. D., & van Lipzig, N. P. M. (2014). The role of atmospheric rivers in anomalous snow accumulation in East Antarctica. *Geophysical Research Letters*, *41*, 6199–6206. https://doi.org/10.1002/2014GL060881

Gorodetskaya, I. V., van Lipzig, N. P. M., van den Broeke, M. R., Mangold, A., Boot, W., & Reijmer, C. H. (2013). Meteorological regimes and accumulation patterns at Utsteinen, Dronning Maud Land, East Antarctica: Analysis of two contrasting years. *Journal of Geophysical Research: Atmospheres*, *118*, 1700–1715. https://doi.org/10.1002/jgrd.50177

Goujon, C., Barnola, J.-M., & Ritz, C. (2003). Modeling the densification of polar firn including heat diffusion: Application to close-off characteristics and gas isotopic fractionation for Antarctica and Greenland sites. *Journal of Geophysical Research*, *108*(D24), 4792. https://doi.org/10.1029/2002JD003319

Gow, A. J. (1965). On the accumulation and seasonal stratification of snow at the South Pole. *Journal of Glaciology*, *5*(40), 467–477.

Grazioli, J., Madeleine, J.-B., Gallée, H., Forbes, R. M., Genthon, C., Krinner, G., & Berne, A. (2017). Katabatic winds diminish precipitation contribution to the Antarctic ice mass balance. *Proceedings of the National Academy of Sciences of the United States of America*, *114*(41), 201707633. https://doi.org/10.1073/pnas.1707633114

Greuell, W. (2000). Melt-water accumulation on the surface of the greenland ice sheet: effect on albedo and mass balance. *Geografiska Annaler. Series A, Physical Geography*, *82*(4), 489–498. https://doi.org/10.1111/j.0435-3676.2000.00136.x

Groot Zwaaftink, C. D., Cagnati, A., Crepaz, A., Fierz, C., MacElloni, G., Valt, M., & Lehning, M. (2013). Event-driven deposition of snow on the Antarctic Plateau: Analyzing field measurements with SNOWPACK. *The Cryosphere*, *7*(1), 333–347. https://doi.org/10.5194/tc-7-333-2013

Hanna, E., Cropper, T. E., Hall, R. J., & Cappelen, J. (2016). Greenland blocking index 1851–2015: a regional climate change signal. *International Journal of Climatology*, *36*(15), 4847–4861. https://doi.org/10.1002/joc.4673

Hanna, E., Fettweis, X., & Hall, R. J. (2018). Brief communication: Recent changes in summer Greenland blocking captured by none of the CMIP5 models. *The Cryosphere*, *12*(10), 3287–3292. https://doi.org/10.5194/tc-12-3287-2018

Hanna, E., Huybrechts, P., Cappelen, J., Steffen, K., Bales, R. C., Burgess, E., et al. (2011). Greenland Ice Sheet surface mass balance 1870 to 2010 based on Twentieth Century Reanalysis, and links with global climate forcing. *Journal of Geophysical Research*, *116*, D24121. https://doi.org/10.1029/2011JD016387

Hanna, E., Huybrechts, P., Janssens, I., Cappelen, J., Steffen, K., & Stephens, A. (2005). Runoff and mass balance of the Greenland Ice Sheet: 1958-2003. *Journal of Geophysical Research*, *110*, D13108. https://doi.org/10.1029/2004JD005641

Hanna, E., Huybrechts, P., & Mote, T. L. (2002). Surface mass balance of the Greenland Ice Sheet from Climate-Analyss data and accumulation/runoff models. *Annals of Glaciology*, *35*, 67–72.

Hanna, E., McConnell, J., Das, S., Cappelen, J., & Stephens, A. (2006). Observed and modeled Greenland Ice Sheet snow accumulation, 1958–2003, and links with regional climate forcing. *Journal of Climate*, *19*(3), 344–358. https://doi.org/10.1175/JCLI3615.1

Hanna, E., & Valdes, P. (2001). Validation of ECMWF (re)analysis surface climate data, 1979-98, for Greenland and implications for mass balance modelling of the ice sheet. *International Journal of Climatology*, *21*(2), 171–195.

Harden, B. E., Renfrew, I. A., Petersen, G. N., Harden, B. E., Renfrew, I. A., & Petersen, G. N. (2011). A climatology of wintertime barrier winds off Southeast Greenland. *Journal of Climate*, *24*(17), 4701–4717. https://doi.org/10.1175/2011JCLI4113.1

Hardy, R. A., Nerem, R. S., & Wiese, D. N. (2017). The impact of atmospheric modeling errors on GRACE estimates of mass loss in Greenland and Antarctica. *Journal of Geophysical Research: Solid Earth*, *122*, 10,440–10,458. https://doi.org/10.1002/2017JB014556

Harper, J., Humphrey, N., Pfeffer, W. T., Brown, J., & Fettweis, X. (2012). Greenland ice-sheet contribution to sea-level rise buffered by meltwater storage in firn. *Nature*, *491*(7423), 240–243. https://doi.org/10.1038/nature11566

Hawley, R. L., Brandt, O., Morris, E. M., Kohler, J., Shepherd, A. P., & Wingham, D. J. (2008). Techniques for measuring high-resolution firn density profiles: Case study from Kongsvegen, Svalbard. *Journal of Glaciology*, *54*(186), 463–468.

Hawley, R. L., & Morris, E. M. (2006). Borehole optical stratigraphy and neutron-scattering density measurements at Summit, Greenland. *Journal of Glaciology*, *52*(179), 491–496.

Hermann, M., Box, J. E., Fausto, R. S., Colgan, W. T., Langen, P. L., Mottram, R., et al. (2018). Application of PROMICE Q-transect in situ accumulation and ablation measurements (2000–2017) to constrain mass balance at the southern tip of the Greenland Ice Sheet. *Journal of Geophysical Research: Earth Surface*, *123*, 1235–1256. https://doi.org/10.1029/2017JF004408

Herron, M. M. (1982). Impurity sources of F−, Cl−, NO3− and SO4 2− in Greenland and Antarctic precipitation. *Journal of Geophysical Research*, *87*(C4), 3052–3060. https://doi.org/10.1029/JC087iC04p03052

Herron, M. M., & Langway, C. C. (1980). Firn densification: An empirical model. *Journal of Glaciology*, *25*(93), 373–385. https://doi.org/10.3189/S0022143000015239

Hoffman, M. J., Fountain, A. G., & Liston, G. E. (2008). Surface energy balance and melt thresholds over 11 years at Taylor Glacier, Antarctica. *Journal of Geophysical Research*, *113*, F04014. https://doi.org/10.1029/2008JF001029

Howat, I. M., de la Peña, S., Desilets, D., & Womack, G. (2018). Autonomous ice sheet surface mass balance measurements from cosmic rays. *The Cryosphere*, *12*(6), 2099–2108.

Hui, F., Ci, T., Cheng, X., Scambo, T. A., Liu, Y., Zhang, Y., et al. (2014). Mapping blue-ice areas in Antarctica using ETM+ and MODIS data. *Annals of Glaciology*, *55*(66), 129–137. https://doi.org/10.3189/2014AoG66A069

Hurrell, J. W., Kushnir, Y., Ottersen, G., & Visbeck, M. (2013). An Overview of the North Atlantic Oscillation. The North Atlantic Oscillation: Climatic significance and environmental impact. https://doi.org/10.1029/134GM01

Huybrechts, P., Rybak, O., Steinhage, D., & Pattyn, F. (2009). Past and present accumulation rate reconstruction along the Dome FujiKohnen radio-echo sounding profile, Dronning Maud Land, East Antarctica. *Annals of Glaciology*, *50*(51), 112–120. https://doi.org/10.3189/172756409789097513

James, I. N. (2006). On the forcing of planetary-scale Rossby waves by Antarctica. *Quarterly Journal of the Royal Meteorological Society*, *114*(481), 619–637. https://doi.org/10.1002/qj.49711448105

Janssens, I., & Huybrechts, P. (2000). The treatment of meltwater retention in mass-balance parameterizations of the Greenland ice sheet. *Annals of Glaciology*, *31*, 133–140.

Jones, P. D., & Lister, D. H. (2015). Antarctic near-surface air temperatures compared with ERA-Interim values since 1979. *International Journal of Climatology*, *35*(7), 1354–1366. https://doi.org/10.1002/joc.4061

Kameda, T., Motoyama, H., Fujita, S., & Takahashi, S. (2008). Temporal and spatial variability of surface mass balance at Dome Fuji, East Antarctica, by the stake method from 1995 to 2006. *Journal of Glaciology*, *54*(184), 107–116. https://doi.org/10.3189/002214308784409062

Kanagaratnam, P., Gogineni, S. P., Ramasami, V., & Braaten, D. (2004). A wideband radar for high-resolution mapping of near-surface internal layers in glacial ice. *IEEE Transactions on Geoscience and Remote Sensing*, *42*(3), 483–490. https://doi.org/10.1109/TGRS.2004.823451

Kanagaratnam, P., Markus, T., Lytle, V., Heavey, B., Jansen, P., Prescott, G., & Gogineni, S. P. (2007). Ultrawideband radar measurements of thickness of snow over sea ice. *IEEE Transactions on Geoscience and Remote Sensing*, *45*(9), 2715–2724. https://doi.org/10.1109/TGRS.2007.900673

Kargel, J. S., Ahlstrøm, A. P., Alley, R. B., Bamber, J. L., Benham, T. J., Box, J. E., et al. (2012). Brief communication
 Greenland's shrinking ice cover: “Fast times” but not that fast. *The Cryosphere*, *6*(3), 533–537. https://doi.org/10.5194/tc-6-533-2012

Kaspari, S., Mayewski, P. A., Dixon, D. A., Spikes, V. B., Sneed, S. B., Handley, M. J., & Hamilton, G. S. (2004). Climate variability in West Antarctica derived from annual accumulation-rate records from ITASE firn/ice cores. *Annals of Glaciology*, *39*(1), 585–594. https://doi.org/10.3189/172756404781814447

Kay, J. E., Deser, C., Phillips, A., Mai, A., Hannay, C., Strand, G., et al. (2014). The Community Earth System Model (CESM) large ensemble project: A community resource for studying climate change in the presence of internal climate variability. *Bulletin of the American Meteorological Society*, *96*(8), 1333–1349. https://doi.org/10.1175/BAMS-D-13-00255.1

Kay, J. E., & Gettelman, A. (2009). Cloud influence on and response to seasonal Arctic sea ice loss. *Journal of Geophysical Research*, *114*, D18204. https://doi.org/10.1029/2009JD011773

King, J. C., Anderson, P. S., & Mann, G. W. (2001). The seasonal cycle of sublimation at Halley, Antarctica. *Journal of Glaciology*, *47*(156), 1–8.

King, J. C., Anderson, P. S., Vaughan, D. G., Mann, G. W., Mobbs, S. D., & Vosper, S. B. (2004). Wind-borne redistribution of snow across an Antarctic ice rise. *Journal of Geophysical Research*, *109*, D11104. https://doi.org/10.1029/2003JD004361

King, J. C., Gadian, A., Kirchgaessner, A., Kuipers Munneke, P., Lachlan-Cope, T. A., Orr, A., et al. (2015). Validation of the summertime surface energy budget of Larsen C Ice Shelf (Antarctica) as represented in three high-resolution atmospheric models. *Journal of Geophysical Research: Atmospheres*, *120*, 1335–1347. https://doi.org/10.1002/2014JD022604

Kingslake, J., Ely, J. C., Das, I., & Bell, R. E. (2017). Widespread movement of meltwater onto and across Antarctic ice shelves. *Nature*, *544*(7650), 349–352. https://doi.org/10.1038/nature22049

Kittel, C., Amory, C., Agosta, C., Delhasse, A., Huot, P.-V., Fichefet, T., & Fettweis, X. (2018). Sensitivity of the current Antarctic surface mass balance to sea surface conditions using MAR. *The Cryosphere Discussions*, 1–19. https://doi.org/10.5194/tc-2018-106

Kneifel, S., Maahn, M., Peters, G., & Simmer, C. (2011). Observation of snowfall with a low-power FM-CW K-band radar (Micro Rain Radar). *Meteorology and Atmospheric Physics*, *113*(1), 75–87. https://doi.org/10.1007/s00703-011-0142-z

Kodama, M. (1980). Continuous monitoring of snow water equivalent using cosmic ray neutrons. *Cold Regions Science and Technology*, *3*(4), 295–303.

Kodama, M., Kawasaki, S., & Wada, M. (1975). A cosmic-ray snow gauge. *The International Journal of Applied Radiation and Isotopes*, *26*(12), 774–775.

Kodama, M., Nakai, K., Kawasaki, S., & Wada, M. (1979). An application of cosmic-ray neutron measurements to the determination of the snow-water equivalent. *Journal of Hydrology*, *41*(1–2), 85–92.

Koenig, L. S., Ivanoff, A., Alexander, P. M., MacGregor, J. A., Fettweis, X., Panzer, B., et al. (2016). Annual Greenland accumulation rates (2009–2012) from airborne snow radar. *The Cryosphere*, *10*(4), 1739–1752. https://doi.org/10.5194/tc-10-1739-2016

Koenig, L. S., Lampkin, D. J., Montgomery, L. N., Hamilton, S. L., Turrin, J. B., Joseph, C. A., et al. (2015). Wintertime storage of water in buried supraglacial lakes across the Greenland Ice Sheet. *The Cryosphere*, *9*(4), 1333–1342. https://doi.org/10.5194/tc-9-1333-2015

Krinner, G., Derksen, C., Essery, R., Flanner, M., Hagemann, S., Clark, M., et al. (2018). ESM-SnowMIP: Assessing models and quantifying snow-related climate feedbacks. *Geoscientific Model Development*, *11*(12), 5027–5049. https://doi.org/10.5194/gmd-11-5027-2018

Krinner, G., & Genthon, C. (1997). The Antarctica mass balance in a stretched grid general circulation model. *Annals of Glaciology*, *25*, 73–78.

Krinner, G., Largeron, C., Ménégoz, M., Agosta, C., & Brutel-Vuilmet, C. (2014). Oceanic forcing of Antarctic climate change: A study using a stretched-grid atmospheric general circulation model. *Journal of Climate*, *27*(15), 5786–5800. https://doi.org/10.1175/JCLI-D-13-00367.1

Kuipers Munneke, P., Ligtenberg, S. R. M., Noël, B. P. Y., Howat, I. M., Box, J. E., Mosley-Thompson, E., et al. (2015). Elevation change of the Greenland ice sheet due to surface mass balance and firn processes, 1960–2014. *The Cryosphere*, *9*, 2009–2025. https://doi.org/10.5194/tc-9-2009-2015

Kuipers Munneke, P., Ligtenberg, S. R., van den Broeke, M. R., van Angelen, J. H., & Forster, R. R. (2014). Explaining the presence of perennial liquid water bodies in the firn of the Greenland Ice Sheet. *Geophysical Research Letters*, *41*, 476–483. https://doi.org/10.1002/2013GL058389

Kuipers Munneke, P., Luckman, A. J., Bevan, S. L., Smeets, C. J. P. P., Gilbert, E., van den Broeke, M. R., et al. (2018). Intense winter surface melt on an Antarctic Ice Shelf. *Geophysical Research Letters*, *45*, 7615–7623. https://doi.org/10.1029/2018GL077899

Kuipers Munneke, P., Picard, G., van den Broeke, M. R. R., Lenaerts, J. T. M., & van Meijgaard, E. (2012). Insignificant change in Antarctic snowmelt volume since 1979. *Geophysical Research Letters*, *39*, L01501. https://doi.org/10.1029/2011GL050207

Kuipers Munneke, P., Reijmer, C. H., van den Broeke, M. R., König-Langlo, G., Stammes, P., & Knap, W. H. (2008). Analysis of clear-sky Antarctic snow albedo using observations and radiative transfer modeling. *Journal of Geophysical Research*, *113*, D17118. https://doi.org/10.1029/2007JD009653

Kuipers Munneke, P., Smeets, C. J. P. P., Reijmer, C. H., Oerlemans, J., van de Wal, R. S. W., & van den Broeke, M. R. (2018). The K-transect on the western Greenland Ice Sheet: Surface energy balance (2003-2016). *Arctic Antarctic and Alpine Research*, *50*(1), 1–13. https://doi.org/10.1080/15230430.2017.1420952

Kuipers Munneke, P., van den Broeke, M. R., King, J. C., Gray, T., & Reijmer, C. H. (2012). Near-surface climate and surface energy budget of Larsen C ice shelf, Antarctic Peninsula. *The Cryosphere*, *6*(2), 353–363. https://doi.org/10.5194/tc-6-353-2012

Lachlan-Cope, T. A., Connolley, W. M., & Turner, J. (2001). The role of the non-axisymmetric Antarctic Orography in forcing the observed pattern of variability of the Antarctic Climate. *Geophysical Research Letters*, *28*(21), 4111–4114. https://doi.org/10.1029/2001GL013465

Langley, E. S., Leeson, A. A., Stokes, C. R., & Jamieson, S. S. R. (2016). Seasonal evolution of supraglacial lakes on an East Antarctic outlet glacier. *Geophysical Research Letters*, *43*, 8563–8571. https://doi.org/10.1002/2016GL069511

Larson, K. M., Wahr, J., & Munneke, P. K. (2015). Constraints on snow accumulation and firn density in Greenland using GPS receivers. *Journal of Glaciology*, *61*(225), 101–114. https://doi.org/10.3189/2015JoG14J130

Lathem, T. L., Beyersdorf, A. J., Thornhill, K. L., Winstead, E. L., Cubison, M. J., Hecobian, A., et al. (2013). Sciences ESS atmospheric chemistry and physics climate of the past geoscientific instrumentation methods and data systems analysis of CCN activity of Arctic aerosol and Canadian biomass burning during summer 2008. *Atmospheric Chemistry and Physics*, *13*(5), 2735–2756. https://doi.org/10.5194/acp-13-2735-2013

Lenaerts, J. T. M., Brown, J., van den Broeke, M. R., Matsuoka, K., Drews, R., Callens, D., et al. (2014). High variability of climate and surface mass balance induced by Antarctic ice rises. *Journal of Glaciology*, *60*(224), 1101–1110. https://doi.org/10.3189/2014JoG14J040

Lenaerts, J. T. M., Fyke, J., & Medley, B. (2018). The signature of ozone depletion in recent Antarctic precipitation change: A study with the Community Earth System Model. *Geophysical Research Letters*, *45*, 12,931–12,939. https://doi.org/10.1029/2018GL078608

Lenaerts, J. T. M., Le Bars, D., van Kampenhout, L., Vizcaino, M., Enderlin, E. M. E. M., & van den Broeke, M. R. M. R. (2015). Representing Greenland ice sheet freshwater fluxes in climate models. *Geophysical Research Letters*, *42*, 6373–6381. https://doi.org/10.1002/2015GL064738

Lenaerts, J. T. M., Lhermitte, S., Drews, R., Ligtenberg, S. R. M., Berger, S., Helm, V., et al. (2017). Meltwater produced by wind-albedo interaction stored in an East Antarctic ice shelf. *Nature Climate Change*, *7*(1), 58–62. https://doi.org/10.1038/nclimate3180

Lenaerts, J. T. M., Ligtenberg, S. R. M., Medley, B., van de Berg, W. J., Konrad, H., Nicolas, J. P., et al. (2017). Climate and surface mass balance of coastal West Antarctica resolved by regional climate modelling. *Annals of Glaciology*, *59*(76pt1), 29–41. https://doi.org/10.1017/aog.2017.42

Lenaerts, J. T. M., & van den Broeke, M. R. (2012). Modeling drifting snow in Antarctica with a regional climate model: 2. Results. *Journal of Geophysical Research*, *117*, D05109. https://doi.org/10.1029/2010JD015419

Lenaerts, J. T. M., van den Broeke, M. R., Déry, S. J., van Meijgaard, E., van de Berg, W. J., Palm, S. P., & Sanz Rodrigo, J. (2012). Modeling drifting snow in Antarctica with a regional climate model: 1. Methods and model evaluation. *Journal of Geophysical Research*, *117*, D05108. https://doi.org/10.1029/2011JD016145

Lenaerts, J. T. M., van den Broeke, M. R., Scarchilli, C., & Agosta, C. (2012). Impact of model resolution on simulated wind, drifting snow and surface mass balance in Terre Adélie, East Antarctica. *Journal of Glaciology*, *48*(211), 821–829. https://doi.org/10.3189/2012JoG12J020

Lenaerts, J. T. M., van den Broeke, M. R., van Angelen, J. H., van Meijgaard, E., & Déry, S. J. (2012). Drifting snow climate of the Greenland ice sheet: A study with a regional climate model. *The Cryosphere*, *6*(4), 891–899. https://doi.org/10.5194/tc-6-891-2012

Lenaerts, J. T. M., van den Broeke, M. R., van de Berg, W. J., van Meijgaard, E., & Kuipers Munneke, P. (2012). A new, high-resolution surface mass balance map of Antarctica (1979-2010) based on regional atmospheric climate modeling. *Geophysical Research Letters*, *39*, L04501. https://doi.org/10.1029/2011GL050713

Lenaerts, J. T. M., van Meijgaard, E., van den Broeke, M. R., Ligtenberg, S. R. M., Horwath, M., & Isaksson, E. (2013). Recent snowfall anomalies in Dronning Maud Land, East Antarctica, in a historical and future climate perspective. *Geophysical Research Letters*, *40*, 2684–2688. https://doi.org/10.1002/grl.50559

Lenaerts, J. T. M., Van Tricht, K., Lhermitte, S., & L'Ecuyer, T. S. (2017). Polar clouds and radiation in satellite observations, reanalyses, and climate models. *Geophysical Research Letters*, *44*, 3355–3364. https://doi.org/10.1002/2016GL072242

Lenaerts, J. T. M., Vizcaino, M., Fyke, J., van Kampenhout, L., & van den Broeke, M. R. (2016). Present-day and future Antarctic ice sheet climate and surface mass balance in the Community Earth System Model. *Climate Dynamics*, *47*(5–6), 1367–1381. https://doi.org/10.1007/s00382-015-2907-4

Lewis, G., Osterberg, E., Hawley, R., Whitmore, B., Peter Marshall, H., & Box, J. (2017). Regional Greenland accumulation variability from Operation IceBridge airborne accumulation radar. *The Cryosphere*, *11*, 773–788. https://doi.org/10.5194/tc-11-773-2017

Li, J., & Zwally, H. J. (2011). Modeling of firn compaction for estimating ice-sheet mass change from observed ice-sheet elevation change. *Annals of Glaciology*, *52*(59), 1–7. https://doi.org/10.3189/172756411799096321

Ligtenberg, S. R. M., Helsen, M. M., & van den Broeke, M. R. (2011). An improved semi-empirical model for the densification of Antarctic firn. *The Cryosphere*, *5*(4), 809–819. https://doi.org/10.5194/tc-5-809-2011

Ligtenberg, S. R. M., Lenaerts, J. T. M., van den Broeke, M. R., & Scambos, T. A. (2014). On the formation of blue ice on Byrd Glacier, Antarctica. *Journal of Glaciology*, *60*(219), 41–50. https://doi.org/10.3189/2014JoG13J116

Ligtenberg, S. R. M., van de Berg, W. J., van den Broeke, M. R., Rae, J. G. L., & van Meijgaard, E. (2013). Future surface mass balance of the Antarctic ice sheet and its influence on sea level change, simulated by a regional atmospheric climate model. *Climate Dynamics*, *41*(3–4), 867–884. https://doi.org/10.1007/s00382-013-1749-1

Lindsay, R., Wensnahan, M., Schweiger, A., & Zhang, J. (2014). Evaluation of seven different atmospheric reanalysis products in the Arctic. *Journal of Climate*, *27*(7), 2588–2606. https://doi.org/10.1175/JCLI-D-13-00014.1

Liston, G. E., & Sturm, M. (2002). Winter precipitation patterns in Arctic Alaska determined from a blowing-snow model and snow-depth observations. *Journal of Hydrometeorology*, *3*(6), 646–659. https://doi.org/10.1175/1525-7541(2002)003<0646:WPPIAA>2.0.CO;2

Liston, G. E., Winther, J.-G. G., Liston, G. E., & Winther, J.-G. G. (2005). Antarctic surface and subsurface snow and ice melt fluxes. *Journal of Climate*, *18*(10), 1469–1481. https://doi.org/10.1175/JCLI3344.1

Liu, J., Chen, Z., Francis, J., Song, M., Mote, T., & Hu, Y. (2016). Has Arctic Sea Ice Loss contributed to increased surface melting of the Greenland Ice Sheet? *Journal of Climate*, *29*(9), 3373–3386. https://doi.org/10.1175/JCLI-D-15-0391.1

Löfverström, M., Caballero, R., Nilsson, J., & Kleman, J. (2014). Evolution of the large-scale atmospheric circulation in response to changing ice sheets over the last glacial cycle. *Climate of the Past*, *10*(4), 1453–1471. https://doi.org/10.5194/cp-10-1453-2014

Looyenga, H. (1965). Dielectric constants of heterogeneous mixtures. *Physica*, *31*(3), 401–406. https://doi.org/10.1016/0031-8914(65)90045-5

Lucas-Picher, P., Wulff-Nielsen, M., Christensen, J. H., Aðalgeirsdóttir, G., Mottram, R., & Simonsen, S. B. (2012). Very high resolution regional climate model simulations over Greenland: Identifying added value. *Journal of Geophysical Research*, *117*, D02108. https://doi.org/10.1029/2011JD016267

Luckman, A., Elvidge, A., Jansen, D., Kulessa, B., Kuipers Munneke, P., King, J., & Barrand, N. E. (2014). Surface melt and ponding on Larsen C Ice Shelf and the impact of föhn winds. *Antarctic Science*, *26*(6), 625–635. https://doi.org/10.1017/S0954102014000339

Luthcke, S. B., Zwally, H. J., Abdalati, W., Rowlands, D. D., Ray, R. D., Nerem, R. S., et al. (2006). Recent Greenland ice mass loss by drainage system from satellite gravity observations. *Science*, *314*(5803), 1286–1289. https://doi.org/10.1126/science.1130776

MacGregor, J. A., Matsuoka, K., Koutnik, M. R., Waddington, E. D., Studinger, M., & Winebrenner, D. P. (2009). Millennially averaged accumulation rates for the Vostok Subglacial Lake region inferred from deep internal layers. *Annals of Glaciology*, *50*(51), 25–34. https://doi.org/10.3189/172756409789097441

Machguth, H., MacFerrin, M., van As, D., Box, J. E., Charalampidis, C., Colgan, W., et al. (2016). Greenland meltwater storage in firn limited by near-surface ice formation. *Nature Climate Change*, *6*(4), 390–393. https://doi.org/10.1038/nclimate2899

Markus, T., Neumann, T., Martino, A., Abdalati, W., Brunt, K., Csatho, B., et al. (2017). The Ice, Cloud, and land Elevation Satellite-2 (ICESat-2): science requirements, concept, and implementation. *Remote Sensing of Environment*, *190*, 260–273. https://doi.org/10.1016/J.RSE.2016.12.029

Marshall, G. J. (2009). On the annual and semi-annual cycles of precipitation across Antarctica. *International Journal of Climatology*, *29*(15), 2298–2308. https://doi.org/10.1002/joc.1810

Marshall, G. J., & Thompson, D. W. J. (2016). The signatures of large-scale patterns of atmospheric variability in Antarctic surface temperatures. *Journal of Geophysical Research: Atmospheres*, *121*, 3276–3289. https://doi.org/10.1002/2015JD024665

Marshall, G. J., Thompson, D. W. J. J., & van den Broeke, M. R. (2017). The signature of Southern Hemisphere atmospheric circulation patterns in Antarctic precipitation. *Geophysical Research Letters*, *44*, 11,580–11,589. https://doi.org/10.1002/2017GL075998

Martín-Español, A., King, M. A., Zammit-Mangion, A., Andrews, S. B., Moore, P., & Bamber, J. L. (2016). An assessment of forward and inverse GIA solutions for Antarctica. *Journal of Geophysical Research: Solid Earth*, *121*, 6947–6965. https://doi.org/10.1002/2016JB013154

Martín-Español, A., Zammit-Mangion, A., Clarke, P. J., Flament, T., Helm, V., King, M. A., et al. (2016). Spatial and temporal Antarctic Ice Sheet mass trends, glacio-isostatic adjustment, and surface processes from a joint inversion of satellite altimeter, gravity, and GPS data. *Journal of Geophysical Research: Earth Surface*, *121*, 182–200. https://doi.org/10.1002/2015JF003550

Matsuoka, K., Hindmarsh, R. C. A., Moholdt, G., Bentley, M. J., Pritchard, H. D., Brown, J., et al. (2015). Antarctic ice rises and rumples: Their properties and significance for ice-sheet dynamics and evolution. *Earth-Science Reviews*, *150*, 724–745. https://doi.org/10.1016/j.earscirev.2015.09.004

Mattingly, K. S., Mote, T. L., & Fettweis, X. (2018). Atmospheric river impacts on Greenland Ice Sheet surface mass balance. *Journal of Geophysical Research: Atmospheres*, *123*, 8538–8560. https://doi.org/10.1029/2018JD028714

McConnell, J. R., Arthern, R. J., Mosley-Thompson, E., Davis, C. H., Bales, R. C., Thomas, R., et al. (2000). Changes in Greenland ice sheet elevation attributed primarily to snowaccumulation variability. *Nature*, *406*(6798), 877–879. https://doi.org/10.1038/35022555

McConnell, J. R., Bales, R. C., & Davis, D. R. (1997). Recent intra-annual snow accumulation at South Pole: Implications for ice core interpretation. *Journal of Geophysical Research*, *102*(D18), 21,947–21,954. https://doi.org/10.1029/97JD00848

McConnell, J. R., Lamorey, G. W., Lambert, S. W., & Taylor, K. C. (2002). Continuous ice-core chemical analyses using inductively coupled plasma mass spectrometry. *Environmental Science & Technology*, *36*(1), 7–11. https://doi.org/10.1021/es011088z

McConnell, J. R., Mosley-Thompson, E., Bromwich, D. H., Bales, R. C., & Kyne, J. D. (2000). Interannual variations of snow accumulation on the Greenland Ice Sheet (1985–1996): New observations versus model predictions. *Journal of Geophysical Research*, *105*(D3), 4039–4046. https://doi.org/10.1029/1999JD901049

McMillan, M., Nienow, P., Shepherd, A., Benham, T., & Sole, A. (2007). Seasonal evolution of supra-glacial lakes on the Greenland Ice Sheet. *Earth and Planetary Science Letters*, *262*(3–4), 484–492. https://doi.org/10.1016/J.EPSL.2007.08.002

Medley, B., Joughin, I., Das, S. B., Steig, E. J., Conway, H., Gogineni, S., et al. (2013). Airborne-radar and ice-core observations of annual snow accumulation over Thwaites Glacier, West Antarctica confirm the spatiotemporal variability of global and regional atmospheric models. *Geophysical Research Letters*, *40*, 3649–3654. https://doi.org/10.1002/grl.50706

Medley, B., Joughin, I., Smith, B. E., Das, S. B., Steig, E. J., Conway, H., et al. (2014). Constraining the recent mass balance of Pine Island and Thwaites glaciers, West Antarctica, with airborne observations of snow accumulation. *The Cryosphere*, *8*(4), 1375–1392. https://doi.org/10.5194/tc-8-1375-2014

Medley, B., Ligtenberg, S. R. M., Joughin, I., van den Broeke, M. R., Gogineni, S., & Nowicki, S. (2015). Antarctic firn compaction rates from repeat-track airborne radar data: I. Methods. *Annals of Glaciology*, *56*(70), 155–166. https://doi.org/10.3189/2015AoG70A203

Medley, B., & Thomas, E. R. (2019). Increased snowfall over the Antarctic Ice Sheet mitigated twentieth-century sea-level rise. *Nature Climate Change*, *9*(1), 34–39. https://doi.org/10.1038/s41558-018-0356-x

Meehl, G. A. (1991). A reexamination of the mechanism of the semiannual oscillation in the Southern Hemisphere. *Journal of Climate*, *4*(9), 911–926. https://doi.org/10.1175/1520-0442(1991)004<0911:AROTMO>2.0.CO;2

Miège, C., Forster, R. R., Box, J. E., Burgess, E. W., McConnell, J. R., Pasteris, D. R., & Spikes, V. B. (2013). Southeast Greenland high accumulation rates derived from firn cores and ground-penetrating radar. *Annals of Glaciology*, *54*(63), 322–332. https://doi.org/10.3189/2013AoG63A358

Miège, C., Forster, R. R., Brucker, L., Koenig, L. S., Solomon, D. K., Paden, J. D., et al. (2016). Spatial extent and temporal variability of Greenland firn aquifers detected by ground and airborne radars. *Journal of Geophysical Research: Earth Surface*, *121*, 2381–2398. https://doi.org/10.1002/2016JF003869

Miller, N. B., Shupe, M. D., Lenaerts, J. T. M., Kay, J. E., de Boer, G., & Bennartz, R. (2018). Process-based model evaluation using surface energy budget observations in Central Greenland. *Journal of Geophysical Research: Atmospheres*, *123*, 4777–4796. https://doi.org/10.1029/2017JD027377

Minghu, D., Cunde, X., Yuansheng, L., Jiawen, R., Shugui, H., Bo, J., & Bo, S. (2011). Spatial variability of surface mass balance along a traverse route from Zhongshan station to Dome A, Antarctica. *Journal of Glaciology*, *57*(204), 658–666.

Mohajerani, Y., Velicogna, I., & Rignot, E. (2018). Mass loss of Totten and Moscow University Glaciers, East Antarctica, using regionally optimized GRACE mascons. *Geophysical Research Letters*, *45*, 7010–7018. https://doi.org/10.1029/2018GL078173

Monaghan, A. J., Bromwich, D. H., Fogt, R. L., Wang, S. H., Mayewski, P. A., Dixon, D. A., et al. (2006). Insignificant change in Antarctic snowfall since the International Geophysical Year. *Science*, *313*(5788), 827–831. https://doi.org/10.1126/science.1128243

Moore, G. W. K., Renfrew, I. A., Moore, G. W. K., & Renfrew, I. A. (2005). Tip jets and barrier winds: A QuikSCAT climatology of high wind speed events around Greenland. *Journal of Climate*, *18*(18), 3713–3725. https://doi.org/10.1175/JCLI3455.1

Morlighem, M., Williams, C. N., Rignot, E., An, L., Arndt, J. E., Bamber, J. L., et al. (2017). BedMachine v3: Complete bed topography and ocean bathymetry mapping of Greenland from multibeam echo sounding combined with mass conservation. *Geophysical Research Letters*, *44*, 11,051–11,061. https://doi.org/10.1002/2017GL074954

Morris, E. M., & Cooper, J. D. (2003). Density measurements in ice boreholes using neutron scattering. *Journal of Glaciology*, *49*(167), 599–604.

Mosley-Thompson, E., McConnell, J. R., Bales, R. C., Li, Z., Lin, P. N., Steffen, K., et al. (2001). Local to regional-scale variability of annual net accumulation on the Greenland ice sheet from PARCA cores. *Journal of Geophysical Research*, *106*(D24), 33,839–33,851. https://doi.org/10.1029/2001JD900067

Mottram, R., Nielsen, K. P., Gleeson, E., & Yang, X. (2017). Modelling glaciers in the HARMONIE-AROME NWP model. *Advances in Science and Research*, *14*, 323–334. https://doi.org/10.5194/asr-14-323-2017

Mouginot, J., Rignot, E., & Scheuchl, B. (2014). Sustained increase in ice discharge from the Amundsen Sea Embayment, West Antarctica, from 1973 to 2013. *Geophysical Research Letters*, *41*, 1576–1584. https://doi.org/10.1002/2013GL059069

Moussavi, M. S., Abdalati, W., Pope, A., Scambos, T., Tedesco, M., MacFerrin, M., & Grigsby, S. (2016). Derivation and validation of supraglacial lake volumes on the Greenland Ice Sheet from high-resolution satellite imagery. *Remote Sensing of Environment*, *183*, 294–303. https://doi.org/10.1016/J.RSE.2016.05.024

Nash, D., Waliser, D., Guan, B., Ye, H., & Ralph, F. M. (2018). The role of atmospheric rivers in extratropical and polar hydroclimate. *Journal of Geophysical Research: Atmospheres*, *123*, 6804–6821. https://doi.org/10.1029/2017JD028130

Nereson, N. A., Raymond, C. F., Jacobel, R. W., & Waddington, E. D. (2000). The accumulation pattern across Siple Dome, West Antarctica, inferred from radar-detected internal layers. *Journal of Glaciology*, *46*(152), 75–87. https://doi.org/10.3189/172756500781833449

Nghiem, S. V., Hall, D. K., Mote, T. L., Tedesco, M., Albert, M. R., Keegan, K., et al. (2012). The extreme melt across the Greenland ice sheet in 2012. *Geophysical Research Letters*, *39*, L20502. https://doi.org/10.1029/2012GL053611

Nicolas, J. P., & Bromwich, D. H. (2011). Precipitation changes in high southern latitudes from global reanalyses: A cautionary tale. *Surveys in Geophysics*, *32*(4–5), 475–494. https://doi.org/10.1007/s10712-011-9114-6

Nienow, P. W., Sole, A. J., Slater, D. A., & Cowton, T. R. (2017). Recent advances in our understanding of the role of meltwater in the Greenland Ice Sheet System. *Current Climate Change Reports*, *3*(4), 330–344. https://doi.org/10.1007/s40641-017-0083-9

Nigro, M. A., Cassano, J. J., & Knuth, S. L. (2012). Evaluation of Antarctic Mesoscale Prediction System (AMPS) cyclone forecasts using infrared satellite imagery. *Antarctic Science*. https://doi.org/10.1017/S0954102011000745

Nilsson, J., Vallelonga, P., Simonsen, S. B., Sørensen, L. S., Forsberg, R., Dahl-Jensen, D., et al. (2015). Greenland 2012 melt event effects on CryoSat-2 radar altimetry. *Geophysical Research Letters*, *42*, 3919–3926. https://doi.org/10.1002/2015GL063296

Noël, B., Fettweis, X., van de Berg, W. J., van den Broeke, M. R., & Erpicum, M. (2014). Sensitivity of Greenland Ice Sheet surface mass balance to perturbations in sea surface temperature and sea ice cover: A study with the regional climate model MAR. *The Cryosphere*, *8*(5), 1871–1883. https://doi.org/10.5194/tc-8-1871-2014

Noël, B., van de Berg, W. J., Lhermitte, S., Wouters, B., Machguth, H., Howat, I., et al. (2017). A tipping point in refreezing accelerates mass loss of Greenland's glaciers and ice caps. *Nature Communications*, *8*(9296), 14730. https://doi.org/10.1038/ncomms14730

Noël, B., van de Berg, W. J., van Meijgaard, E., Kuipers Munneke, P., van de Wal, R. S. W., & van den Broeke, M. R. (2015). Evaluation of the updated regional climate model RACMO2.3: Summer snowfall impact on the Greenland Ice Sheet. *The Cryosphere*, *9*(5), 1831–1844. https://doi.org/10.5194/tc-9-1831-2015

Noël, B., van de Berg, W. J., van Wessem, J. M., van Meijgaard, E., van As, D., Lenaerts, J. T. M., et al. (2018). Modelling the climate and surface mass balance of polar ice sheets using RACMO2—Part 1: Greenland (1958-2016). *The Cryosphere*, *12*(3), 811–831. https://doi.org/10.5194/tc-12-811-2018

Nye, J. F. (1963). Correction factor for accumulation measured by the thickness of the annual layers in an ice sheet. *Journal of Glaciology*, *4*, 785–788.

Oerter, H., Wilhelms, F., Jung-Rothenhäusler, F., Göktas, F., Miller, H., Graf, W., & Sommer, S. (2000). Accumulation rates in Dronning Maud Land, Antarctica, as revealed by dielectric-profiling measurements of shallow firn cores. *Annals of Glaciology*, *30*(1), 27–34.

Ohmura, A., & Reeh, N. (1991). New precipitation and accumulation maps for Greenland. *Journal of Glaciology*, *37*(125), 140–148. https://doi.org/10.3189/S0022143000042891

Oliva, M., Navarro, F., Hrbáček, F., Hernández, A., Nývlt, D., Pereira, P., et al. (2017). Recent regional climate cooling on the Antarctic Peninsula and associated impacts on the cryosphere. *Science of the Total Environment*, *580*, 210–223. https://doi.org/10.1016/J.SCITOTENV.2016.12.030

Overland, J. E., Francis, J. A., Hanna, E., & Wang, M. (2012). The recent shift in early summer Arctic atmospheric circulation. *Geophysical Research Letters*, *39*, L19804. https://doi.org/10.1029/2012GL053268

Overly, T. B., Hawley, R. L., Helm, V., Morris, E. M., & Chaudhary, R. N. (2016). Greenland annual accumulation along the EGIG line, 1959–2004, from ASIRAS airborne radar and neutron-probe density measurements. *The Cryosphere*, *10*(4), 1679–1694. https://doi.org/10.5194/tc-10-1679-2016

Pail, R., Bingham, R., Braitenberg, C., Dobslaw, H., Eicker, A., Güntner, A., et al., & IUGG Expert Panel (2015). Science and user needs for observing global mass transport to understand global change and to benefit society. *Surveys in Geophysics*, *36*(6), 743–772. https://doi.org/10.1007/s10712-015-9348-9

Palerme, C., Kay, J. E., Genthon, C., L'Ecuyer, T., Wood, N. B., & Claud, C. (2014). How much snow falls on the Antarctic ice sheet? *The Cryosphere*, *8*(4), 1577–1587. https://doi.org/10.5194/tc-8-1577-2014

Palm, S. P., Kayetha, V., Yang, Y., & Pauly, R. (2017). Blowing snow sublimation and transport over Antarctica from 11 years of CALIPSO observations. *The Cryosphere*, *11*(6), 2555–2569. https://doi.org/10.5194/tc-11-2555-2017

Palm, S. P., Yang, Y., Spinhirne, J. D., & Marshak, A. (2011). Satellite remote sensing of blowing snow properties over Antarctica. *Journal of Geophysical Research*, *116*, D16123. https://doi.org/10.1029/2011JD015828

Palmer, S. J., Dowdeswell, J. A., Christoffersen, P., Young, D. A., Blankenship, D. D., Greenbaum, J. S., et al. (2013). Greenland subglacial lakes detected by radar. *Geophysical Research Letters*, *40*, 6154–6159. https://doi.org/10.1002/2013GL058383

Parish, T. R. (1983). The influence of the Antarctic Peninsula on the wind field over the western Weddell Sea. *Journal of Geophysical Research*, *88*(C4), 2684–2692. https://doi.org/10.1029/JC088iC04p02684

Parish, T. R., & Bromwich, D. H. (1987). The surface windfield over the Antarctic Ice Sheets. *Nature*, *328*, 51–54.

Petersen, G. N., Renfrew, I. A., & Moore, G. W. K. (2009). An overview of barrier winds off southeastern Greenland during the Greenland Flow Distortion experiment. *Quarterly Journal of the Royal Meteorological Society*, *135*(645), 1950–1967. https://doi.org/10.1002/qj.455

Pfeffer, W. T., Illangasekare, T. H., & Meier, M. F. (1990). Analysis and modelling of melt-water refreezing in dry snow. *Journal of Glaciology*, *36*(123), 238–246.

Phillpot, H. R., & Zillman, J. W. (1970). The surface temperature inversion over the Antarctic Continent. *Journal of Geophysical Research*, *75*(21), 4161–4169. https://doi.org/10.1029/JC075i021p04161

Picard, G., Domine, F., Krinner, G., Arnaud, L., & Lefebvre, E. (2012). Inhibition of the positive snow-albedo feedback by precipitation in interior Antarctica. *Nature Climate Change*, *2*(11), 795–798. https://doi.org/10.1038/nclimate1590

Picciotto, E., & Wilgain, S. (1963). Fission products in Antarctic snow, a reference level for measuring accumulation. *Journal of Geophysical Research*, *68*(21), 5965–5972. https://doi.org/10.1029/JZ068i021p05965

Powers, J. G., Manning, K. W., Bromwich, D. H., Cassano, J. J., & Cayette, A. M. (2012). A decade of antarctic science support through AMPS. *Bulletin of the American Meteorological Society*, *93*(11), 1699–1712. https://doi.org/10.1175/BAMS-D-11-00186.1

Powers, J. G., Monaghan, A. J., Cayette, A. M., Bromwich, D. H., Kuo, Y. H., & Manning, K. W. (2003). Real-time mesoscale modeling over Antarctica: The Antarctic Mesoscale Prediction System. *Bulletin of the American Meteorological Society*, *84*(11), 1533–1546. https://doi.org/10.1175/BAMS-84-11-1533

Pritchard, H. D., Ligtenberg, S. R. M., Fricker, H. a., Vaughan, D. G., van den Broeke, M. R., & Padman, L. (2012). Antarctic ice-sheet loss driven by basal melting of ice shelves. *Nature*, *484*(7395), 502–505. https://doi.org/10.1038/nature10968

Proksch, M., Löwe, H., & Schneebeli, M. (2015). Density, specific surface area, and correlation length of snow measured by high-resolution penetrometry. *Journal of Geophysical Research: Earth Surface*, *120*, 346–362. https://doi.org/10.1002/2014JF003266

Qin, D., Xiao, C., Allison, I., Bian, L., Stephenson, R., Ren, J., & Yan, M. (2004). Snow surface height variations on the Antarctic ice sheet in Princess Elizabeth Land, Antarctica: 1 year of data from an automatic weather station. *Annals of Glaciology*, *39*, 181–187. https://doi.org/10.3189/172756404781814546

Radok, U., & Lile, R. C. (1977). A year of snow accumulation at plateau station. *Antarctic Research Series*, *25*, 17–26. https://doi.org/10.1002/9781118664872.CH2

Rae, J. G. L., Aðalgeirsdóttir, G., Edwards, T. L., Fettweis, X., Gregory, J. M., Hewitt, H. T., et al. (2012). Greenland ice sheet surface mass balance: Evaluating simulations and making projections with regional climate models. *The Cryosphere*, *6*(6), 1275–1294. https://doi.org/10.5194/tc-6-1275-2012

Raphael, M. N. (2004). A zonal wave 3 index for the Southern Hemisphere. *Geophysical Research Letters*, *31*, L23212. https://doi.org/10.1029/2004GL020365

Reeves Eyre, J. E. J. J., & Zeng, X. (2017). Evaluation of Greenland near surface air temperature datasets. *The Cryosphere*, *11*(4), 1591–1605. https://doi.org/10.5194/tc-11-1591-2017

Reijmer, C. H., & van den Broeke, M. R. (2001). Moisture source of precipitation in Western Dronning Maud Land, Antarctica. *Antarctic Science*, *13*(2), 210–220. https://doi.org/10.1017/S0954102001000293

Rémy, F., & Parouty, S. (2009). Antarctic Ice Sheet and radar altimetry: A review. *Remote Sensing*, *1*(4), 1212–1239. https://doi.org/10.3390/rs1041212

Rennermalm, A. K., Smith, L. C., Stroeve, J. C., & Chu, V. W. (2009). Does sea ice influence Greenland ice sheet surface-melt? *Environmental Research Letters*, *4*(2), 024011. https://doi.org/10.1088/1748-9326/4/2/024011

Rhoades, A. M., Huang, X., Ullrich, P. A., & Zarzycki, C. M. (2015). Characterizing Sierra Nevada snowpack using variable-resolution CESM. *Journal of Applied Meteorology and Climatology*, *55*(1), 173–196. https://doi.org/10.1175/JAMC-D-15-0156.1

Ricaud, P., Bazile, E., del Guasta, M., Lanconelli, C., Grigioni, P., & Mahjoub, A. (2017). Genesis of diamond dust, ice fog and thick cloud episodes observed and modelled above Dome C, Antarctica. *Atmospheric Chemistry and Physics*, *17*(8), 5221–5237. https://doi.org/10.5194/acp-17-5221-2017

Richardson, C., Aarholt, E., Hamran, S.-E., Holmlund, P., & Isaksson, E. (1997). Spatial distribution of snow in western Dronning Maud Land, East Antarctica, mapped by a ground-based snow radar. *Journal of Geophysical Research*, *102*(B9), 20,343–20,353. https://doi.org/10.1029/97JB01441

Rignot, E., Mouginot, J., Scheuchl, B., van den Broeke, M., van Wessem, M. J., & Morlighem, M. (2019). Four decades of Antarctic Ice Sheet mass balance from 1979–2017. *Proceedings of the National Academy of Sciences of the United States of America*, *116*(4), 1095–1103. https://doi.org/10.1073/pnas.1812883116

Rignot, E., Velicogna, I., van den Broeke, M. R. R., Monaghan, A., & Lenaerts, J. T. M. (2011). Acceleration of the contribution of the Greenland and Antarctic ice sheets to sea level rise. *Geophysical Research Letters*, *38*, L05503. https://doi.org/10.1029/2011GL046583

Robinson, A., Calov, R., & Ganopolski, A. (2012). Multistability and critical thresholds of the Greenland ice sheet. *Nature Climate Change*, *2*(6), 429–432. https://doi.org/10.1038/nclimate1449

Rodriguez-Morales, F., Gogineni, S., Leuschen, C. J., Paden, J. D., Li, J., Lewis, C. C., et al. (2014). Advanced multifrequency radar instrumentation for polar research. *IEEE Transactions on Geoscience and Remote Sensing*, *52*(5), 2824–2842. https://doi.org/10.1109/TGRS.2013.2266415

Rotschky, G., Eisen, O., Wilhelms, F., Nixdorf, U., & Oerter, H. (2004). Spatial distribution of surface mass balance on Amundsenisen plateau, Antarctica, derived from ice-penetrating radar studies. *Annals of Glaciology*, *39*(1), 265–270. https://doi.org/10.3189/172756404781814618

Sasgen, I., Dobslaw, H., Martinec, Z., & Thomas, M. (2010). Satellite gravimetry observation of Antarctic snow accumulation related to ENSO. *Earth and Planetary Science Letters*, *299*(3-4), 352–358. https://doi.org/10.1016/j.epsl.2010.09.015

Sasgen, I., van den Broeke, M., Bamber, J. L., Rignot, E., Sørensen, L. S., Wouters, B., et al. (2012). Timing and origin of recent regional ice-mass loss in Greenland. *Earth and Planetary Science Letters*, *333-334*, 293–303. https://doi.org/10.1016/J.EPSL.2012.03.033

Sato, N., Kikuchi, K., Barnard, S. C., & Hogan, A. W. (1981). Some characteristic properties of ice crystal precipitation in the summer season at South Pole Station, Antarctica. *Journal of the Meteorological Society of Japan. Series II*, *59*(5), 772–780. https://doi.org/10.2151/jmsj1965.59.5_772

Scambos, T., Hulbe, C., & Fahnestock, M. (2003). Climate-induced ice shelf disintegration in the Antarctic Peninsula. In *Antarctic Peninsula Climate Variability: Historical and Paleoenvironmental Perspectives* (Vol. 79, pp. 79–92). Washington, DC: American Geophysical Union. https://doi.org/10.1177/095968360501500217

Scambos, T. A., Frezzotti, M., Haran, T., Bohlander, J., Lenaerts, J. T. M., van den Broeke, M. R., et al. (2012). Extent of low-accumulation "wind glaze" areas on the East Antarctic plateau: Implications for continental ice mass balance. *Journal of Glaciology*, *58*(210), 633–647. https://doi.org/10.3189/2012JoG11J232

Schlegel, N.-J., Wiese, D. N., Larour, E. Y., Watkins, M. M., Box, J. E., Fettweis, X., & van den Broeke, M. R. (2016). Application of GRACE to the assessment of model-based estimates of monthly Greenland Ice Sheet mass balance (2003-2012). *The Cryosphere*, *10*(5), 1965–1989. https://doi.org/10.5194/tc-10-1965-2016

Schlosser, E., Manning, K. W., Powers, J. G., Duda, M. G., Birnbaum, G., & Fujita, K. (2010). Characteristics of high-precipitation events in Dronning Maud Land, Antarctica. *Journal of Geophysical Research*, *115*, D14107. https://doi.org/10.1029/2009JD013410

Schmidt, R. A. (1982). Vertical profiles of wind speed, snow concentration and humidity in blowing snow. *Boundary-Layer Meteorology*, *23*(2), 223–246. https://doi.org/10.1007/BF00123299

Schneider, D. P., & Fogt, R. L. (2018). Artifacts in century-length atmospheric and coupled reanalyses over Antarctica due to historical data availability. *Geophysical Research Letters*, *45*, 964–973. https://doi.org/10.1002/2017GL076226

Schuenemann, K. C., Cassano, J. J., & Finnis, J. (2009). Synoptic forcing of precipitation over Greenland: Climatology for 1961–99. *Journal of Hydrometeorology*, *10*(1), 60–78. https://doi.org/10.1175/2008JHM1014.1

Scott, J. B. T., Smith, A. M., Bingham, R. G., & Vaughan, D. G. (2010). Crevasses triggered on Pine Island Glacier, West Antarctica, by drilling through an exceptional melt layer. *Annals of Glaciology*, *51*(55), 65–70. https://doi.org/10.3189/172756410791392763

Screen, J. A., & Simmonds, I. (2011). Erroneous Arctic temperature trends in the ERA-40 reanalysis: A closer look. *Journal of Climate*, *24*(10), 2620–2627. https://doi.org/10.1175/2010JCLI4054.1

Serreze, M. C., & Hurst, C. M. (2000). Representation of mean Arctic precipitation from NCEP-NCAR and ERA reanalyses. *Journal of Climate*, *13*(1), 182–201. https://doi.org/10.1175/1520-0442(2000)013<0182:ROMAPF>2.0.CO;2

Shean, D. E., Christianson, K., Larson, K. M., Ligtenberg, S. R. M., Joughin, I. R., Smith, B. E., et al. (2017). GPS-derived estimates of surface mass balance and ocean-induced basal melt for Pine Island Glacier ice shelf, Antarctica. *The Cryosphere*, *11*(6), 2655–2674. https://doi.org/10.5194/tc-11-2655-2017

Shepherd, A., Ivins, E., Rignot, E., Smith, B., van den Broeke, M., Velicogna, I., et al. (2018). Mass balance of the Antarctic Ice Sheet from 1992 to 2017. *Nature*, *558*(7709), 219–222. https://doi.org/10.1038/s41586-018-0179-y

Shepherd, A., Ivins, E. R., A, G., Barletta, V. R., Bentley, M. J., Bettadpur, S., et al. (2012). A reconciled estimate of ice-sheet mass balance. *Science*, *338*(6111), 1183–1189. https://doi.org/10.1126/science.1228102

Shupe, M. D., Intrieri, J. M., Shupe, M. D., & Intrieri, J. M. (2004). Cloud radiative forcing at the Arctic surface: The influence of cloud properties, surface albedo, and solar zenith angle. *Journal of Climate*, *17*(3), 616–628. https://doi.org/10.1175/1520-0442(2004)017<0616:CRFOTA>2.0.CO;2

Shupe, M. D., Turner, D. D., Walden, V. P., Bennartz, R., Cadeddu, M. P., Castellani, B. B., et al. (2013). High and dry: New observations of tropospheric and cloud properties above the Greenland Ice Sheet. *Bulletin of the American Meteorological Society*, *94*(2), 169–186. https://doi.org/10.1175/BAMS-D-11-00249.1

Siegert, M. J., & Payne, A. J. (2004). Past rates of accumulation in central West Antarctica. *Geophysical Research Letters*, *31*, L12403. https://doi.org/10.1029/2004GL020290

Siegfried, M. R., Medley, B., Larson, K. M., Fricker, H. A., & Tulaczyk, S. (2017). Snow accumulation variability on a West Antarctic ice stream observed with GPS reflectometry, 2007–2017. *Geophysical Research Letters*, *44*, 7808–7816. https://doi.org/10.1002/2017GL074039

Simonsen, S. B., Stenseng, L., Aðalgeirsdóttir, G., Fausto, R. S., Hvidberg, C. S., & Lucas-Picher, P. (2013). Assessing a multilayered dynamic firn-compaction model for Greenland with ASIRAS radar measurements. *Journal of Glaciology*, *59*(215), 545–558. https://doi.org/10.3189/2013JoG12J158

Sinisalo, A., Grinsted, A., & Moore, J. C. (2004). Dynamics of the Scharffenbergbotnen blue-ice area, Dronning Maud Land, Antarctica. *Annals of Glaciology*, *39*, 417–422. https://doi.org/10.3189/172756404781814177

Smeets, C. J. P. P., & van den Broeke, M. R. (2008). Temporal and spatial variations of the aerodynamic roughness length in the ablation zone of the greenland ice sheet. *Boundary-Layer Meteorology*, *128*(3), 315–338. https://doi.org/10.1007/s10546-008-9291-0

Smith, L. C., Chu, V. W., Yang, K., Gleason, C. J., Pitcher, L. H., Rennermalm, A. K., et al. (2015). Efficient meltwater drainage through supraglacial streams and rivers on the southwest Greenland ice sheet. *Proceedings of the National Academy of Sciences of the United States of America*, *112*(4), 1001–1006. https://doi.org/10.1073/pnas.1413024112

Sodemann, H., Schwierz, C., & Wernli, H. (2008). Interannual variability of Greenland winter precipitation sources: Lagrangian moisture diagnostic and North Atlantic Oscillation influence. *Journal of Geophysical Research*, *113*, D03107. https://doi.org/10.1029/2007JD008503

Sodemann, H., & Stohl, A. (2009). Asymmetries in the moisture origin of Antarctic precipitation. *Geophysical Research Letters*, *36*, L22803. https://doi.org/10.1029/2009GL040242

Souverijns, N., Gossart, A., Lhermitte, S., Gorodetskaya, I. V., Grazioli, J., Berne, A., et al. (2018). Evaluation of the CloudSat surface snowfall product over Antarctica using ground-based precipitation radars. *The Cryosphere Discussions*, 1–21. https://doi.org/10.5194/tc-2018-111

Speirs, J. C., Steinhoff, D. F., McGowan, H. A., Bromwich, D. H., & Monaghan, A. J. (2010). Foehn winds in the McMurdo Dry Valleys, Antarctica: The origin of extreme warming events. *Journal of Climate*, *23*(13), 3577–3598. https://doi.org/10.1175/2010JCLI3382.1

Spencer, M. K., Alley, R. B., & Creyts, T. T. (2001). Preliminary firn-densification model with 38-site dataset. *Journal of Glaciology*, *47*(159), 671–676.
Spikes, V. B., Hamilton, G. S., Arcone, S. A., Kaspari, S., & Mayewski, P. A. (2004). Variability in accumulation rates from GPR profiling on the West Antarctic plateau. *Annals of Glaciology*, *39*(1), 238–244. https://doi.org/10.3189/172756404781814393
Steger, C. R., Reijmer, C. H., van den Broeke, M. R., Wever, N., Forster, R. R., Koenig, L. S., et al. (2017). Firn meltwater retention on the Greenland Ice Sheet: A model comparison. *Frontiers in Earth Science*, *5*, 3. https://doi.org/10.3389/feart.2017.00003
Steig, E. J., & Neff, P. D. (2018). The prescience of paleoclimatology and the future of the Antarctic ice sheet. *Nature Communications*, *9*(1), 2730. https://doi.org/10.1038/s41467-018-05001-1
Steinhoff, D. F., Bromwich, D. H., Lambertson, M., Knuth, S. L., & Lazzara, M. A. (2008). A dynamical investigation of the May 2004 McMurdo Antarctica severe wind event using AMPS. *Monthly Weather Review*, *136*(1), 7–26. https://doi.org/10.1175/2007MWR1999.1
Stibal, M., Box, J. E., Cameron, K. A., Langen, P. L., Yallop, M. L., Mottram, R. H., et al. (2017). Algae drive enhanced darkening of bare ice on the Greenland Ice Sheet. *Geophysical Research Letters*, *44*, 11,463–11,471. https://doi.org/10.1002/2017GL075958
Stroeve, J. C., Mioduszewski, J. R., Rennermalm, A., Boisvert, L. N., Tedesco, M., & Robinson, D. (2017). Investigating the local-scale influence of sea ice on Greenland surface melt. *The Cryosphere*, *11*(5), 2363–2381. https://doi.org/10.5194/tc-11-2363-2017
Sundal, A. V., Shepherd, A., Nienow, P., Hanna, E., Palmer, S., & Huybrechts, P. (2009). Evolution of supra-glacial lakes across the Greenland Ice Sheet. *Remote Sensing of Environment*, *113*(10), 2164–2171. https://doi.org/10.1016/J.RSE.2009.05.018
Sutterley, T. C., Velicogna, I., Fettweis, X., Rignot, E., Noël, B., & van den Broeke, M. (2018). Evaluation of reconstructions of snow/ice melt in Greenland by regional atmospheric climate models using laser altimetry data. *Geophysical Research Letters*, *45*, 8324–8333. https://doi.org/10.1029/2018GL078645
Sutterley, T. C., Velicogna, I., Rignot, E., Mouginot, J., Flament, T., van den Broeke, M. R., et al. (2014). Mass loss of the Amundsen Sea Embayment of West Antarctica from four independent techniques. *Geophysical Research Letters*, *41*, 8421–8428. https://doi.org/10.1002/2014GL061940
Thomas, E. R., Hosking, J. S., Tuckwell, R. R., Warren, R. A., & Ludlow, E. C. (2015). Twentieth century increase in snowfall in coastal West Antarctica. *Geophysical Research Letters*, *42*, 9387–9393. https://doi.org/10.1002/2015GL065750
Thomas, E. R., van Wessem, J. M., Roberts, J., Isaksson, E., Schlosser, E., Fudge, T. J., et al. (2017). Regional Antarctic snow accumulation over the past 1000 years. *Climate of the Past Discussions*, *13*(11), 1–42. https://doi.org/10.5194/cp-2017-18
Trusel, L. D., Das, S. B., Osman, M. B., Evans, M. J., Smith, B. E., Fettweis, X., et al. (2018). Nonlinear rise in Greenland runoff in response to post-industrial Arctic warming. *Nature*, *564*(7734), 104–108. https://doi.org/10.1038/s41586-018-0752-4
Trusel, L. D., Frey, K. E., & Das, S. B. (2012). Antarctic surface melting dynamics: Enhanced perspectives from radar scatterometer data. *Journal of Geophysical Research*, *117*, F02023. https://doi.org/10.1029/2011JF002126
Trusel, L. D., Frey, K. E., Das, S. B., Karnauskas, K. B., Kuipers Munneke, P., van Meijgaard, E., & van den Broeke, M. R. (2015). Divergent trajectories of Antarctic surface melt under two twenty-first-century climate scenarios. *Nature Geoscience*, *8*(12), 927–932. https://doi.org/10.1038/ngeo2563
Trusel, L. D., Frey, K. E., Das, S. B., Munneke, P. K., & van den Broeke, M. R. (2013). Satellite-based estimates of Antarctic surface meltwater fluxes. *Geophysical Research Letters*, *40*, 6148–6153. https://doi.org/10.1002/2013GL058138
Turner, J., Lachlan-Cope, T. A., Marshall, G. J., Morris, E. M., Mulvaney, R., & Winter, W. (2002). Spatial variability of Antarctic Peninsula net surface mass balance. *Journal of Geophysical Research*, *107*(D13), 4173. https://doi.org/10.1029/2001JD000755
Turner, J., Lu, H., White, I., King, J. C., Phillips, T., Hosking, J. S., et al. (2016). Absence of 21st century warming on Antarctic Peninsula consistent with natural variability. *Nature*, *535*(7612), 411–415. https://doi.org/10.1038/nature18645
Turner, J., Orr, A., Gudmundsson, G. H., Jenkins, A., Bingham, R. G., Hillenbrand, C.-D., & Bracegirdle, T. J. (2017). Atmosphere-ocean-ice interactions in the Amundsen Sea Embayment, West Antarctica. *Reviews of Geophysics*, *55*, 235–276. https://doi.org/10.1002/2016RG000532
Turner, J., Phillips, T., Hosking, J. S., Marshall, G. J., & Orr, A. (2013). The Amundsen Sea low. *International Journal of Climatology*, *33*(7), 1818–1829. https://doi.org/10.1002/joc.3558
Urbini, S., Frezzotti, M., Gandolfi, S., Vincent, C., Scarchilli, C., Vittuari, L., & Fily, M. (2008). Historical behaviour of Dome C and Talos Dome (East Antarctica) as investigated by snow accumulation and ice velocity measurements. *Global and Planetary Change*, *60*(3–4), 576–588. https://doi.org/10.1016/j.gloplacha.2007.08.002
Våge, K., Spengler, T., Davies, H. C., & Pickart, R. S. (2009). Multi-event analysis of the westerly Greenland tip jet based upon 45 winters in ERA-40. *Quarterly Journal of the Royal Meteorological Society*, *135*(645), 1999–2011. https://doi.org/10.1002/qj.488
van Angelen, J. H., Lenaerts, J. T. M., Lhermitte, S., Fettweis, X., Kuipers Munneke, P., van den Broeke, M. R., et al. (2012). Sensitivity of Greenland Ice Sheet surface mass balance to surface albedo parameterization: A study with a regional climate model. *The Cryosphere*, *6*(5), 1175–1186. https://doi.org/10.5194/tc-6-1175-2012
van Angelen, J. H., Lenaerts, J. T. M., van den Broeke, M. R., Fettweis, X., & van Meijgaard, E. (2013). Rapid loss of firn pore space accelerates 21st century Greenland mass loss. *Geophysical Research Letters*, *40*, 2109–2113. https://doi.org/10.1002/grl.50490
van Angelen, J. H., van den Broeke, M. R., & van de Berg, W. J. (2011). Momentum budget of the atmospheric boundary layer over the Greenland ice sheet and its surrounding seas. *Journal of Geophysical Research*, *116*, D10101. https://doi.org/10.1029/2010JD015485
van Angelen, J. H., van den Broeke, M. R., Wouters, B., & Lenaerts, J. T. M. (2014). Contemporary (1960–2012) evolution of the climate and surface mass balance of the Greenland Ice Sheet. *Surveys in Geophysics*, *35*(5), 1155–1174. https://doi.org/10.1007/s10712-013-9261-z
van Dalum, C. T., van de Berg, W. J., Libois, Q., Picard, G., & van den Broeke, M. R. (2018). A method to convert spectral to narrowband snow albedo for use in climate models. *Geoscientific Model Development Discussion*, 1–26. https://doi.org/10.5194/gmd-2018-175
van de Berg, W. J., van den Broeke, M. R., Reijmer, C. H., & van Meijgaard, E. (2006). Reassessment of the Antarctic surface mass balance using calibrated output of a regional atmospheric climate model. *Journal of Geophysical Research*, *111*, D11104. https://doi.org/10.1029/2005JD006495
van de Wal, R. S. W., Greuell, W., van den Broeke, M. R., Reijmer, C. H., & Oerlemans, J. (2005). Surface mass-balance observations and automatic weather station data along a transect near Kangerlussuaq, West Greenland. *Annals of Glaciology*, *42*, 311–316.
van den Broeke, M., Bamber, J., Ettema, J., Rignot, E., Schrama, E., van de Berg, W. J., et al. (2009). Partitioning recent Greenland mass loss. *Science*, *326*(5955), 984–986. https://doi.org/10.1126/science.1178176
van den Broeke, M., Box, J., Fettweis, X., Hanna, E., Noël, B., Tedesco, M., et al. (2017). Greenland Ice Sheet surface mass loss: Recent developments in observation and modeling. *The Cryosphere Discussions*, 1–12. https://doi.org/10.5194/tc-2017-201
van den Broeke, M., Smeets, P., & Ettema, J. (2009). Surface layer climate and turbulent exchange in the ablation zone of the west Greenland ice sheet. *International Journal of Climatology*, *29*(15), 2309–2323. https://doi.org/10.1002/joc.1815

van den Broeke, M., van de Berg, W. J., & van Meijgaard, E. (2006). Snowfall in coastal West Antarctica much greater than previously assumed. *Geophysical Research Letters*, *33*, L02505. https://doi.org/10.1029/2005GL025239
van den Broeke, M. R. (1997). Spatial and temporal variation of sublimation on Antarctica: Results of a high-resolution general circulation model. *Journal of Geophysical Research*, *102*(D25), 29,765–29,777. https://doi.org/10.1029/97JD01862
van den Broeke, M. R. (1998). The semi-annual oscillation and Antarctic climate. Part 1: influence on near surface temperatures (1957–79). *Antarctic Science*, *10*(2), 175–183. https://doi.org/10.1017/S0954102098000248
van den Broeke, M. R., Bamber, J., Lenaerts, J. T. M., & Rignot, E. (2011). Ice sheets and sea level: Thinking outside the box. *Surveys in Geophysics*, *32*(4–5), 495–505. https://doi.org/10.1007/s10712-011-9137-z
van den Broeke, M. R., Enderlin, E. M., Howat, I. M., Kuipers Munneke, P., Noël, B. P. Y., van de Berg, W. J., et al. (2016). On the recent contribution of the Greenland ice sheet to sea level change. *The Cryosphere*, *10*(5), 1933–1946. https://doi.org/10.5194/tc-10-1933-2016
van den Broeke, M. R., & Gallée, H. (1996). Observation and simulation of barrier winds at the western margin of the Greenland ice sheet. *Quarterly Journal of the Royal Meteorological Society*, *122*(534), 1365–1383.
van den Broeke, M. R., König-Langlo, G., Picard, G., Kuipers Munneke, P., & Lenaerts, J. T. M. (2009). Surface energy balance, melt and sublimation at Neumayer Station, East Antarctica. *Antarctic Science*, *22*(1), 87. https://doi.org/10.1017/S0954102009990538
van den Broeke, M. R., Reijmer, C. H., van As, D., van de Wal, R. S. W., & Oerlemans, J. (2005). Seasonal cycles of Antarctic surface energy balance from automatic weather stations. *Annals of Glaciology*, *41*, 131–139.
van den Broeke, M. R., Reijmer, C. H., & van de Wal, R. S. W. (2004). A study of the surface mass balance in Dronning Maud Land, Antarctica, using automatic weather stationS. *Journal of Glaciology*, *50*(171), 565–582. https://doi.org/10.3189/172756504781829756
van den Broeke, M. R., Tijm-Reijmer, C. H., & Boot, W. (2013). Advances on Ice. *International Innovation - Climate Issue*, 47–49.
van den Broeke, M. R., van As, D., Reijmer, C. H., & van de Wal, R. S. W. (2005). Sensible heat exchange at the Antarctic snow surface: A study with automatic weather stations. *International Journal of Climatology*, *25*(8), 1081–1101. https://doi.org/10.1002/joc.1152
van den Broeke, M. R., & van Lipzig, N. P. M. (2004). Changes in Antarctic temperature, wind and precipitation in response to the Antarctic Oscillation. *Annals of Glaciology*, *39*, 119–126. https://doi.org/10.3189/172756404781814654
van den Broeke, M. R., van Lipzig, N. P. M., & van Meijgaard, E. (2003). Factors controlling the near-surface wind field in Antarctica. *Monthly Weather Review*, *131*(4), 733–743. https://doi.org/10.1175/1520-0493(2003)131<0733:FCTNSW>2.0.CO;2
van den Broeke, M. R., van Lipzig, N. P. M., & van Meijgaard, E. (2002). Momentum budget of the East Antarctic atmospheric boundary layer: Results of a regional climate model. *Journal of the Atmospheric Sciences*, *59*(21), 3117–3129. https://doi.org/10.1175/1520-0469(2002)059<3117:MBOTEA>2.0.CO;2
van Kampenhout, L., Lenaerts, J. T. M., Lipscomb, W. H., Sacks, W. J., Lawrence, D. M., Slater, A. G., & van den Broeke, M. R. (2017). Improving the representation of polar snow and firn in the Community Earth System Model. *Journal of Advances in Modeling Earth Systems*, *9*, 2583–2600. https://doi.org/10.1002/2017MS000988
van Kampenhout, L., Rhoades, A. M., Herrington, A. R., Zarzycki, C. M., Lenaerts, J. T. M., Sacks, W. J., & van den Broeke, M. R. (2018). Regional grid refinement in an Earth system model: Impacts on the simulated Greenland surface mass balance. *The Cryosphere Discussions*, 1–25. https://doi.org/10.5194/tc-2018-257
van Lipzig, N. P. M., King, L. J. C., Lachlan-Cope, T. A., & van den Broeke, M. R. (2004). Precipitation, sublimation, and snow drift in the Antarctic Peninsula region from a regional atmospheric model. *Journal of Geophysical Research*, *109*, D24106. https://doi.org/10.1029/2004JD004701
van Lipzig, N. P. M., van Meijgaard, E., & Oerlemans, J. (2002). The spatial and temporal variability of the surface mass balance in Antarctica: Results from a regional climate model. *International Journal of Climatology*, *22*(10), 1197–1217.
van Loon, H. (1967). The half-yearly oscillations in middle and high southern latitudes and the coreless winter. *Journal of the Atmospheric Sciences*, *24*(5), 472–486. https://doi.org/10.1175/1520-0469(1967)024<0472:THYOIM>2.0.CO;2
van Ommen, T. D., Morgan, V., & Curran, M. A. J. (2004). Deglacial and Holocene changes in accumulation at Law Dome, East Antarctica. *Annals of Glaciology*, *39*, 359–365. https://doi.org/10.3189/172756404781814221
Van Tricht, K., Lhermitte, S., Lenaerts, J. T. M., Gorodetskaya, I. V., L'Ecuyer, T. S., Noël, B., et al. (2016). Clouds enhance Greenland ice sheet meltwater runoff. *Nature Communications*, *7*(1), 10266. https://doi.org/10.1038/ncomms10266
van Wessem, J. M., Ligtenberg, S. R. M., Reijmer, C. H., van de Berg, W. J., van den Broeke, M. R., Barrand, N. E., et al. (2016). The modelled surface mass balance of the Antarctic Peninsula at 5.5 km horizontal resolution. *The Cryosphere*, *10*(1), 271–285. https://doi.org/10.5194/tc-10-271-2016
van Wessem, J. M., Reijmer, C. H., Morlighem, M., Mouginot, J., Rignot, E., Medley, B., et al. (2014). Improved representation of East Antarctic surface mass balance in a regional atmospheric climate model. *Journal of Glaciology*, *60*(222), 761–770. https://doi.org/10.3189/2014JoG14J051
van Wessem, J. M., van de Berg, W. J., Noël, B. P. Y., van Meijgaard, E., Amory, C., Birnbaum, G., et al. (2018). Modelling the climate and surface mass balance of polar ice sheets using RACMO2—Part 2: Antarctica (1979–2016). *The Cryosphere*, *12*(4), 1479–1498. https://doi.org/10.5194/tc-12-1479-2018
Vaughan, D. G., Marshall, G. J., Connolley, W. M., Parkinson, C., Mulvaney, R., Hodgson, D. A., et al. (2003). Recent rapid regional climate warming on the Antarctic Peninsula. *Climatic Change*, *60*(3), 243–274. https://doi.org/10.1023/A:1026021217991
Velicogna, I., Sutterley, T. C., & van den Broeke, M. R. (2014). Regional acceleration in ice mass loss from Greenland and Antarctica using GRACE time-variable gravity data. *Geophysical Research Letters*, *41*, 8130–8137. https://doi.org/10.1002/2014GL061052
Velicogna, I., & Wahr, J. (2005). Greenland mass balance from GRACE. *Geophysical Research Letters*, *32*, L18505. https://doi.org/10.1029/2005GL023955
Velicogna, I., & Wahr, J. (2006). Measurements of time-variable gravity show mass loss in Antarctica. *Science*, *311*, 1754–1756.
Vignon, E., Hourdin, F., Genthon, C., van de Wiel, B. J. H., Gallée, H., Madeleine, J.-B., & Beaumet, J. (2018). Modeling the dynamics of the atmospheric boundary layer over the Antarctic Plateau with a general circulation model. *Journal of Advances in Modeling Earth Systems*, *10*, 98–125. https://doi.org/10.1002/2017MS001184
Vizcaino, M. (2014). Ice sheets as interactive components of Earth System Models: Progress and challenges. *Wiley Interdisciplinary Reviews: Climate Change*, *5*(4), 557–568. https://doi.org/10.1002/wcc.285
Vizcaíno, M., Lipscomb, W. H., Sacks, W. J., van Angelen, J. H., Wouters, B., & van den Broeke, M. R. (2013). Greenland surface mass balance as simulated by the Community Earth System Model. Part I: Model evaluation and 1850–2005 results. *Journal of Climate*, *26*(20), 7793–7812. https://doi.org/10.1175/JCLI-D-12-00615.1

Vizcaino, M., Mikolajewicz, U., Ziemen, F., Rodehacke, C. B., Greve, R., & Broeke, M. R. (2015). Coupled simulations of Greenland ice sheet and climate change up to AD 2300. *Geophysical Research Letters*, *42*, 3927–3935. https://doi.org/10.1002/2014GL061142
von Walden, P., Warren, S. G., & Tuttle, E. (2003). Atmospheric ice crystals over the Antarctic Plateau in winter. *Journal of Applied Meteorology and Climatology*, *42*(10), 1391–1405. https://doi.org/10.1175/1520-0450(2003)042<1391:AICOTA>2.0.CO;2
Wacker, U., Ries, H., & Schättler, U. (2009). Precipitation simulation for dronning maud land using the COSMO model. *Antarctic Science*, *21*(6), 643–662. https://doi.org/10.1017/S0954102009990149
Waddington, E. D., Neumann, T. A., Koutnik, M. R., Marshall, H. P., & Morse, D. L. (2007). Inference of accumulation-rate patterns from deep layers in glaciers and ice sheets. *Journal of Glaciology*, *53*(183), 694–712.
Wahr, J., Molenaar, M., & Bryan, F. (1998). Time variability of the Earth's gravity field: Hydrological and oceanic effects and their possible detection using GRACE. *Journal of Geophysical Research*, *103*, 30,205–30,229. https://doi.org/10.1029/98JB02844
Wang, X., Key, J. R., Wang, X., & Key, J. R. (2005). Arctic surface, cloud, and radiation properties based on the AVHRR polar pathfinder dataset. Part I: Spatial and temporal characteristics. *Journal of Climate*, *18*(14), 2558–2574. https://doi.org/10.1175/JCLI3438.1
Wang, X., & Zender, C. S. (2010). Constraining MODIS snow albedo at large solar zenith angles: Implications for the surface energy budget in Greenland. *Journal of Geophysical Research*, *115*, F04015. https://doi.org/10.1029/2009JF001436
Warren, S. G., & Wiscombe, W. J. (1980). A model for the spectral albedo of snow. II: Snow containing atmospheric aerosols. *Journal of the Atmospheric Sciences*, *37*(12), 2734–2745. https://doi.org/10.1175/1520-0469(1980)037<2734:AMFTSA>2.0.CO;2
Weijer, W., Veneziani, M., Stössel, A., Hecht, M. W., Jeffery, N., Jonko, A., et al. (2017). Local atmospheric response to an open-ocean Polynya in a high-resolution climate model. *Journal of Climate*, *30*(5), 1629–1641. https://doi.org/10.1175/JCLI-D-16-0120.1
Wientjes, I. G. M., van de Wal, R. S. W., Reichart, G. J., Sluijs, A., & Oerlemans, J. (2011). Dust from the dark region in the western ablation zone of the Greenland ice sheet. *The Cryosphere*, *5*(3), 589–601. https://doi.org/10.5194/tc-5-589-2011
Wilhelms, F. (2005). Explaining the dielectric properties of firn as a density-and-conductivity mixed permittivity (DECOMP). *Geophysical Research Letters*, *32*, L16501. https://doi.org/10.1029/2005GL022808
Wille, J. D., Bromwich, D. H., Cassano, J. J., Nigro, M. A., Mateling, M. E., & Lazzara, M. A. (2014). Evaluation of the AMPS boundary layer simulations on the Ross Ice Shelf, Antarctica, with unmanned aircraft observations. *Journal of Applied Meteorology and Climatology*, *56*(8), 2239–2258. https://doi.org/10.1175/JAMC-D-16-0339.1
Wingham, D. J., Francis, C. R., Baker, S., Bouzinac, C., Brockley, D., Cullen, R., et al. (2006). CryoSat: A mission to determine the fluctuations in Earth's land and marine ice fields. *Advances in Space Research*, *37*(4), 841–871. https://doi.org/10.1016/j.asr.2005.07.027
Winkelmann, R., Levermann, A., Martin, M. A., & Frieler, K. (2012). Increased future ice discharge from Antarctica owing to higher snowfall. *Nature*, *492*(7428), 239–242.
Winther, J. G., Jespersen, M. N., & Liston, G. E. (2001). Blue-ice areas in Antarctica derived from NOAA AVHRR satellite data. *Journal of Glaciology*, *47*(157), 325–334.
Wiscombe, W. J., & Warren, S. G. (1980). A model for the spectral albedo of snow. I: Pure snow. *Journal of the Atmospheric Sciences*, *37*, 2712–2733.
Wiscombe, W. J., Warren, S. G., Wiscombe, W. J., & Warren, S. G. (1980). A model for the spectral albedo of snow. I: Pure snow. *Journal of the Atmospheric Sciences*, *37*(12), 2712–2733. https://doi.org/10.1175/1520-0469(1980)037<2712:AMFTSA>2.0.CO;2
Wood, N. B., L'Ecuyer, T. S., Heymsfield, A. J., Stephen, G. L., Hudak, D. R., & Rodriguez, P. (2014). Estimating snow microphysical properties using collocated multisensor observations. *Journal of Geophysical Research: Atmospheres*, *119*, 8941–8961. https://doi.org/10.1002/2013JD021303
Wouters, B., Bamber, J. L. L., van den Broeke, M. R. R., Lenaerts, J. T. M. T. M., & Sasgen, I. (2013). Limits in detecting acceleration of ice sheet mass loss due to climate variability. *Nature Geoscience*, *6*(8), 613–616. https://doi.org/10.1038/ngeo1874
Wouters, B., Bonin, J. A., Chambers, D. P., Riva, R. E. M., Sasgen, I., & Wahr, J. (2014). GRACE, time-varying gravity, Earth system dynamics and climate change. *Reports on Progress in Physics*, *77*(11), 116801. https://doi.org/10.1088/0034-4885/77/11/116801
Wouters, B., Chambers, D., & Schrama, E. J. O. O. (2008). GRACE observes small-scale mass loss in Greenland. *Geophysical Research Letters*, *35*, L20501. https://doi.org/10.1029/2008GL034816
Yuan, X., Kaplan, M. R., & Cane, M. A. (2018). The interconnected global climate system-a review of tropical-polar teleconnections. *Journal of Climate*, *31*(15), 5765–5792. https://doi.org/10.1175/JCLI-D-16-0637.1
Zhang, T., Stamnes, K., Bowling, S. A., Zhang, T., Stamnes, K., & Bowling, S. A. (1996). Impact of clouds on surface radiative fluxes and snowmelt in the Arctic and Subarctic. *Journal of Climate*, *9*(9), 2110–2123. https://doi.org/10.1175/1520-0442(1996)009<2110:IOCOSR>2.0.CO;2
Zielinski, G. A., Mayewski, P. A., Meeker, L. D., Whitlow, S., Twickler, M. S., Morrison, M., et al. (1994). Record of volcanism since 7000 B. C. from the GISP2 Greenland ice core and implications for the volcano-climate system. *Science*, *264*(5161), 948–952. https://doi.org/10.1126/science.264.5161.948
Zwally, H. J., Giovinetto, M. B., Li, J., Cornejo, H. G., Beckley, M. A., Brenner, A. C., et al. (2005). Mass changes of the Greenland and Antarctic ice sheets and shelves and contributions to sea-level: 1992-2002. *Journal of Glaciology*, *51*(175), 509–527. https://doi.org/10.3189/172756505781829007
Zwally, H. J., Li, J., Robbins, J. W., Saba, J. L., Yi, D., & Brenner, A. C. (2015). Mass gains of the Antarctic ice sheet exceed losses. *Journal of Glaciology*, *61*(230), 1019–1036. https://doi.org/10.3189/2015JoG15J071